TARGETING DNA MISMATCHES WITH LUMINESCENT RUTHENIUM COMPLEXES

Thesis by

Adam N. Boynton

In Partial Fulfillment of the Requirements

for the Degree of

Doctor of Philosophy in Chemistry

California Institute of Technology

Pasadena, CA

2017

(Defended June 5, 2017)

Acknowledgements

None of the work presented here would have been possible without the guidance and support of my research advisor, Jackie Barton. Your passion and enthusiasm for science is unparalleled, and your positive energy has truly made it a pleasure to conduct research at Caltech. Between running the lab and being chair of the department, I honestly don't know how you manage to juggle all of your responsibilities. But the fact that I can almost always knock on your door to talk shows me that you truly care about each and every one of us. I've had my share of ups and downs here, but no matter what, you've always been there to let me know that everything will be okay. Thanks for helping me see the glass as half full!

I would also like to thank the members of my committee: Harry Gray, Doug Rees, and Dave Tirrell. You are all incredibly kind and supportive, and your constructive critiques have guided me towards becoming a better scientist.

I want to thank the administrative assistants who have helped hold the lab together. Mo, it was a pleasure to get to know you and I am grateful for all the hard work you put in over the years to keep the lab running smoothly. Elisha, you're one of the nicest people I've met and thanks for everything that you do for us (that includes supplying the upstairs with ample candy).

I must give special thanks to past Barton group members who guided me through my scientific endeavors over the years. Alexis Komor and Alyson Weidmann, you were there when I first joined the group to show me the ropes on rhodium synthesis, cell biology, and running gels, and I thank you for your patience and wisdom. Anna McConnell, while we only overlapped for half a year, much of what I know about ruthenium chemistry comes from your notebooks and our overseas email correspondence. I don't think I've ever sent you an email that you didn't respond to within a day. Thank you so much for always being willing to answer my questions, no matter

how simple. Anna Arnold, you were the one who actually taught me how to use the fluorometer, and I could always turn to you whenever I had a question. Your incredible attention to detail and scientific rigor is an inspiration to us all. Aaron Sattler, we didn't overlap for long, but in a brief period you taught me proper Schlenk line techniques and other insider synthesis tips that I still use to this day. Finally, Lionel Marcelis, much of what is presented in this thesis would not have been possible without your help and guidance. You've taught me so much about ruthenium chemistry and how to properly conduct luminescence experiments, which I am forever thankful for. You're a great co-worker and a wonderful friend.

Other past Barton group members have made my time here very enjoyable. Natalie Muren, you were an awesome desk mate and you filled the corner with so much positive energy. Ariel Furst, it was great having you on the south side of the lab. You were always a source of humor and I miss having someone to talk to about the ridiculous things we've encountered at the gym. Katie Schaeffer, you're a prime example of someone who lives life to the fullest, and your adventurous spirit is a serious inspiration. I'll miss Friday hangouts at the Rath, and of course puppy girl Leia.

To the current group members: you are all fantastic. Kelsey, you're such a smart, talented, and methodical scientist, something we should all strive to be. It's been a pleasure to work with you on various things, and thanks for many insightful discussions. Liz, we joined the lab around the same time and it's been a pleasure to witness your growth and accomplishments as a scientist. Phil, your diligence to research sets an example for everyone. Ted, I'm so impressed by the risks that you are willing to take and the confidence with which you approach new, unexplored research projects. Andy, you're hilarious and such a bright spot in the lab – keep rocking it, champ! Speaking of bright spots – Bekah, you're one of the kindest, most genuine people I know. Your jovial personality and sense of humor always brightens my day. Steph, I truly admire your hard

work and thanks for keeping it chill on the south side. Siobhán, your fun and upbeat attitude has been a great addition to the group. And to all the postdocs – Ed, Levi, Adela, and Yingxin – thank you for sage advice and for keeping various aspects of the lab running like a well-oiled machine. I aspire to the sheer passion you all show for conducting research.

I next must pay thanks to the various members of the CCE department who have made my research possible. Scott Virgil, I don't know how you find the time to do everything that you do, but the fact that you are always there to help either with a ligand synthesis or to fix our HPLC is something I am truly grateful for. Your dedication to helping researchers is truly unmatched. To all who keep the various instrument facilities running smoothly – Mona Shahgholi, Dave VanderVelde, Andres Collazo, Nathan Dalleska – thanks for everything. Joe Drew and Nathan Siladke, thanks for making sure we're always working in a safe lab. And Jay Winkler, data from the laser lab is a critical part of my research. Thank you so much for your guidance and assistance on the ns1 instrument.

Julie Bailis, it's been a pleasure to collaborate. Thank you for taking interest in our compounds and spending the time to study them in your lab. It was great to be able to spend a few days at Amgen to see what a real industry lab looks like.

To all my Caltech friends – I've had such a blast here with you over the years. Mike Post, you were an awesome housemate and I'm glad we keep sharing good tunes with each other. Nick Cowper, you're one of the best friends I've had – you're hilarious, fun, supportive, and always down to chill. Not to mention you've got a great taste in music and I know we'll keep the good tunes rolling for a long time. The whole Lake Street house – Paul, Trevor, Mark, Ben, JingXin, Jenna – you guys really know how to have a good time, and thanks for tons of great hangouts. And Paul, your high energy and humor are one-of-a-kind, not to mention your coffee roasting skills are

on point. Matt Davis, you're one of the coolest guys I know and I'm going to miss heading to Dodger stadium after lab to catch a game. Mike Grodick, life hasn't been the same since you graduated; we had some great times together and you're one of the most loyal friends anyone could hope for.

Finally, to my family: thank you so much for your unwavering love and support throughout life and especially my time at Caltech. I would not have made it this far without your wisdom and guidance in all walks of life.

Abstract

DNA base pair mismatches occur naturally in cells, typically as a result of errors during replication. Cells have evolved a DNA damage response pathway called mismatch repair (MMR) that identifies and corrects base pair mismatches in newly synthesized DNA. However, proteins involved in MMR can undergo mutations, rendering them incapable of correcting mismatches. Such deficiencies in MMR leads to an increase in genetic mutations and are associated with several forms of cancer. Because a higher mismatch frequency serves as an early indicator of cancer progression, DNA mismatches are a promising target in the design of small molecule therapeutics and diagnostics. In this context, transition metal complexes are prime candidates, owing to their valuable spectroscopic and photophysical properties and versatile coordination sphere geometries. Our laboratory focuses on generating octahedral rhodium and ruthenium complexes that selectively target DNA mismatches. A class of rhodium complexes bearing sterically expansive planar ligands bind DNA mismatches with high selectivity and exhibit preferential cytotoxicity towards MMR-deficient cancer cells. These compounds bind to DNA through metalloinsertion, in which the bulky ligand inserts into the duplex at the thermodynamically destabilized mismatch site, displacing the mismatched bases into the DNA groove.

Herein we describe recent advances in the development of luminescent ruthenium complexes that selectively probe DNA mismatches. We demonstrate that $[Ru(Me_4phen)_2(dppz)]^{2+}$ (Me_4phen = 3,4,7,8-tetramethyl-1,10-phenanthroline; dppz = dipyrido[3,2-*a*:2’,3’-*c*]phenazine) is a DNA “light switch” that exhibits a significantly brighter steady-state emission in the presence of a DNA duplex containing a mismatch relative to completely well-matched DNA. Importantly, the bulky Me_4phen ancillary ligands discourage deep intercalation of dppz between well-matched base pairs, and instead, $[Ru(Me_4phen)_2(dppz)]^{2+}$ favors metalloinsertion at thermodynamically

destabilized mismatches. $[Ru(Me_4phen)_2(dppz)]^{2+}$ possesses a higher binding affinity towards a DNA mismatch relative to well-matched base pairs, and furthermore exhibits a longer excited-state emission lifetime when bound to a mismatch compared to that when intercalated at well-matched sites; both of these observations contribute to the dramatic steady-state emission enhancement detected with the mismatched DNA duplex. Additionally, we reveal that the right-handed delta (Δ) isomer of $[Ru(Me_4phen)_2(dppz)]^{2+}$ is the enantiomer which imparts all mismatch selectivity, consistent with the handedness of B-form DNA.

Another mismatch-specific luminescent probe presented in this work is $[Ru(bpy)_2(BNIQ)]^{2+}$ (bpy = 2,2'-bipyridine; BNIQ = benzo[c][1,7]naphthyridine-1-isoquinoline). In contrast to $[Ru(Me_4phen)_2(dppz)]^{2+}$, the BNIQ complex exploits a bulky inserting ligand that selectively undergoes metalloinsertion at a DNA mismatch. This compound too exhibits a brighter steady-state emission in the presence of a mismatched duplex compared to entirely well-matched DNA, which we attribute to the fact that $[Ru(bpy)_2(BNIQ)]^{2+}$ possesses nearly a 500-fold higher binding affinity for the mismatch site compared to well-matched base pairs. Taken together, $[Ru(Me_4phen)_2(dppz)]^{2+}$ and $[Ru(bpy)_2(BNIQ)]^{2+}$ represent two different yet valid approaches in the rational design of mismatch-specific small molecules, one based on ancillary ligand functionalization and the other on incorporating a sterically expansive inserting ligand.

A third approach towards the design of mismatch-specific luminescent ruthenium probes that is briefly explored here is the modification of the intercalating dppz ligand of $[Ru(bpy)_2(dppz)]^{2+}$. Bearing a dppz ligand substituted with four methyl groups, $[Ru(bpy)_2(tmdppz)]^{2+}$ (tmdppz = 3,4,7,8-tetramethyl dipyridophenazine) shows no luminescence discrimination between mismatched and well-matched duplexes. This observation ostensibly arises from the fact that the appended methyl groups shield the dppz phenazine nitrogen atoms

from interactions with water when intercalated within the DNA.

With mismatch-specific luminescent metalloinsertors such as $[Ru(Me_4phen)_2(dppz)]^{2+}$ in hand, we have commenced biological investigations to see whether these compounds can serve as luminescent proxies for rhodium metalloinsertors in MMR-deficient cancer cells. Confocal microscopy of HCT116N and HCT116O cells reveals that $[Ru(Me_4phen)_2(dppz)]^{2+}$ does preferentially localize to mitochondria, unlike potent cell-selective rhodium complexes such as $[Rh(chrysi)(phen)(PPO)]^{2+}$ (PPO = 2-(pyridine-2-yl)propan-2-ol; chrysi = 5,6-chrysenequinone diimine); however, $[Ru(Me_4phen)_2(dppz)]^{2+}$ shows some degree of nuclear entry. Here our goal is the application of the mismatch-specific luminescent probe in co-localization experiments to investigate what proteins are involved in the DNA damage response that is activated upon metalloinsertor binding *in cellulo.*

The work presented here expands beyond the study of luminescent ruthenium complexes. Amino acid conjugates of the earlier-generation rhodium metalloinsertor $[Rh(HDPA)_2(chrysi)]^{3+}$ (HDPA = 2,2'-dipyridylamine) were synthesized. While these conjugates exhibit mismatch binding affinities comparable to other rhodium metalloinsertors, they lose cell-selective biological activity, which may arise from altered uptake and/or sub-cellular localization. Finally, preliminary investigations were conducted on $[Re(CO)_3(pyOEt)(dppn)]^{+}$ (pyOEt = ethyl 3-(pyridin-4-yl)propanoate; dppn = benzodipyridophenazine) and $[Ru(CN)(tpy)(dppz)]^{+}$ (tpy = terpyridine; CN = cyano), which were designed as IR-active probes to study the kinetics of DNA-mediated charge transport (CT) by time-resolved infrared (TRIR) spectroscopy. While these complexes do not possess the desired spectral TRIR properties as originally intended, steady-state luminescence experiments do suggest that this donor-acceptor pair is capable of undergoing DNA-mediated electron transfer.

Altogether, this work demonstrates the versatility of transition metal complexes as non-covalent probes for DNA. Importantly, through the rational modification of their three-dimensional ligand scaffold, one can achieve site-specific recognition of clinically relevant biomarkers such as DNA mismatches.

Published Content and Contributions

Boynton, A.N.; Marcelis, L.; Barton, J.K. *J. Am. Chem. Soc.* **2016**, *138*, 5020-5023.
DOI: 10.1021/jacs.6b02022
A. Boynton was the primary author on the manuscript, synthesized and characterized ruthenium complexes, and performed steady-state and time-resolved luminescence experiments with DNA.

Boynton, A.N.; Marcelis, L.; McConnell, A.J.; Barton, J.K. *Inorg. Chem*. **2017**, *56*, 8381-8389.
DOI: 10.1021/acs.inorgchem.7b01037
A. Boynton was the primary author on the manuscript, optimized the last few steps of the BNIQ ligand synthesis, generated the $[Ru(bpy)_2(BNIQ)]^{2+}$ complex, and performed steady-state and time-resolved luminescence experiments with DNA.

Contents

Chapter 1

Introduction: Targeting DNA Mismatches with Transition Metal Complexes

Adapted from: Barton, J.K.; Boynton, A.N.; Boyle, K.M. In *DNA-Targeting Molecules as Therapeutic Agents*; Waring, M.J., Ed.; The Royal Society of Chemistry, Chapter 15 (*in press*).

1.1 Transition Metal Complexes as Non-Covalent Probes for Nucleic Acids

Coordination complexes offer distinct advantages as probes for nucleic acid structure. Transition metals possess an array of unique photophysical, spectroscopic, and reactive properties, which can be finely tuned by varying the identity of the metal center and surrounding ligands. Furthermore, the relative ease with which different ligands can be exchanged for one another allows the researcher to explore a range of DNA recognition properties. Owing to this modular nature, one can generate families of closely related complexes to assist in structure-function studies. The Barton laboratory has focused on developing transition metal complexes that target DNA through non-covalent interactions, with an emphasis on rhodium- and ruthenium-based agents. Typically, these positively charged, water-soluble compounds are coordinatively saturated and substitutionally inert. Additionally, these are rigid, three-dimensional systems with well-defined stereochemistry, all highly valuable properties in the context of non-covalent DNA recognition.

Perhaps the simplest non-covalent interaction between a cationic transition metal complex and DNA is electrostatic association with the duplex (Figure 1.1a). Also referred to as ionic site binding, the driving force behind this mode is the electrostatic attraction between the positively charged transition metal complex and the negatively charged DNA polyanion.[1] However, this binding mode offers no site-specific molecular recognition of the DNA. Electrostatic binding is embodied by the classic ruthenium polypyridyl complex $[Ru(bpy)_3]^{2+}$ (bpy = 2,2'-bipyridine).[2,3,4] Although the electrostatic interactions may have some stabilizing effects, this attraction results in very weak binding affinities towards the duplex, on the order of 10^2 M^{-1}.[2]

Groove binding is another type of non-covalent interaction that a transition metal complex may undergo with DNA (Figure 1.1b). This mode involves hydrophobic association in the minor

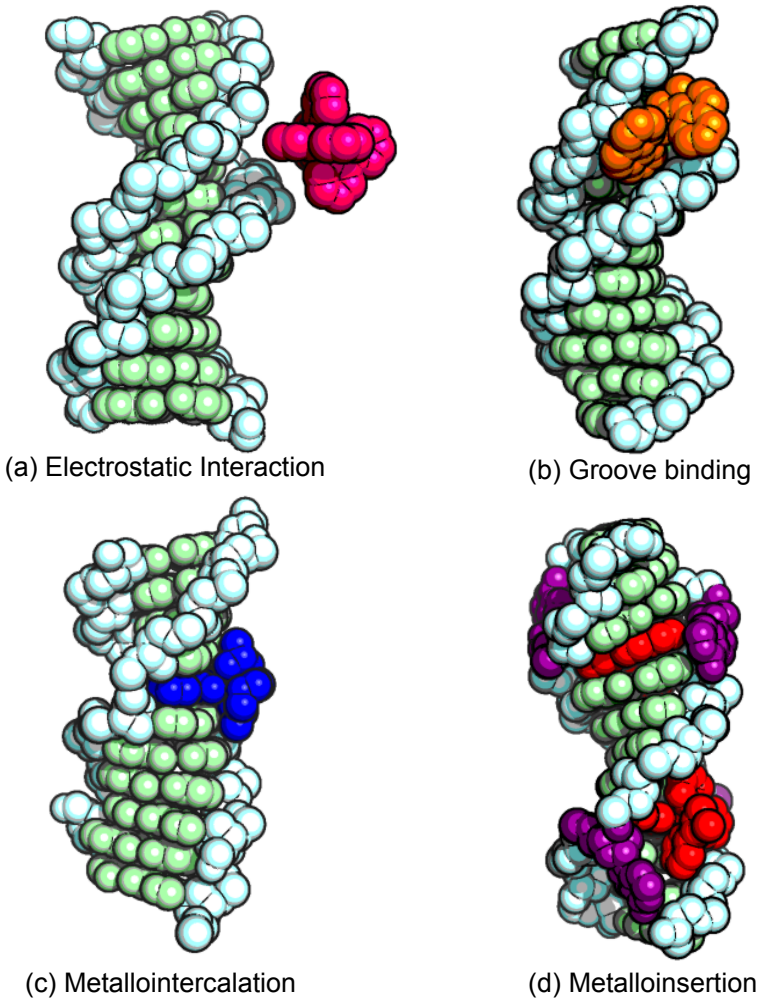

Figure 1.1. Four modes of non-covalent interactions between transition metal complexes and DNA: (a) electrostatic interactions between $[Ru(bpy)_3]^{2+}$ and the negatively-charged DNA, (b) groove binding of $Cu(phen)_2^{2+}$ in the minor groove of DNA, (c) intercalation of [Rh[(*R,R*)-Me_2trien]phi]$^{3+}$ between DNA base pairs, and (d) metalloinsertion of $[Rh(bpy)_2(chrysi)]^{3+}$ into two AC mismatched sites. In all images, the DNA sugar-phosphate backbone is shown in blue, well-matched DNA base pairs are shown in green, and the mismatched bases in part (d) are highlighted in purple. Figure created from PDB structures 4C64, 1VTJ, 3GSK, 454D and CCDC structures ABAFAN and LUQGEL.

groove of the helix. An example of a minor groove-specific binder is $Cu(phen)_2^{2+}$ (phen = 1,10-phenanthroline), which was thoroughly studied by Sigman et al. and functions as a DNA cleaving agent in the presence of hydrogen peroxide.[5,6,7] Another complex that is known to associate with the DNA helix *via* groove binding is $[Ru(phen)_3]^{2+}$, whose interactions with DNA have extensively been characterized by Barton et al.[8] It is critical to note, however, that $[Ru(phen)_3]^{2+}$ is a chiral

molecule; owing to its octahedral coordination geometry and three bidentate phen ligands, it possesses a left-handed enantiomer, designated as Λ, and a right-handed enantiomer, or Δ. Early work deduced that the Λ isomer exhibits preferential binding with B-DNA through association in the minor groove.[2,4]

In contrast to Λ-$[Ru(phen)_3]^{2+}$, the Δ isomer preferentially binds to DNA through a third non-covalent interaction called intercalation. In this binding mode, a planar, aromatic, heterocyclic ligand stacks between the DNA base pairs, typically from the major groove, causing slight unwinding of the helix as well as a small increase in rise (Figure 1.1c).[9] Lippard et al. pioneered the early development of metallointercalators in the 1970s with their square planar platinum(II) complexes.[10,11] In the case of $[Ru(phen)_3]^{2+}$, the phen ligands possess a sufficiently extended π-system to intercalate, albeit partially, between the base pairs of the helix. This intercalation raises the binding affinity towards the DNA relative to groove binding or electrostatic associations. However, the binding affinity of $[Ru(phen)_3]^{2+}$ towards DNA is still relatively meager, on the order of 10^3 M^{-1}. Increasing the intercalative binding affinity for a transition metal probe can be accomplished by increasing the surface area of the intercalating ligand, so as to achieve greater π-stacking between the base pairs of the helix.

Two of the best known examples of strongly intercalating ligands are phi (9,10-phenanthrequinone diimine) and dppz (dipyrido[3,2-*a*:2',3'-*c*]phenazine). Ruthenium(II) complexes bearing the dppz ligand, such as $[Ru(bpy)_2(dppz)]^{2+}$, favorably intercalate into B-form DNA with an affinity on the order of $>10^6$ M^{-1}.[12] While $[Ru(bpy)_2(dppz)]^{2+}$ binds somewhat non-specifically, it does exhibit a preference towards AT-rich regions in the duplex.[13] $[Ru(bpy)_2(dppz)]^{2+}$ and related complexes are described in greater detail in Chapter 2.

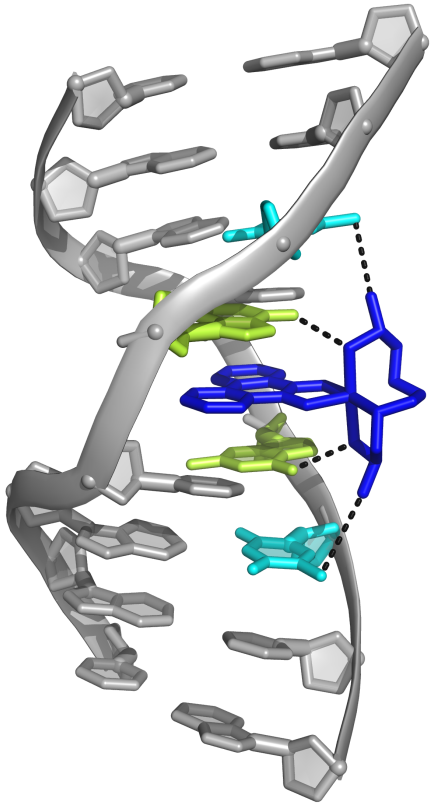

Figure 1.2. [Rh[(*R,R*)-Me_2trien]phi]$^{3+}$ binds specifically to a 5'-TGCA-3' site in this 1.2 Å crystal structure. Van der Waals Me-Me interactions between [Rh[(*R,R*)-Me_2trien]phi]$^{3+}$ (blue) and T (cyan) as well as hydrogen bond interactions between [Rh[(*R,R*)-Me_2trien]phi]$^{3+}$ and the O6 of G (green) are shown as black dotted lines.

Phi is another well-studied intercalating ligand, primarily in the context of rhodium(III) complexes. A classic intercalating complex is [$Rh(phen)_2(phi)$]$^{3+}$, which binds double helical DNA with high affinity ($\geq 10^7$ M^{-1}) owing to the ability of the phi ligand to overlap significantly with the base pairs.[14] Phi complexes of rhodium are capable of cleaving DNA at their intercalative site upon irradiation with UV light, a property with tremendous utility for determining site-specific DNA binding. For example, [$Rh(phen)_2(phi)$]$^{3+}$ exhibits some shape-selective recognition by preferentially photocleaving DNA at 5'-Py-Py-Pu-3' sites. This sequence in particular generates a greater opening of the major groove, which alleviates steric interactions between the DNA and the ancillary phen ligands, allowing the complex to intercalate more deeply. Metallointercalators have

also been developed as sequence-specific recognition agents, exemplified by Δ-α-[Rh[(*R,R*)-Me_2trien]phi]$^{3+}$((*R,R*)-Me_2trien = 2*R*,9*R*-diamino-4,7-diazadecane), which photocleaves specifically at the sequence 5'-TGCA-3'.[15] A high-resolution crystal structure of this metallointercalator bound to DNA revealed that the DNA slightly unwinds at the binding site to permit deep intercalation of the rhodium complex, which occurs from the major groove (Figure 1.2).[16] The sequence-specificity results from an ensemble of non-covalent interactions between functionalities on the ancillary Me_2trien ligand posed into the major groove by rigid intercalation of the octahedral complex. The intercalation results in a doubling of the rise at the binding site, and thus, the phi ligand behaves simply as if it were another base pair in the helix.

The molecules described thus far represent several approaches to target DNA with coordination complexes. Moving forward, however, it becomes interesting not only to target DNA, but to target DNA in a manner that is relevant in the context of therapeutics or diagnostics. Furthermore, this targeting should be selective towards a biomarker of cancer, so as to avoid off-target damage that is often seen with traditional DNA-binding therapeutics, such as cisplatin.[17] Even the most selective complex described here, Δ-α-[Rh[(*R,R*)-Me_2trien]phi]$^{3+}$, serves merely as a proof-of-concept molecule since its target, 5'-TGCA-3' DNA, is not specifically implicated in any disease. With this considered, it becomes the task of the researcher not only to target DNA, but to identify and target DNA biomarkers that are unique to disease.

1.2 Rhodium Metalloinsertors as Probes for DNA Mismatches

The Barton laboratory has considered that potential targets for the design of new complexes might include sites of DNA damage or DNA lesions, which can be caused by both endogenous and exogenous sources such as replication errors or interactions with reactive oxygen species.[18,19] Since the genomic integrity of DNA is essential to mutation-free replication, cells usually have

several mechanisms to repair these types of DNA insults.[20,21,22] One such repair mechanism, mismatch repair (MMR), is responsible for the correction of DNA base pair mismatches, which, if left uncorrected, propagate into point mutations upon cellular replication (Figure 1.3).[23,24] Deficiencies in this repair pathway are associated with many types of cancer, including

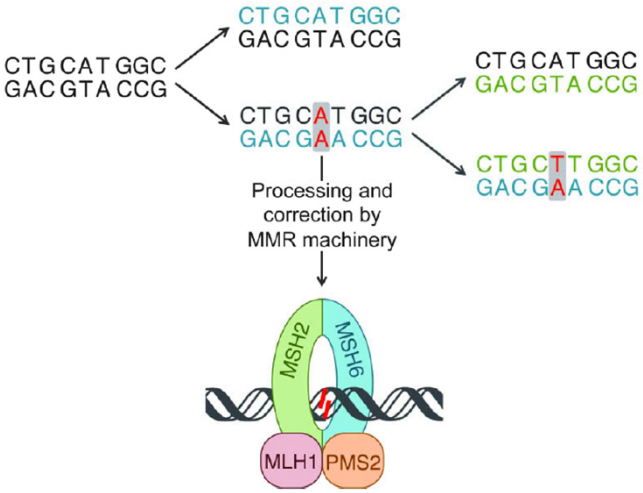

Figure 1.3. Cartoon of the mismatch repair (MMR) machinery. A replication error can result in an AA mismatch (red), which is identified and corrected by the MMR machinery (bottom). However, if the AA mismatch is not processed correctly, a subsequent iteration of replication will result in a TA mutation (red). Reprinted with permission from ref. 23, © 2016 Elsevier B.V.

tumorigenesis in up to 75% of individuals with Lynch syndrome (a genetic condition involving MMR deficiencies) and up to 20% of all solid tumors.[25,26] Additionally, cancers featuring microsatellite instabilities (MSI) are associated with resistance to many first-line cancer treatments, such as cisplatin and alkylating agents.[27,28] As such, MMR deficiencies and the associated increase in uncorrected DNA base pair mismatches represent a promising target for therapeutic and diagnostic design.

The first example of a small transition metal complex capable of selectively targeting a DNA base pair mismatch came in 1997 with the development of a unique rhodium complex, $[Rh(bpy)_2(chrysi)]^{3+}$ (chrysi = 5,6-chrysenequinone diimine) (Figure 1.4).[29] $[Rh(bpy)_2(chrysi)]^{3+}$

was inspired by complexes such as $[Rh(phen)_2(phi)]^{3+}$ and $[Rh(phi)_2(bpy)]^{3+}$, which exploit inert, redox capable metal centers that allow them to cleave DNA upon irradiation with UV-light.[30,31] To impart mismatch selectivity upon this family of complexes, the phi ligand framework was expanded upon with an additional phenyl ring to generate the chrysi ligand. At 11.3 Å, the chrysi ligand is about 2.1 Å wider than phi and about 0.5 Å wider than a well-matched base pair, making intercalation a less favorable binding possibility due to steric clashing between the ligand and the sugar-phosphate backbone (Figure 1.4). Instead, it was hypothesized that rhodium complexes containing this bulky ligand would preferentially interact with DNA at thermodynamically destabilized sites, such as mismatches and abasic sites, which may be better able to accommodate the expansive ligand.

As predicted, $[Rh(bpy)_2(chrysi)]^{3+}$ was shown to photocleave DNA in a surprisingly selective and robust manner. Initial experiments revealed the rhodium complex could photocleave mismatches of all identities, and that the extent of photocleavage (and therefore the level of detection) was dependent primarily on the thermodynamic destabilization of the targeted mismatch.[32] Overall, it was found that 80% of mismatches in all possible sequence contexts (as well as thermodynamically destabilized abasic sites and single base bulges) were detected by $[Rh(bpy)_2(chrysi)]^{3+}$.[33,34] Guanine-containing mismatches are frequently undetected by $[Rh(bpy)_2(chrysi)]^{3+}$ due to their low destabilization; they are in fact quite similar to well-matched base pairs. Remarkably, in binding a highly destabilized site, such as a CC mismatch, high selectivity of the Rh complex is maintained even in a large 2725 base pair linearized plasmid containing only a single CC mismatch: incubation of $[Rh(bpy)_2(chrysi)]^{3+}$ with this plasmid produced discrete cleavage products that corresponded exclusively with cleavage at the mismatched site.[33] In comparison, no photocleavage was observed in an analogous well-matched

plasmid.

These early studies showed that $[Rh(bpy)_2(chrysi)]^{3+}$ was a promising answer to DNA mismatch targeting, but it was not fully understood *how* $[Rh(bpy)_2(chrysi)]^{3+}$ targeted mismatches until Δ-$[Rh(bpy)_2(chrysi)]^{3+}$ was co-crystallized with DNA containing an AC mismatch (Figure 1.4).[35] The crystal structure revealed that the rhodium complex did not bind DNA mismatches *via* intercalation, but instead bound DNA through insertion. This distinct binding mode was initially proposed by L.S. Lerman in 1961, but the binding mode had not been directly observed until this structure.[36] Accordingly, $[Rh(bpy)_2(chrysi)]^{3+}$ and future complexes became known as rhodium metalloinsertors and their binding mode as metalloinsertion.

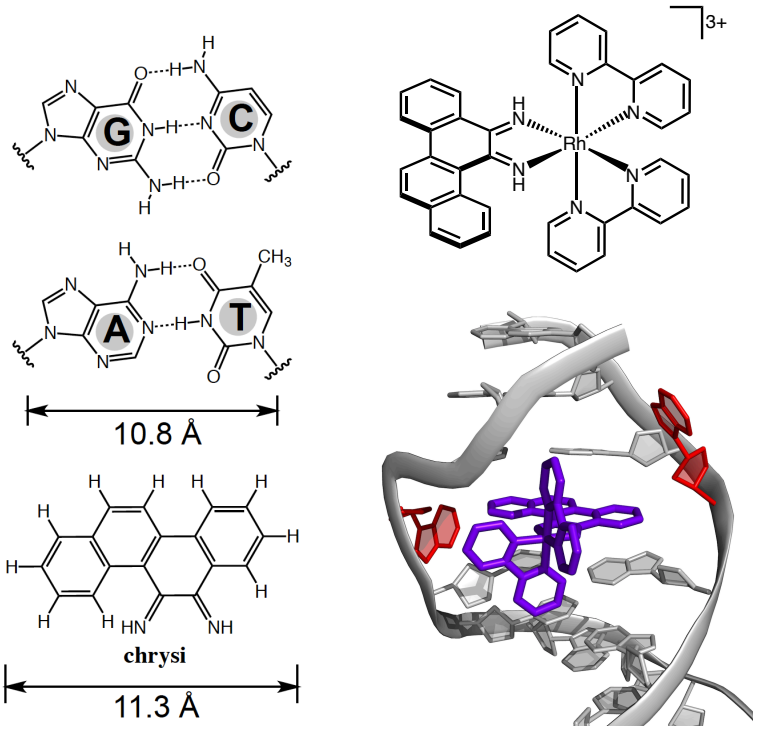

Figure 1.4. (*Left*) The chrysi ligand is 0.5 Å wider than a well-matched base pair, making intercalation unfavorable. (*Upper right)* The structure of Δ-$[Rh(bpy)_2(chrysi)]^{3+}$. (*Lower Right*) A crystal structure revealed that Δ-$Rh(bpy)_2(chrysi)]^{3+}$ (purple) binds to a mismatch *via* metalloinsertion, in which the complex inserts from the minor groove and extrudes the mismatched bases (red) (figure created from PDB structure 3GSK).

In metalloinsertion, the chrysi ligand of the Δ-enantiomer *inserts* into the DNA helix from the minor groove at a mismatch site by displacing and ejecting the mismatched bases (Figure 1.4). This insertion allows the chrysi ligand to replace the destabilized DNA mispair and π-stack with the neighboring well-matched bases. Unlike intercalation, there is little unwinding of the DNA nor a rise in the DNA helix. This is a highly stable binding interaction, with most metalloinsertors having binding affinities on the order of 10^6 to 10^7 M^{-1}. Moreover, for most metalloinsertors, the binding is highly enantioselective; only the Δ-isomer can fit into the right-handed minor groove. The features of this unique binding mode also clarified the thermodynamic dependence of metalloinsertion on mismatch stability – proper hydrogen bond contacts between well-matched base pairs are too stabilizing to permit insertion of the chrysi ligand. This binding mode was later verified with additional crystal structures using AA-mismatched DNA as well as an NMR-solution structure using CC-mismatched DNA.[37,38] In particular, the NMR structure confirmed that the crystallographically observed metalloinsertion was not simply an artifact of crystal packing forces.

1.3 Rhodium Metalloinsertors as Chemotherapeutics

After nearly a decade of *in vitro* work elucidating the binding properties and selectivity of rhodium metalloinsertors, it became clear that these complexes could find even greater significance as potential therapeutics. As discussed previously, deficiencies in MMR are associated with some cancers and can lead to an increase in persistent DNA base pair mismatches.[39] However, due to the high fidelity and proofreading abilities of DNA polymerases, even MMR-deficient cells have extremely few mismatches. Since there are so few mismatch targets, it is necessary that a therapeutically relevant small molecule should have a generic affinity for all mismatches, not just certain mispairs. As such, rhodium metalloinsertors, which have high selectivity and bind an abundance of mismatches in various sequence contexts, are an ideal

therapeutic scaffold for MMR-deficient cancers.

To test if *in vitro* results would translate to *ex vivo* cellular models, rhodium metalloinsertors were tested *via* cell proliferation and cell viability assays in isogenic MMR-proficient and deficient cell lines. Remarkably, $[Rh(bpy)_2(chrysi)]^{3+}$ preferentially targets MMR-deficient cells over their MMR-proficient counterparts.[40] Since the discovery of this unique biological selectivity, several generations of rhodium metalloinsertors have been developed to further improve this selective biological activity.[41,42] One metalloinsertor in particular, $[Rh(chrysi)(phen)(PPO)]^{2+}$ (PPO = 2-(pyridine-2-yl)propan-2-ol), is highly potent and selective towards MMR-deficient cancer cells compared to MMR-proficient cells.[43] This compound has been shown to inhibit DNA synthesis and induce cell death by necrosis in the MMR-deficient HCT116O cell line.[43] Recent results have demonstrated that Rh-PPO activates a DNA damage response that leads to cell death.[44] It is proposed that upon binding to a DNA mismatch *via* metalloinsertion, an event which extrudes the mismatched bases from the helix, a novel lesion is created that is recognized by the cellular DNA damage response, and an inability to repair this lesion results in cell death. Thus, rhodium metalloinsertors hold great promise as chemotherapeutic agents directed towards mismatch repair-deficient cancers.

1.4 Luminescent Probes for DNA Mismatches

In addition to developing octahedral rhodium complexes as potential therapeutics targeted to mismatches, there is also considerable interest in designing mismatch-specific luminescent small molecules to serve as diagnostic probes for the early detection of MMR-deficient cancers, which may represent early diagnostics of carcinogenesis. While rhodium metalloinsertors are non-luminescent upon excitation, one avenue for developing a diagnostic probe for DNA mismatches is to fluorescently tag a rhodium metalloinsertor. In one design, a negatively charged fluorophore,

Oregon Green 514, was tethered to a positively charged rhodium metalloinsertor to generate the conjugate RhOG (Figure 1.5).[45] The motivation behind this design was that the fluorescence of the dye would be quenched in free solution, or in the presence of well-matched DNA, due to ion-pairing with the rhodium moiety. However, if a mismatch were present, the rhodium would undergo metalloinsertion, causing the negatively charged dye to be repelled by the sugar-phosphate DNA backbone, resulting in "turn-on" fluorescence. As expected, the fluorescence of the RhOG conjugate is considerably quenched relative to free Oregon Green, and compared to an equimolar solution of free Oregon Green and free metalloinsertor. Importantly, in fluorescence titrations of the conjugate with well-matched and CC-mismatched 17-mer oligonucleotides, the conjugate exhibits a 3.2-fold brighter emission intensity in the presence of the sequence containing the mismatch. Additionally, PAGE experiments utilizing ^{32}P-labeled oligonucleotides revealed

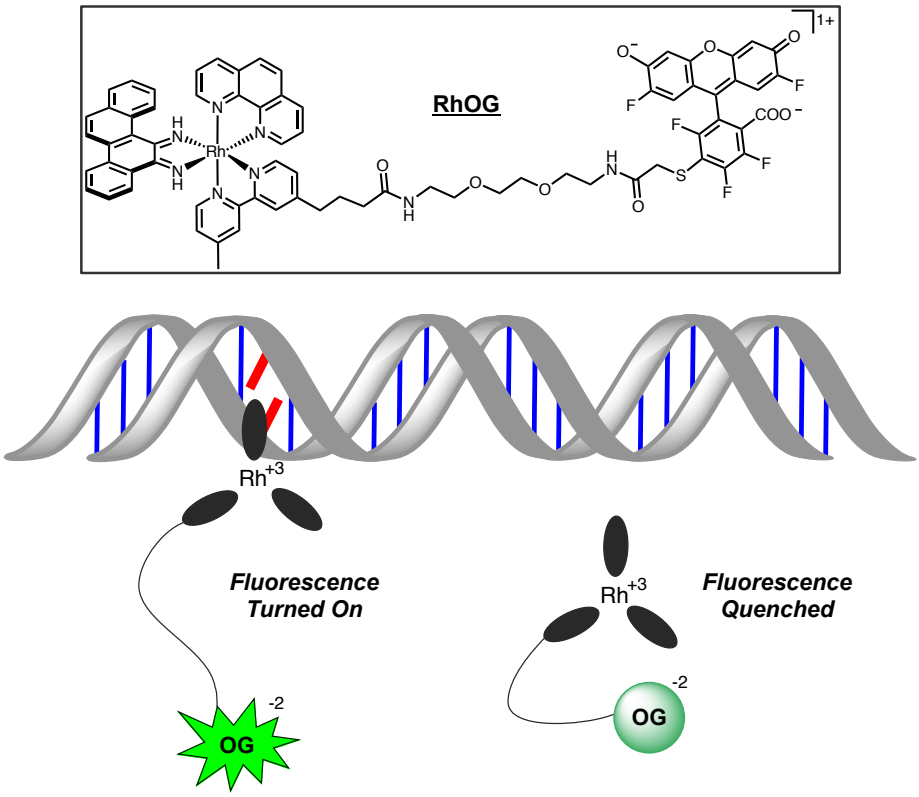

Figure 1.5. Illustration of the design behind the rhodium metalloinsertor-Oregon Green conjugate (RhOG).

specific photocleavage at the CC mismatch. However, one drawback of this RhOG conjugate is that even in the presence of the mismatched sequence, the maximum fluorescence reached by the fluorophore was only 6% that of free Oregon Green; rhodium quenching even in the extended form could not be eliminated.

More recently, another rhodium-fluorophore conjugate has been studied, in which a positively charged cyanine dye was tethered to a metalloinsertor scaffold *via* a PEG linker.[46] In this design, the cyanine dye was chosen because it weakly fluoresces in aqueous solution but emits quite brightly upon intercalating into DNA. The rationale behind this conjugate design was that in the presence of well-matched DNA, the rhodium metalloinsertor would have a low affinity for the duplex, and thus only a weak emission from the conjugate would be observed in solution. Conversely, the metalloinsertor would readily bind to a mismatch site, thus permitting the cyanine dye to intercalate between the base pairs of the duplex, yielding a significant increase in fluorescence. Indeed, upon the addition of well-matched DNA, no change in the conjugate's cyanine fluorescence is seen; however, upon the addition of a 27-mer duplex containing a single CC mismatch, a substantial increase in fluorescence intensity is observed.

While conjugated organic fluorophores certainly play an important role in the context of DNA detection, the use of a singular transition metal center that is inherently luminescent is highly attractive owing to synthetic accessibility and the ability to study longer-lived emission lifetimes *via* time-resolved spectroscopy. In particular, ruthenium(II) polypyridyl complexes possess an intense metal-to-ligand charge transfer (MLCT) transition which, upon excitation, yields a bright, long-lived emission in the visible region. Like the rhodium complexes discussed in this chapter, ruthenium(II) polypyridyl compounds are coordinatively saturated, making them inert to ligand substitution and stable in aqueous solutions.

The ensuing chapters of this thesis discuss recent progress that has been made towards developing mismatch-specific luminescent ruthenium(II) complexes. Mismatch-targeting by small molecules represents a new strategy for therapeutic and diagnostic design, one based upon the application of octahedral metal complexes targeted to thermodynamically destabilized DNA mismatches through non-covalent interactions.

References

1. Turro, N.J.; Barton, J.K.; Tomalia, D. A. *Acc. Chem. Res.* **1991**, *24*, 332–340.

2. Pyle, A. M.; Rehmann, J. P.; Meshoyrer, R.; Kumar, C. V.; Turro, N. J.; Barton, J. K. *J. Am. Chem. Soc.* **1989**, *111*, 3051–3058.

3. Barton, J. K.; Goldberg, J. M.; Kumar, C. V.; Turro, N. J. *J. Am. Chem. Soc.* **1986**, *108*, 2081–2088.

4. Kumar, C. V.; Barton, J. K.; Turro, N. J. *J. Am. Chem. Soc.* **1985**, *107*, 5518–5523.

5. Thederahn, T. B.; Kuwabara, M. D.; Larsen, T. A.; Sigman, D. S. *J. Am. Chem. Soc.* **1989**, *111*, 4941–4946.

6. Sigman, D. S.; Mazumder, A.; Perrin, D. M. *Curr. Opin. Chem. Biol.* **1993**, *93*, 2295–2316.

7. Sigman, D. S.; Chen, C. B. *Annu. Rev. Biochem.* **1990**, *59*, 207–236.

8. Barton, J. K. *Science* **1986**, *233*, 727–735.

9. Erkkila, K. E.; Odom, D. T.; Barton, J. K. *Chem. Rev.* **1999**, *99*, 2777–2796.

10. Jennette, K. W.; Lippard, S. J.; Vassiliades, G. A.; Bauer, W. R. *Proc. Natl. Acad. Sci.* **1974**, *71*, 3839–3843.

11. Bond, P. J.; Langridge, R.; Jennette, K. W.; Lippard, S. J. *Proc. Natl. Acad. Sci.* **1975**, *72*, 4825–4829.

12. Friedman, A. E.; Chambron, J.-C.; Sauvage, J.-P.; Turro, N. J.; Barton, J. K. *J. Am. Chem. Soc.* **1990**, *112*, 4960–4962.

13. Holmlin, R. E.; Stemp, E. D.; Barton, J. K. *Inorg. Chem.* **1998**, *37*, 29–34.

14. Sitlani, A.; Long, E. C.; Pyle, A. M.; Barton, J. K. *J. Am. Chem. Soc.* **1992**, *114*, 2303–2312.

15. Krotz, A. H.; Hudson, B. P.; Barton, J. K. *J. Am. Chem. Soc.* **1993**, *115*, 12577–12578.

16. Kielkopf, C. L.; Erkkila, K. E.; Hudson, B. P.; Barton, J. K.; Rees, D. C. *Nat. Struct. Biol.* **2000**, *7*, 117–121.

17. Shoshan, M. C.; Linder, S. *Expert Opin. Drug Metab. Toxicol.* **2008**, *4*, 273–280.

18. Friedberg, E. C.; McDaniel, L. D.; Schultz, R. a. *Curr. Opin. Genet. Dev.* **2004**, *14*, 5–10.

19. Jackson, A. L.; Loeb, L. A. *Mutat. Res.* **2001**, *477*, 7–21.

20. Sancar, A.; Lindsey-Boltz, L. A.; Unsal-Kacmaz, K.; Linn, S. *Annu. Rev. Biochem.* **2004**, *73*, 39–85.

21. Jackson, S.; Bartek, J. *Nature* **2009**, *461*, 1071–1078.

22. Helleday, T.; Petermann, E.; Lundin, C.; Hodgson, B.; Sharma, R. A. *Nat. Rev. Cancer* **2008**, *8*, 193–204.

23. Boyle, K.M.; Barton, J.K. *Inorg. Chim. Acta.* **2016**, *452*, 3-11.

24. Glaab, W. E.; Tindall, K. R. *Carcinogenesis* **1997**, *18*, 1–8.

25. Barrow, E.; Hill, J.; Gareth Evans, D. *Fam. Cancer* **2013**, *12*, 229–240.

26. Arzimanoglou, I. I.; Gilbert, F.; Barber, H. R. *Cancer* **1998**, *82*, 1808–1820.

27. Fink, D.; Aebi, S.; Howell, S. B. *Clin. Cancer Res.* **1998**, *4*, 1–6.

28. Martin, L. P.; Hamilton, T. C.; Schilder, R. J. *Clin. Cancer Res.* **2008**, *14*, 1291–1295.

29. Jackson, B. A.; Barton, J. K. *J. Am. Chem. Soc.* **1997**, *119*, 12986–12987.

30. Uchida, K.; Pyle, A. M.; Morii, T.; Barton, J. K. *Nucleic Acids Res.* **1989**, *17*, 10259–10279.

31. Pyle, A. M.; Chiang, M. Y.; Barton, J. K. *Inorg. Chem.* **1990**, *29*, 4487–4495.

32. Jackson, B. A.; Barton, J. K. *Biochemistry* **2000**, *39*, 6176–6182.

33. Jackson, B. A.; Alekseyev, V. Y.; Barton, J. K. *Biochemistry* **1999**, *38*, 4655–4662.

34. Zeglis, B. M.; Boland, J. A.; Barton, J. K. *J. Am. Chem. Soc.* **2008**, *130*, 7530–7531.

35. Pierre, V. C.; Kaiser, J. T.; Barton, J. K. *Proc. Natl. Acad. Sci.* **2007**, *104*, 429–434.

36. Lerman, L. S. S. *J. Mol. Biol.* **1961**, *3*, 18–30.

37. Zeglis, B. M.; Pierre, V. C.; Kaiser, J. T.; Barton, J. K. *Biochemistry* **2009**, *48*, 4247–4253.

38. Cordier, C.; Pierre, V. C.; Barton, J. K. *J. Am. Chem. Soc.* **2007**, *129*, 12287–12295.

39. Kunkel, T. A.; Erie, D. A. *Annu. Rev. Genet.* **2015**, *49*, 291–313.

40. Hart, J. R.; Glebov, O.; Ernst, R. J.; Kirsch, I. R.; Barton, J. K. *Proc. Natl. Acad. Sci. U. S. A.* **2006**, *103*, 15359–15363.

41. Ernst, R.J.; Komor, A.C.; Barton, J.K. *Biochemistry* **2011**, *50*, 10919-10928.

42. Komor, A.C.; Schneider, C.J.; Weidmann, A.G.; Barton, J.K. *J. Am. Chem. Soc.* **2012**, *134*, 19223-19233.

43. Komor, A.C.; Barton, J.K. *J. Am. Chem. Soc.* **2014**, *136*, 14160-14172.

44. Bailis, J.M.; Weidmann, A.G.; Barton, J.K. *Submitted*.

45. Zeglis, B. M.; Barton, J. K. *J. Am. Chem. Soc.* **2006**, *128*, 5654–5655.

46. Nano, A.; Barton, J. K. *Manuscript in preparation*.

Chapter 2

$[Ru(Me_4phen)_2(dppz)]^{2+}$, a Light Switch for DNA Mismatches

Adapted from: Boynton, A.N.; Marcelis, L.; Barton, J.K. *J. Am. Chem. Soc.* **2016**, *138*, 5020-5023. L. Marcelis calculated $[Ru(Me_4phen)_2(dppz)]^{2+}$ binding affinities through titration curve-fitting analysis and assisted in excited-state lifetime measurements.

2.1 Introduction

The DNA mismatch repair (MMR) pathway identifies and corrects base pair mismatches that can occur during replication as a result of failed proofreading by polymerases.[1] If left uncorrected, DNA base pair mismatches lead to mutations in subsequent rounds of replication.[2,3] Deficiencies in the MMR protein machinery are associated with several forms of cancer, including 80% of hereditary non-polyposis colon cancers and 15-20% of all solid tumors.[4,5] Furthermore, commonly used chemotherapeutics such as cisplatin and DNA alkylating agents exhibit a decreased effectiveness towards MMR-deficient cancers.[6,7]

The design of small molecules that target DNA mismatches holds promise for chemotherapeutic and diagnostic applications. As discussed in Chapter 1, a class of octahedral rhodium complexes, bearing the sterically expansive chrysi ligand, bind DNA mismatches with high selectivity and exhibit preferential cytotoxicity towards MMR-deficient cancer cells.[8,9] These compounds bind to DNA through metalloinsertion, in which the bulky chrysi ligand inserts into the duplex at the thermodynamically destabilized mismatch site, displacing the mismatched bases into the DNA groove.[10,11]

Luminescent reporters of mismatches may represent early diagnostics of carcinogenesis. In an effort to develop new selective, signal-on probes for DNA mismatches, we have focused our attention on derivatives of $[Ru(bpy)_2(dppz)]^{2+}$ (dppz = dipyridophenazine), which serve as molecular "light switches" for duplex DNA (Figure 2.1).[12] While these complexes do luminesce in organic, aprotic solvents such as acetonitrile, in aqueous solution, their luminescence is quenched due to hydrogen bonding between solvent water molecules and the phenazine nitrogen atoms of the dppz ligand. However, upon intercalating into well-matched duplex DNA, these compounds luminesce brightly owing to protection of the dppz ligand from the aqueous

environment.[13,14]

While $[Ru(bpy)_2(dppz)]^{2+}$ intercalates non-specifically into duplex DNA, the complex luminesces more brightly in the presence of a DNA mismatch relative to completely well-matched DNA (Figure 2.1).[15] A crystal structure of Δ-$[Ru(bpy)_2(dppz)]^{2+}$ bound to a 12-mer DNA oligonucleotide containing two AA mismatches was obtained at 0.92 Å resolution (Figure 2.1).[16] The asymmetric unit revealed five ruthenium complexes bound to the DNA duplex. In this

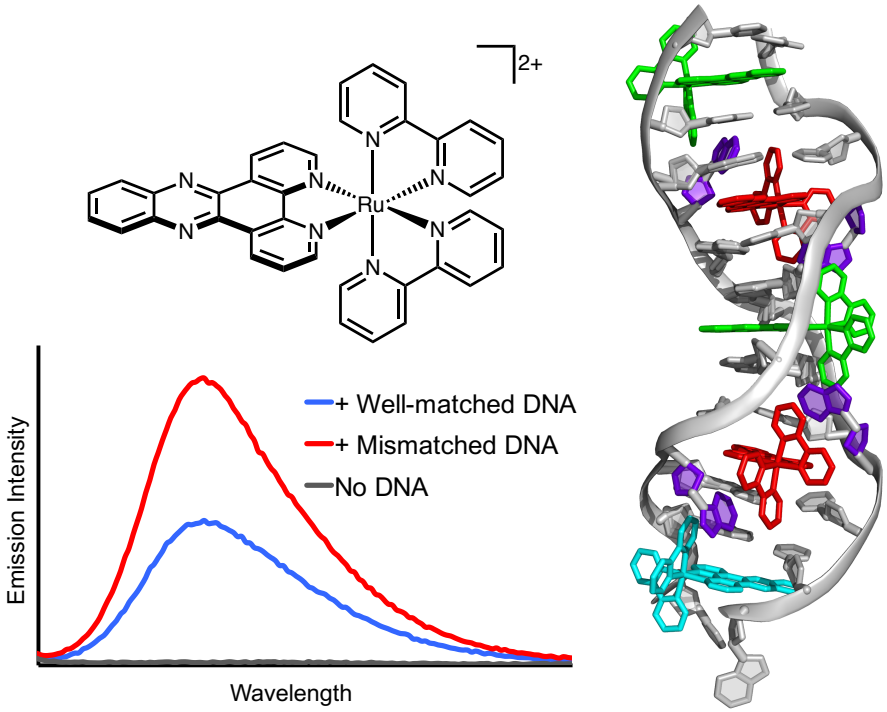

Figure 2.1. *(Left)* $[Ru(bpy)_2(dppz)]^{2+}$ is a molecular "light switch" for duplex DNA in aqueous solution, and luminesces more brightly in the presence of DNA containing a mismatch. (*Right*) Δ-$[Ru(bpy)_2(dppz)]^{2+}$ was co-crystallized with a short DNA duplex containing two AA mismatches (mismatched base pairs are highlighted in purple), and three binding modes of the complex were observed: metalloinsertion (red) at the mismatched sites, intercalation (green) at well-matched sites, and end-capping between two duplexes (cyan). Figure created from PDB structure 4E1U.

structure, the complex was bound to the DNA in three distinct binding modes: (i) intercalation at well-matched sites, (ii) metalloinsertion at the mismatched sites, and (iii) end-capping between two duplexes. At the mismatched sites, the complex binds from the minor groove and inserts deeply into the base stack, completely extruding the mismatched adenosines. Interestingly, at both

AA sites, each adenosine is displaced back towards the minor groove and stacks with the bpy ancillary ligands of the ruthenium complex. Furthermore, because the dppz ligand is relatively narrow and also symmetric, a minimal widening of the DNA minor groove is observed. This crystal structure also illustrates two Δ-$[Ru(bpy)_2(dppz)]^{2+}$ molecules bound *via* intercalation at well-matched sites. Both complexes are intercalated in the minor groove, an observation that differs from what is suggested by solution-phase experiments, namely that $[Ru(bpy)_2(dppz)]^{2+}$ intercalates at well matched sites *via* the major groove.[17,18,19] However, in this structure, there are clear stacking interactions between the bpy ligands of the intercalated complexes and the neighboring mismatched adenosines, interactions that ostensibly stabilize the complexes in the minor groove at well-matched sites. Thus, these results suggest that there is likely a relatively small energetic difference when comparing intercalation from the minor and major groove for $[Ru(bpy)_2(dppz)]^{2+}$.

Despite exhibiting a 1.5 to 2-fold luminescence enhancement in the presence of a DNA defect compared to fully well-matched DNA, $[Ru(bpy)_2(dppz)]^{2+}$ is not mismatch-specific. A mismatch-specific luminescent compound could be particularly valuable in the context of developing diagnostic probes for detecting deficiencies in mismatch repair. In this chapter, we investigate the role of ancillary ligand modification for achieving mismatch specificity. In particular, we rationalized that incorporating methyl groups on the ancillary ligands of $[Ru(phen)_2(dppz)]^{2+}$ and $[Ru(bpy)_2(dppz)]^{2+}$ would disfavor binding to well-matched sites as a result of steric clashing between the ancillary ligands and the DNA backbone. Moreover, bulkier ancillary ligands would disfavor deep intercalation of dppz at well-matched sites and instead favor shielding of the phenazine nitrogen atoms with insertion at a mismatch. Inspiration for this rationale arose from two prior reports in the Barton group which described incorporating methyl

substituents into the phenanthroline ligands of $[Ru(phen)_2(dppz)]^{2+}$ and $[Os(phen)_2(dppz)]^{2+}$. C. Puckett synthesized the methyl-substituted complex $[Ru(Me_4phen)_2(dppz)]^{2+}$ (Me_4phen = 3,4,7,8-tetramethyl-1,10-phenanthroline, Figure 2.2) and observed that it displays a significant reduction in steady-state emission intensity relative to $[Ru(phen)_2(dppz)]^{2+}$ with calf thymus DNA.[20] E. Holmlin et al. synthesized a series of $[Os(L)_2(dppz)]^{2+}$ complexes – which also function as DNA light switches – bearing various ancillary ligand modifications.[21] Of particular interest is the observation that $[Os(4,7\text{-dmp})_2(Me_2\text{-dppz})]^{2+}$ (4,7-dmp = 4,7-dimethylphenanthroline; Me_2-dppz = 7,8-dimethyldipyridophenazine) possesses a significantly reduced emission intensity with DNA compared to the parent $[Os(phen)_2(Me_2\text{-dppz})]^{2+}$ complex. This was attributed to two mechanisms working together: first, the methyl groups at the 4-position of phenanthroline likely prevent full intercalation of the complex due to steric interactions with the DNA backbone. Second, it was found that the 4,7-complex is more sensitive to quenching by water due to an increase in excited-state pK_a at the phenazine nitrogen atoms. The methyl groups at the 4,7 positions stabilize the Os(III) oxidation state, meaning that an excited-state reduction of the phenazine portion of the dppz ligand is more favorable. Mismatch binding was not investigated in these prior reports; however, based on the evidence that appending simple methyl groups onto the ancillary ligands discourages intercalation at well-matched sites in duplex DNA, we believed that $[Ru(Me_4phen)_2(dppz)]^{2+}$ might favor metalloinsertion at mismatched base pairs.

2.2 Experimental Protocols

2.2.1. Materials

All chemicals and starting materials were purchased from commercial vendors and used as received. Dipyrido[3,2-*a*:2',3'-*c*]phenazine (dppz) was prepared according to the literature.[22] UV-

Visible spectra were recorded on a Beckman DU 7400 UV-Visible spectrophotometer (Beckman Coulter). Oligonucleotides were synthesized using standard phosphoramidite chemistry at Integrated DNA Technologies (Coralville, IA) and purified by HPLC using a C_{18} reverse-phase column (Varian, Inc.) on a Hewlett-Packard 1100 HPLC. The copper complex $Cu(phen)_2^{2+}$ was generated *in situ* by combining $CuCl_2$ with phen ligand in a 1:3 ratio.

2.2.2. Synthesis

$Ru(Me_4phen)_2Cl_2$. Following a modified literature report,[23] $RuCl_3 \bullet nH_2O$ (0.217 g, 0.830 mmol), 3,4,7,8-tetramethyl-1,10-phenanthroline (0.494 g, 2.09 mmol), and LiCl (0.298 g, 7.03 mmol) were combined in a Schlenk flask under argon. The contents were dissolved in anhydrous DMF (5 mL), and the solution was heated to 140°C and stirred for 4 h while being protected from light. The contents were cooled to room temperature, diluted with acetone (20 mL), and stored in the freezer overnight. The black precipitate was collected by vacuum filtration, washed three times with 5 mL portions of H_2O and three times with 5 mL portions of diethyl ether, and dried. The product was used subsequently without further purification (0.495 g, 73%).

$Ru(Me_2bpy)_2Cl_2$. $RuCl_3 \bullet nH_2O$ (0.281 g, 1.07 mmol) was reacted with 5,5'-dimethyl-2,2'-dipyridine (0.500 g, 2.71 mmol) and LiCl (0.385 g, 9.08 mmol) in DMF (15 mL) under the conditions described for the synthesis of $Ru(Me_4phen)_2Cl_2$. The product was isolated and used subsequently without further purification (0.304 g, 63%).

$[Ru(Me_4phen)_2(dppz)]X_2$ ($X = PF_6$ or Cl). Dppz ligand (0.025 g, 0.089 mmol) was combined with $Ru(Me_4phen)_2Cl_2$ (0.057 g, 0.089 mmol) in ethylene glycol (8 mL) and heated to 130°C and stirred for 5 h. The reaction was cooled to room temperature and diluted with H_2O (8 mL). Excess NH_4PF_6 was added to precipitate the product, which was collected by filtration, washed copiously with H_2O and diethyl ether, and dried. (0.084 g, 82%). ESI(+)MS (*m/z*): $[M/2]^+$

found 428.2. The complex was converted to its water-soluble Cl salt by anion exchange chromatography (Sephadex QAE) and further purified by preparative HPLC using an isocratic method of 65% MeOH and 35% H_2O (containing 0.1% TFA) over 60 min. ^{1}H NMR (500 MHz, DMSO-d_6) δ 9.58 (dd, *J* = 8.2, 1.3 Hz, 2H), 8.54 (dd, *J* = 6.3, 3.4 Hz, 2H), 8.52 (d, *J* = 0.9 Hz, 4H), 8.22 (dd, *J* = 6.6, 3.4 Hz, 2H), 8.13 (dd, *J* = 5.4, 1.3 Hz, 2H), 7.90 (m, 4H), 7.76 (s, 2H), 2.82 (d, *J* = 1.3 Hz, 12H), 2.27 (d, *J* = 3.7 Hz, 12H). The complex was again converted to its Cl salt by anion exchange chromatography to remove TFA anions present from the HPLC purification ($\varepsilon_{422\ nm}$ = 21,200 M^{-1} cm^{-1}).[20]

[Ru(Me$_2$bpy)$_2$(dppz)]X$_2$ (X = PF$_6$ or Cl). Dppz ligand (0.240 g, 0.851 mmol) was combined with $Ru(Me_2bpy)_2Cl_2$ (0.304 g, 0.563 mmol) in ethylene glycol and reacted as described for the Me_4phen complex, and the product was collected as its PF_6 salt (0.521 g, 89%). ESI(+)MS (*m/z*): $[M/2]^+$ found 376.2. The complex was converted to its water-soluble Cl salt by anion exchange chromatography (Sephadex QAE) and further purified by preparative HPLC using a gradient of H_2O (with 0.1% TFA) to CH_3CN over 60 min. ^{1}H NMR (500 MHz, DMSO-d_6) δ 9.62 (dd, *J* = 8.2, 1.3 Hz, 2H), 8.71 (d, *J* = 8.4 Hz, 2H), 8.67 (d, *J* = 8.4 Hz, 2H), 8.52 (m, 2H), 8.21 (m, 4H), 8.04 (m, 4H), 7.94 (dd, *J* = 8.4, 1.9 Hz, 2H), 7.54 (dt, *J* = 1.8, 0.8 Hz, 2H), 7.48 (dt, *J* = 1.4, 0.7 Hz, 2H), 2.26 (d, *J* = 0.7 Hz, 6H), 2.08 (d, *J* = 0.7 Hz, 6H). The complex was again converted to its Cl salt by anion exchange chromatography to remove TFA anions present from the HPLC purification.

2.2.3 [Ru(Me$_4$phen)$_2$(dppz)]$^{2+}$ Enantiomer Separation

Enantiomeric separations were performed using an Astec CYCLOBOND I 2000 DMP semi-preparative chiral HPLC column. Separation was achieved with an isocratic 60% acetonitrile/40% 0.1 M KPF_6 method over one hour. Following the preparative HPLC runs, the

fractions of each enantiomer were pooled and the solvent was evaporated. Each isomer was re-dissolved in a minimal volume of water/acetonitrile and run through a Sep-Pak C18 cartridge (Waters) to remove the potassium ions from the KPF_6. The isomers were then converted to their water-soluble Cl salts using Sephadex QAE. Isomers were confirmed by circular dichroism and assigned as reported.[16,24] The lambda (Λ) isomer elutes first, followed by the delta (Δ).

2.2.4. Luminescence Measurements

Steady-State Luminescence. Luminescence spectra were recorded on an ISS-K2 spectrofluorometer at 25°C. $[Ru(Me_4phen)_2(dppz)]^{2+}$ and $[Ru(Me_2bpy)_2(dppz)]^{2+}$ were excited at 440 nm, and emission spectra were integrated from 564-820 nm. The Cl salts of the complexes were used for all experiments. In all cases, [DNA] is defined as the concentration of full sequence.

Time-Resolved Luminescence. Time-resolved spectroscopic measurements were carried out at the Beckman Institute Laser Resource Center (BILRC) and were conducted using instrumentation that has been described.[25] Briefly, a 460 nm light produced by OPO pumped with a 10 Hz, Qswitched Nd:YAG laser (Spectra-Physics Quanta-Ray PRO-Series) was used as an excitation source (pump pulse duration ≈8 ns). The emitted light was detected at 650 nm with a photomultiplier tube (Hamamatsu R928) following wavelength selection by a double monochromator (Instruments SA DH-10). Scattered laser light was removed from the detectors using suitable filters. The samples were held in 1 cm path length quartz cuvettes (Starna) equipped with stir bars and irradiated at 460 nm with 500−1000 laser pulses at 3 mJ/pulse. Kinetic traces were fit to exponential equations of the form $I(t) = a_0 + \Sigma\ a_n \exp(-t/\tau_n)$, where $I(t)$ is the signal intensity as a function of time, a_0 is the intensity at long time, a_n is a pre-exponential factor that represents the relative contribution from the nth component to the trace, and τ_n is the lifetime of the nth component, convoluted with a Gaussian function to take into account the Instrument

Response Function (fwmh = 8ns). The errors are evaluated to be equal to 5%, but the incertitude on the short component (associated with complexes bond to well-matched DNA, *i.e.* 33-35 ns) being close to the IRF time characteristic is subject to a greater error (+/- 8 ns).

2.3 Results and Discussion

2.3.1. Luminescence of $[Ru(Me_4phen)_2(dppz)]^{2+}$ with 27-mer DNA Duplexes

As expected, $[Ru(Me_4phen)_2(dppz)]^{2+}$ is not luminescent in aqueous solution upon excitation at 440 nm (MLCT transition). We studied the steady-state luminescence response of the complex towards a well-matched 27-mer DNA duplex and the analogous DNA duplex containing a single CC mismatch (Figure 2.2). Indeed, the ruthenium complex acts as a DNA light switch. Excitation in the presence of either duplex yields emission spectra centered at 640-650 nm (Figure 2.2). Importantly, we observe appreciable luminescence enhancement with the 27-mer containing the single CC mismatch in comparison to the same 27-mer sequence lacking a mismatch. From DNA titrations of $[Ru(Me_4phen)_2(dppz)]^{2+}$ (Appendix A.1), we calculate binding affinities of 6.8 x 10^4 M^{-1} and 1.8 x 10^6 M^{-1} for well-matched and mismatched sites, respectively (Table 2.1). Given the 26-fold difference in binding affinities, we can conclude that the complex is quite selective for binding to the single base mismatch.

To determine whether the differential luminescence observed in the steady-state experiments is due not only to a higher binding affinity towards the mismatch but also to an increase in relative emissivity, we measured excited state emission lifetimes of $[Ru(Me_4phen)_2(dppz)]^{2+}$ with the well-matched and mismatched 27-mer (Table 2.1). In the presence of the well-matched sequence, a short emission lifetime equal to 35 ns is detected.

5'-GAC CAG CTT ATC A**C**C CCT AGA TAA GCG-3'
WM: 3'-CTG GTC GAA TAG T**G**G GGA TCT ATT CGC-5'
MM: 3'-CTG GTC GAA TAG T**C**G GGA TCT ATT CGC-5'

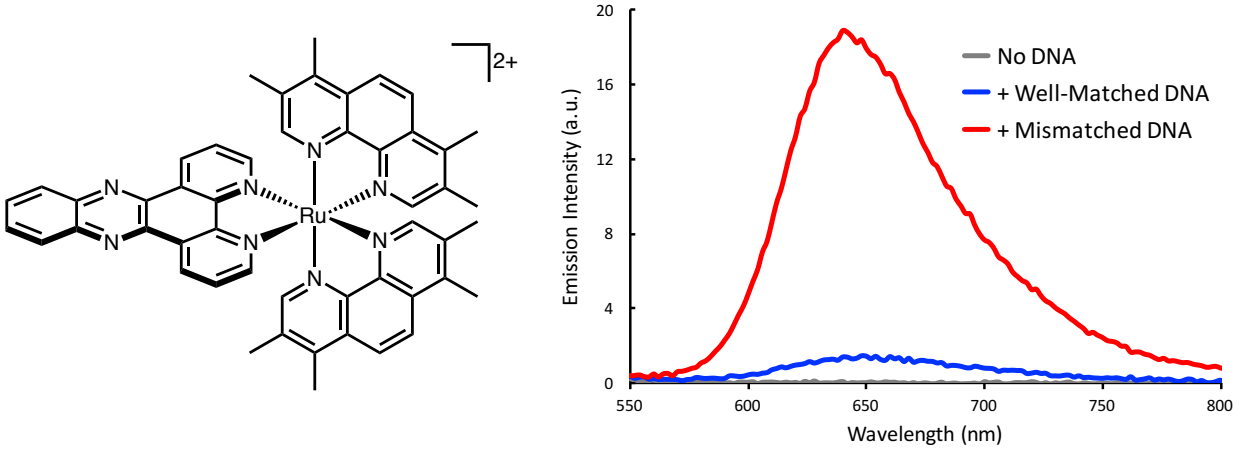

Figure 2.2. (*Top*) DNA sequences used in this study. (*Bottom left*) Structure of $[Ru(Me_4phen)_2(dppz)]^{2+}$. (*Bottom right*) Steady-state luminescence spectra of *rac*-$[Ru(Me_4phen)_2(dppz)]^{2+}$ with no DNA (gray), well-matched (blue) duplex, and with the duplex containing a single CC mismatch (red). Samples were prepared in 5 mM tris, 200 mM NaCl, pH 7.5. [Ru] = 2 μM, [DNA duplex] = 2 μM, λ_{ex} = 440 nm.

However, with the mismatched duplex, the luminescence decays as a bi-exponential function with components equal to 33 ns and 160 ns. We attribute this additional longer lifetime component, 81% of the overall decay, to the population of excited complex bound to the mismatch. This longer-lived component is similar in luminescence lifetime of the complex in dry acetonitrile (Table 2.1). This similarity in excited state lifetime illustrates how effectively the inserted complex is protected from quenching within its mismatched binding site.

Table 2.1. Binding Affinities and Emission Lifetimes of *rac*-$[Ru(Me_4phen)_2(dppz)]^{2+}$ with Well-Matched and Mismatched DNA Duplexes

	Well-matched DNA	Mismatched DNA	CH_3CN
K_a (M^{-1})[a]	6.8 x 10^4	1.8 x 10^6	-
Emission Lifetime (ns)[b]	35	33 (19%), 160 (81%)	189[c]

[a] Titrations were performed with DNA sequences shown in Figure 2.2 in 5 mM tris, 200 mM NaCl, pH 7.5. [Ru] = 2 μM, λ_{ex} = 440 nm. The binding affinity is expressed per binding site. [b] Samples containing 4 μM Ru and 4 μM DNA were prepared in 5 mM tris, 200 mM NaCl, pH 7.5 using DNA sequences shown in Figure 2.2. λ_{ex} = 460 nm, λ_{em} = 650 nm. Percentages reflect relative contributions of each lifetime to the overall decay. [c] Obtained in degassed, anhydrous acetonitrile.

2.3.2 $[Ru(Me_4phen)_2(dppz)]^{2+}$ Evidence for Metalloinsertion

We also investigated whether $[Ru(Me_4phen)_2(dppz)]^{2+}$ is capable of probing other types of DNA base mismatches using hairpin oligonucleotides (Figure 2.3) containing a variable base pair (XY). The emission intensity of the complex with the well-matched GC and AT sequences is compared to GG, AA, CT, TT, CA, and CC mismatches, as well as an abasic site (CR). The greatest emission enhancement occurs in the presence of the most thermodynamically destabilized mismatch, CC, followed by CA. We detect negligible enhancement with the GG mismatch as expected given its stability. Only a small enhancement is observed with the AA mismatch, which is generally more stable than CC, CA, and CT mismatches.[26,27] Figure 2.3 shows similar emission intensities for CT and TT mismatches, although we might anticipate a greater emission intensity for CT based on relative stabilities; we have previously noted that for $[Ru(bpy)_2(dppz)]^{2+}$, hydrogen bonding interactions between thymine and the dppz ligand at the mismatch may lead to partial quenching.[15]

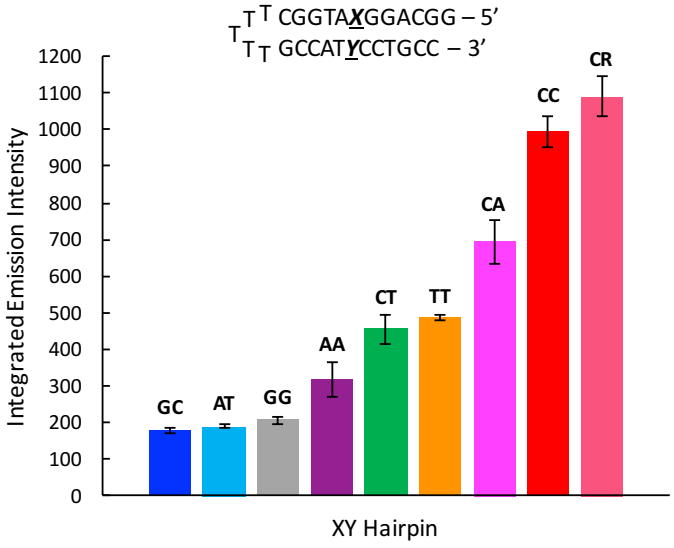

Figure 2.3. Plot of integrated emission intensity of *rac*-$[Ru(Me_4phen)_2(dppz)]^{2+}$ (2 μM) with DNA hairpins (2 μM) containing a variable XY base pair. "R" denotes a tetrahydrofuranyl abasic site. λ_{ex} = 440 nm. Samples prepared in 5 mM tris, 50 mM NaCl, pH 7.5.

We also examined the luminescence response towards an abasic site (CR), and we find that the enhancement is comparable to that with the CC mismatch, consistent with relative stabilities. Generally, then, the relative thermodynamic destabilization of the mismatch site correlates with the luminescence intensities seen in Figure 2.3. This dependence on the instability of the mismatch is consistent with metalloinsertion.[28]

Metalloinsertion by octahedral metal complexes occurs from the minor groove side of DNA. To probe whether $[Ru(Me_4phen)_2(dppz)]^{2+}$ does in fact bind at the mismatch from the minor groove, we tested $Cu(phen)_2^{2+}$ as a minor groove quencher (Figure 2.4).[16,29,30] With the DNA mismatch, as [Cu]/[Ru] increases, there is significant quenching of $[Ru(Me_4phen)_2(dppz)]^{2+}$

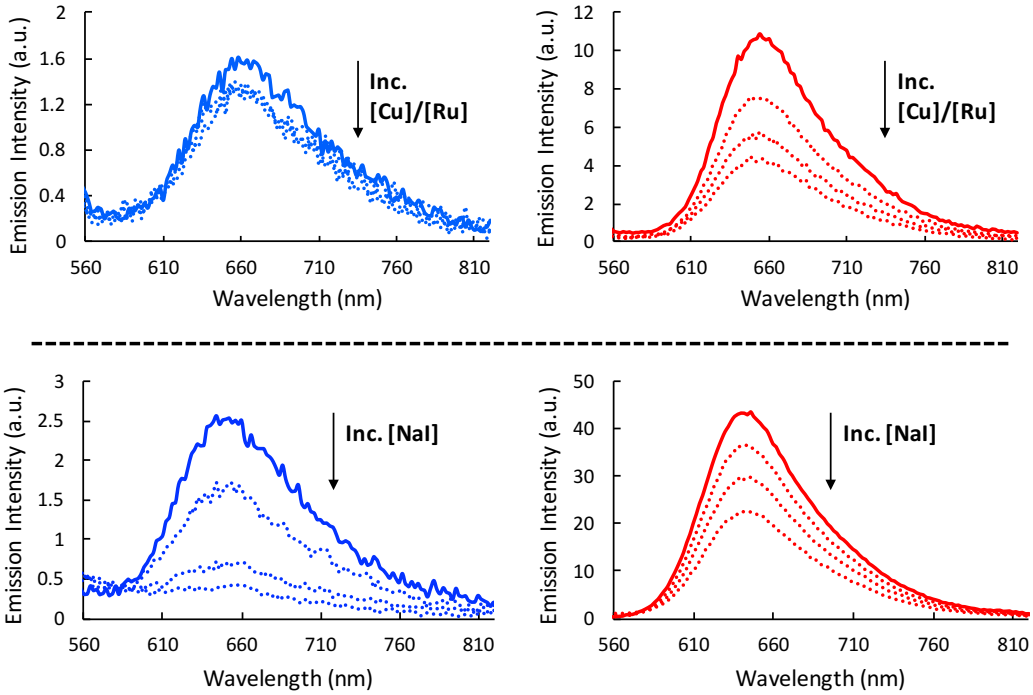

Figure 2.4. (*Top*) Steady-state $Cu(phen)_2^{2+}$ quenching of *rac*-$[Ru(Me_4phen)_2(dppz)]^{2+}$ (2 μM) bound to well-matched (left, blue) and mismatched (right, red) DNA (2 μM). Solid lines indicate no Cu present; dotted lines are increasing concentrations of Cu such that [Cu]/[Ru] = 7, 40, and 100, respectively. λ_{ex} = 440 nm. Samples were prepared in 5 mM tris, 50 mM NaCl, pH 7.5. The DNA sequences are as in Figure 2.2. (*Bottom*) Steady-state NaI quenching of *rac*-$[Ru(Me_4phen)_2(dppz)]^{2+}$ (2 μM) bound to well-matched (left, blue) and mismatched (right, red) DNA (2 μM). Solid lines indicate no NaI present, and dotted lines represent increasing NaI concentrations of 25, 50, and 75 mM, respectively. λ_{ex} = 440 nm. Samples were prepared in 5 mM tris, 200 mM NaCl, pH 7.5.

luminescence (Figure 2.4). Conversely, with well-matched DNA, there is little change in luminescence with increasing $Cu(phen)_2^{2+}$ concentration. These observations indicate ruthenium binding at the mismatch *via* the minor groove, consistent with metalloinsertion. Moreover, the results suggest that binding to well-matched sites by the Me_4phen derivative occurs through the major groove. This latter conclusion is further supported by quenching experiments employing sodium iodide (NaI). Iodide, an anionic quencher, is expected to preferentially quench a small molecule bound in the major groove of the DNA helix compared to the minor groove.[15] Thus, NaI can be used to improve the luminescence differential between mismatched and well-matched samples of $[Ru(Me_4phen)_2(dppz)]^{2+}$ (Figure 2.4). NaI was employed to preferentially quench the luminescence associated with well-matched DNA. It is evident that a more dramatic quenching is observed with the well-matched duplex compared to the duplex containing the CC mismatch. This suggests that at well-matched sites, the complex is bound in the more accessible major groove. However, we do note appreciable quenching of the mismatched signal, implying that the iodide quencher is still capable of accessing the mismatch-bound complex. Nonetheless, with this quenching method, we are able to completely abolish the well-matched emission signal, while maintaining a strong signal associated with mismatch binding, thus improving the luminescence differential between the two duplexes.

2.3.3. Model for $[Ru(Me_4phen)_2(dppz)]^{2+}$ Binding to Well-Matched and Mismatched DNA

To help explain the differential luminescence observed between the mismatched and well-matched DNA samples, we explored models of $[Ru(Me_4phen)_2(dppz)]^{2+}$ bound to well-matched and mismatched sites. Using the DNA coordinates from the crystal structure of Δ-$[Rh(bpy)_2(chrysi)]^{3+}$ bound by metalloinsertion to an AC mismatch,[10] we oriented Δ-$[Ru(Me_4phen)_2(dppz)]^{2+}$ into the mismatch site from the minor groove while minimizing steric

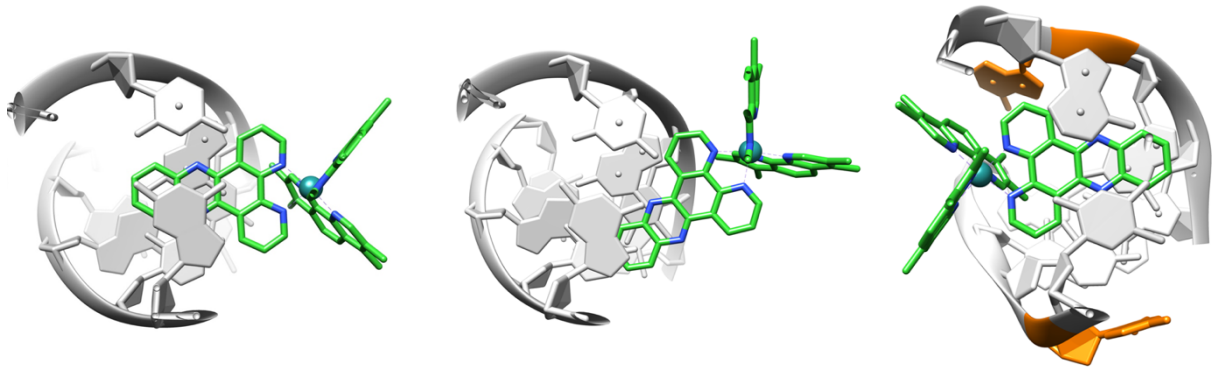

Figure 2.5. Views down the helix axis of Δ-$[Ru(Me_4phen)_2(dppz)]^{2+}$ modeled into the crystal structures of DNA duplexes. The ruthenium complex is shown in green with nitrogen atoms in blue. (*Left*) Head-on intercalation at a well-matched site from the major groove. (*Middle*) Side-on intercalation at a well-matched site from the major groove. (*Right*) Metalloinsertion at a mismatch site from the minor groove; the extruded mismatched bases are shown in orange.

clashes with the Me_4phen ancillary ligands and DNA (Figure 2.5). From this view, we can see that the dppz ligand is capable of deeply inserting into the mismatch site, allowing for significant protection from quenching by water. We also modeled major groove binding using the coordinates for intercalation by another rhodium complex.[31] For intercalation at a well-matched site, we consider two possible binding orientations:[14,21] (i) the dppz ligand intercalates in a "head-on" fashion (Figure 2.5), leaving both phenazine nitrogen atoms relatively well-surrounded by the base stack; (ii) the dppz ligand binds "side-on", achieving overlap with the bases but with one of the phenazine nitrogen atoms being highly exposed to solvent quenching (Figure 2.5). Given the very short 35 ns lifetime observed for the complex with the well-matched duplex, we hypothesize that this side-on intercalation is the dominant binding mode when $[Ru(Me_4phen)_2(dppz)]^{2+}$ is bound to a well-matched site.

2.3.4. Further Investigating the Influence of Methyl Group Incorporation on DNA Binding: $[Ru(Me_2bpy)_2(dppz)]^{2+}$

We prepared another methyl-substituted Ru derivative, $[Ru(Me_2bpy)_2(dppz)]^{2+}$ (Me_2bpy = 5,5'-dimethylbipyridine, Figure 2.6), to gain more insight into the role that methyl substituents

5'-GAC CAG CTT ATC A**C**C CCT AGA TAA GCG-3'
WM: 3'-CTG GTC GAA TAG T**G**G GGA TCT ATT CGC-5'
MM: 3'-CTG GTC GAA TAG T**C**G GGA TCT ATT CGC-5'

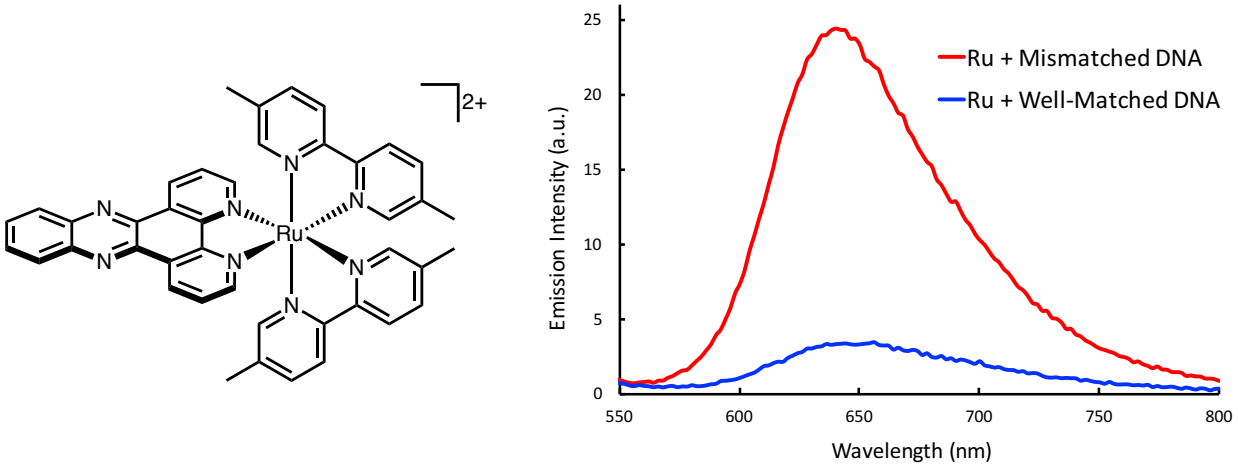

Figure 2.6. (*Top*) DNA sequences used in this study. (*Bottom left*) Structure of $[Ru(Me_2bpy)_2(dppz)]^{2+}$. (*Bottom right*) Steady-state luminescence spectra of *rac*-$[Ru(Me_2bpy)_2(dppz)]^{2+}$ with well-matched (blue) duplex and with the duplex containing a single CC mismatch (red). Samples were prepared in 5 mM tris, 200 mM NaCl, pH 7.5. [Ru] = 2 μM, [DNA duplex] = 2 μM, λ_{ex} = 440 nm.

located on the ancillary ligands play with respect to DNA binding. $[Ru(Me_2bpy)_2(dppz)]^{2+}$ possesses methyl groups at the 5,5' positions of its bpy ligands, which are analogous to the 3,8 methyl groups on Me_4phen; however, unlike $[Ru(Me_4phen)_2(dppz)]^{2+}$, the Me_2bpy derivative does not contain methyl groups that are axial (para) to the Ru center. Thus, $[Ru(Me_2bpy)_2(dppz)]^{2+}$ will provide insight into how methyl groups that are oriented more directly towards the DNA helix influence DNA interactions.

As demonstrated in Figure 2.6, $[Ru(Me_2bpy)_2(dppz)]^{2+}$ exhibits an appreciable luminescence differential in the presence of the mismatched *vs*. well-matched DNA duplexes. The ~7-fold luminescence enhancement observed with the mismatched sequence is a clear improvement over the 1.5 to 2-fold luminescence differential seen with the unsubstituted parent complex $[Ru(bpy)_2(dppz)]^{2+}$ using the same DNA sequences (Figure 2.1). This result indicates that methyl groups oriented toward the DNA helix – as in the 5,5' methyl groups of Me_2bpy and

analogous 3,8 methyl groups of Me_4phen – play a major steric role in disfavoring intercalation at well-matched sites. However, given that $[Ru(Me_4phen)_2(dppz)]^{2+}$ exhibits a ~10-fold emission enhancement when a mismatch is present, this suggests that the additional methyl groups located axial to the Ru center also play a role in the DNA-binding interactions. Furthermore, excited state emission lifetimes of $[Ru(Me_2bpy)_2(dppz)]^{2+}$ with the mismatched DNA duplex reveal a long component (272 ns, 41% of the overall decay) and shorter component (55 ns, 59% of the overall decay). The long-lived 272 ns lifetime is reflective of mismatch binding, while the shorter component is presumably well-matched intercalation. With the completely well-matched sequence, we observe a predominantly short component (27 ns, 88%), and a small portion of a longer lifetime (125 ns, 12%). These data imply that the complex is primarily intercalated in a side-on orientation in which the emission is rapidly quenched, with a small population intercalated in a perpendicular fashion where the dppz ligand is better protected from the aqueous solvent.

2.3.5. $[Ru(Me_4phen)_2(dppz)]^{2+}$ Enantiomer Separation

It is well-established that the right-handed (delta, Δ) enantiomer of $[Ru(phen)_3]^{2+}$-derived ruthenium complexes preferentially bind to B-form DNA compared to their left-handed counterparts (lambda, Λ).[32] Thus, we investigated the chiral preferences in binding to well-matched and mismatched DNA for $[Ru(Me_4phen)_2(dppz)]^{2+}$. Chiral HPLC was utilized to separate the Δ and Λ enantiomers of the complex. An Astec CYCLOBOND I 2000 DMP semi-preparative chiral column was employed for enantiomer separation. Separation was achieved using an isocratic method of 60% acetonitrile with 40% 0.1 M KPF_6 (Figure 2.7). The enantiomers were confirmed and assigned using circular dichroism (Figure 2.7). In these separations, the Λ enantiomer elutes first, followed by the Δ enantiomer. With the two isomers in hand, we sought to investigate their steady-state and time-resolved luminescent properties with the well-matched and mismatched 27-

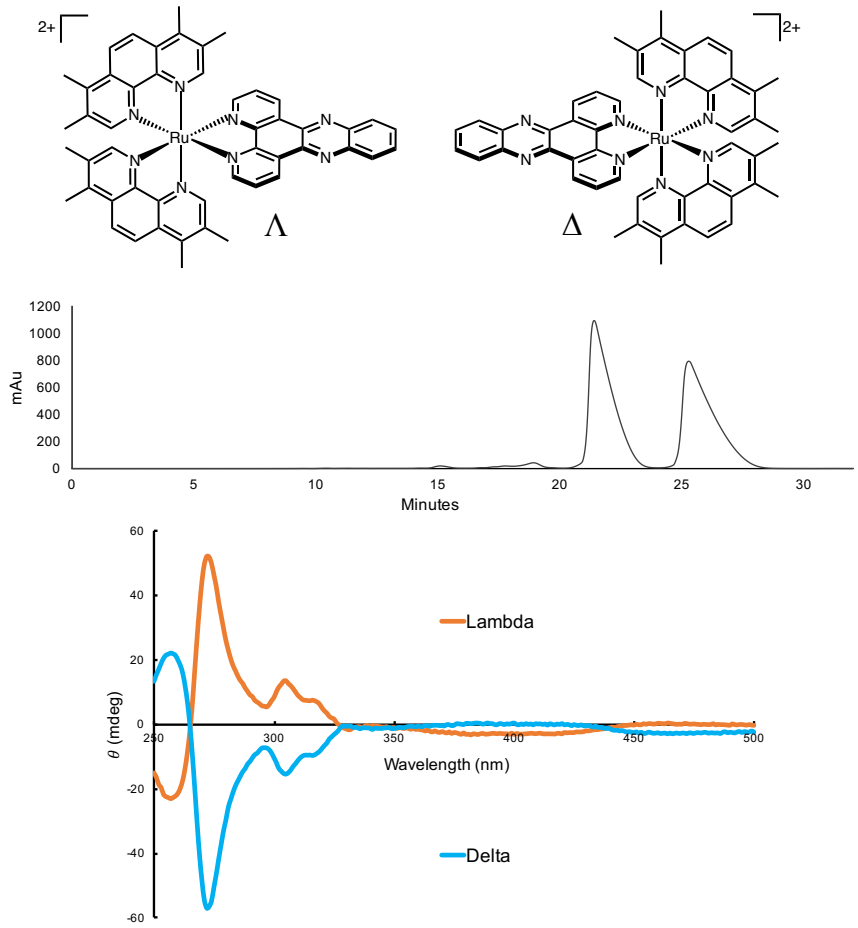

Figure 2.7. (*Top*) Chemical structures of Δ- and Λ-$[Ru(Me_4phen)_2(dppz)]^{2+}$. (*Middle)* HPLC spectrum of *rac*-$[Ru(Me_4phen)_2(dppz)]^{2+}$, obtained with the Astec CYCLOBOND I 2000 DMP chiral column, showing separation of the two enantiomers (60% MeCN/40% 0.1M KPF_6). (*Bottom*) CD spectra of isolated enantiomers (50 μM samples prepared in water).

mer DNA duplexes. We see in Figure 2.8 that the dramatic steady-state emission enhancement in the presence of the CC mismatch is entirely due to binding by the Δ isomer; the Λ enantiomer exhibits a relatively weak light-switch effect in the presence of either duplex.

To confirm the steady-state luminescence behavior of these two enantiomers, we measured their excited state emission lifetimes in the presence of the DNA duplexes (Figure 2.9). Consistent with the steady-state emission spectra, Figure 2.9 illustrates that the excited state emission of Δ-$[Ru(Me_4phen)_2(dppz)]^{2+}$ in the presence of the CC mismatch is substantially longer-lived compared to the fully-matched duplex. Furthermore, the Λ complex exhibits relatively fast emission

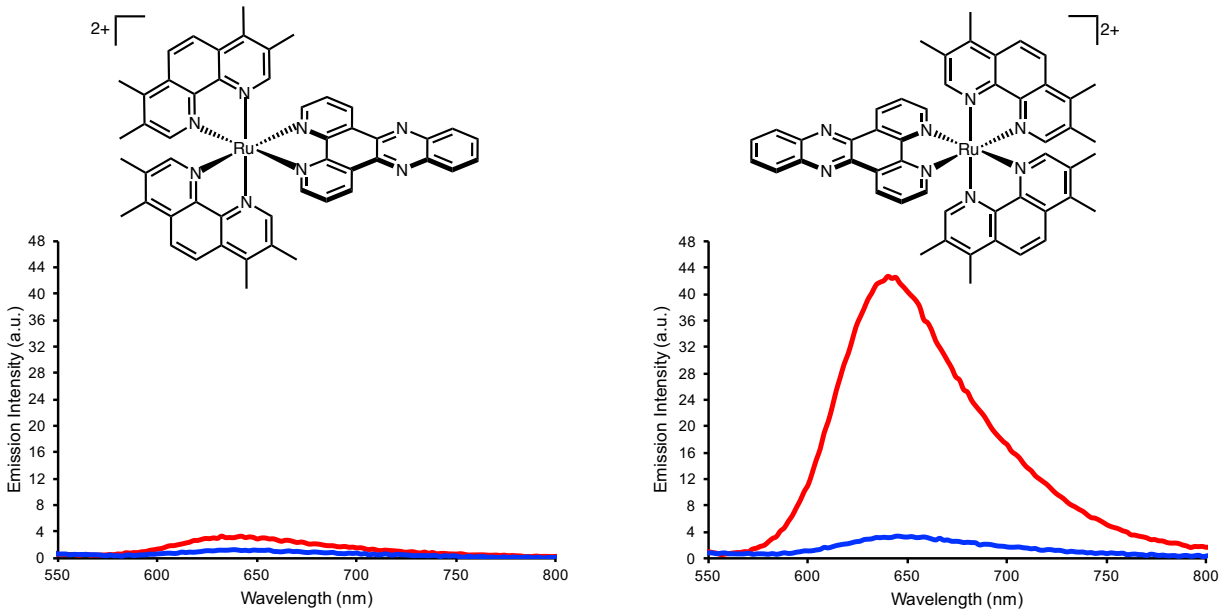

Figure 2.8. Steady-state luminescence spectra of Λ- and Δ-$[Ru(Me_4phen)_2(dppz)]^{2+}$ (left and right, respectively) with the well-matched (blue) duplex and with the duplex containing a single CC mismatch (red). Samples were prepared in 5 mM tris, 200 mM NaCl, pH 7.5. [Ru] = 2 μM, [DNA duplex] = 2 μM, λ_{ex} = 440 nm.

decays in the presence of both sequences. Importantly, the emission decay of Δ-$[Ru(Me_4phen)_2(dppz)]^{2+}$ with the mismatched sequence reveals a satisfactory fit to a mono-exponential function, with a corresponding emission lifetime of 161 ns. This value is consistent with mismatch-bound complex, and these data imply that the Δ isomer is exclusively bound at the mismatched site. Additionally, this isomer possesses a predominantly short-lived (21 ns) lifetime with the fully well-matched sequence, consistent with side-on intercalation of the dppz ligand. A small proportion of a longer-lived (115 ns) species is also detected, attributed to head-on intercalation of dppz. As expected, Λ-$[Ru(Me_4phen)_2(dppz)]^{2+}$ exhibits predominantly short-lived lifetimes (12-15 ns) in the presence of either duplex, reflecting a species that is rapidly quenched by water. However, with the well-matched sequence, a longer-lived component (121 ns) is also detected, indicating that this isomer is capable of intercalation. This longer-lived component is enhanced to ~145 ns when the CC site is present, suggesting that binding to the mismatch may

provide further protection of Λ-$[Ru(Me_4phen)_2(dppz)]^{2+}$ from quenching by water.

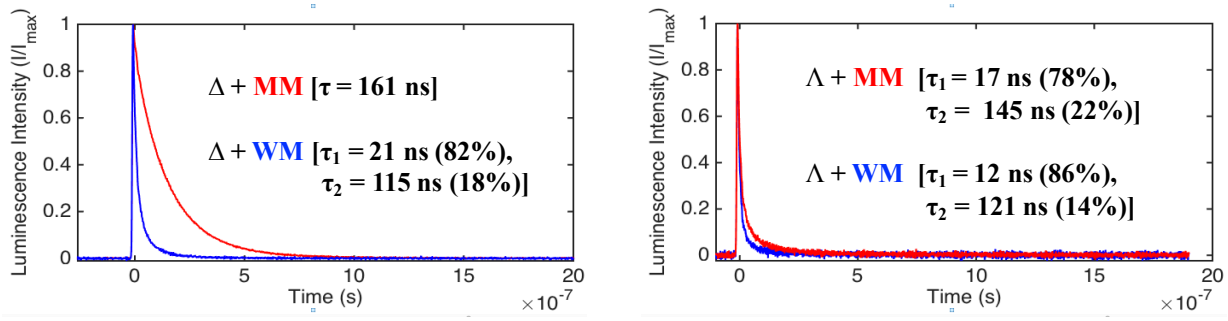

Figure 2.9. Time-resolved luminescence decays of Δ-$[Ru(Me_4phen)_2(dppz)]^{2+}$ (left) and Λ-$[Ru(Me_4phen)_2(dppz)]^{2+}$ (right) with well-matched (blue) duplex and with the duplex containing a single base pair CC mismatch (red). Insets are the calculated emission lifetimes for the various samples, fit to mono- or bi-exponential decays as indicated. Samples were in 5 mM tris, 200 mM NaCl, pH 7.5. [Ru] = 4 μM, [DNA duplex] = 4 μM, λ_{ex} = 460 nm, λ_{em} = 650 nm.

2.4 Conclusions

By incorporating methyl groups into the ancillary ligands of the $[Ru(phen)_2(dppz)]^{2+}$ scaffold, we have thus prepared a luminescent light switch that is highly selective in probing a DNA mismatch. This selectivity is the result of both a higher binding affinity towards mismatched DNA and a longer excited state emission lifetime when bound to a mismatch. Furthermore, consistent with the handedness of B-form DNA, we see that Δ-$[Ru(Me_4phen)_2(dppz)]^{2+}$ is the isomer which imparts all mismatch selectivity. This work demonstrates that ancillary ligand modification offers a new approach in the design of mismatch-specific transition metal complexes.

References

1. Boyle, K.M.; Barton, J.K. *Inorg. Chim. Acta.* **2016**, *452*, 3-11.

2. Glab, W.E.; Tindall, K.R. *Carcinogenesis* **1997**, *18*, 1-8.

3. Parsons, R. et al. *Cell* **1993**, *75*, 1227-1236.

4. Kolodner, R.D. *Trends Biochem. Sci*. **1995**, *20*, 397-401.

5. Arzimanoglou, I.I.; Gilbert, F.; Barber, H.R.K. *Cancer* **1998,** *82*, 1808-1820.

6. Fink, D.; Aebi, S.; Howell, S.B. *Clin. Cancer Res.* **1998**, *4*, 1-6.

7. Martin, L.P.; Hamilton, T.C.; Schilder, R.J. *Clin. Cancer Res.* **2008**, *14*, 1291-1295.

8. Komor, A.C.; Barton, J.K. *J. Am. Chem. Soc.* **2014**, *136,* 14160-14172.

9. Komor, A.C.; Scheider, C.J.; Weidmann, A.G.; Barton, J.K. *J. Am. Chem. Soc.* **2012**, *134,* 19223-19233.

10. Pierre, V.C.; Kaiser, J.T.; Barton, J.K. *Proc. Natl. Acad. Sci.* **2007**, *104*, 429-434.

11. Zeglis, B.M.; Pierre, V.C.; Kaiser, J.T.; Barton, J.K. *Biochemistry* **2009**, *48*, 4247-4253.

12. Friedman, A.E.; Chambron, J.C.; Sauvage, J.P.; Turro, N.J.; Barton, J.K. *J. Am. Chem. Soc.* **1990**, *112*, 4960-4962.

13. Jenkins, Y.; Friedman, A.E.; Turro, N.J.; Barton, J.K. *Biochemistry* **1992**, *31*, 10809-10816.

14. Hartshorn, R.M.; Barton, J.K. *J. Am. Chem. Soc.* **1992**, *114*, 5919-5925.

15. Lim, M. H.; Song, H.; Olmon, E. D.; Dervan, E. E.; Barton, J. K. *Inorg. Chem.* **2009**, *48*, 5392–5397.

16. Song, H.; Kaiser, J. T.; Barton, J. K. *Nat. Chem.* **2012**, *4*, 615–620.

17. Holmlin, R. E.; Stemp, E. D. a.; Barton, J. K. *Inorg. Chem.* **1998**, *37*, 29–34.

18. Dupureur, C. M.; Barton, J. K. *J. Am. Chem. Soc.* **1994**, *116*, 10286–10287.

19. Dupureur, C. M.; Barton, J. K. *Inorg. Chem.* **1997**, *36*, 33–43.

20. Puckett, C.A. *The Cellular Uptake of Luminescent Ruthenium Complexes*. Ph.D. Thesis, California Institute of Technology, Pasadena, CA. 2010.

21. Holmlin, R.E.; Yao, J.A.; Barton, J.K. *Inorg. Chem.* **1999**, *38*, 174-189.

22. Dickerson, J.E.; Summers, L.A. *Aust. J. Chem.* **1970**, *23*, 1023-1027.

23. Nakabayashi, Y.; Watanabe, Y.; Nakao, T.; Yamauchi, O. *Inorg. Chim. Acta* **2004**, *357*, 2553-2560.

24. Liu, J.-G. et al. *J. Biol. Inorg. Chem*. **2000**, *5*, 119–128.

25. Dempsey, J. L.; Winkler, J. R.; Gray, H. B. *J. Am. Chem. Soc.* **2010**, *132*, 1060−1065.

26. Peyret, N.; Senevirante, A.; Allawi, H.T.; SantaLucia, J. *Biochemistry* **1999**, *38,* 3468-3477.

27. SantaLucia, J.; Hicks, D. *Annu. Rev. Biophys. Biomol. Struct.* **2004**, *33*, 415-440.

28. Jackson, B.A.; Barton, J.K. *Biochemistry* **2000**, *39*, 6176-6182.

29. Sigman, D.S.; Chen, C.-H.B. *Annu. Rev. Biochem.* **1990**, *59*, 207-236.

30. Lim, M.H.; Lau, I.H.; Barton, J.K. *Inorg. Chem.* **2007**, *46*, 9528-9530.

31. Kielkopf, C.L.; Erkkila, K.E.; Hudson, B.A.; Barton, J.K.; Rees, D.C. *Nat. Stuct. Biol.* **2000**, *7*, 117-121.

32. Barton, J. K. *Science* **1986**, *233*, 727–735.

Chapter 3

$[Ru(bpy)_2(BNIQ)]^{2+}$ is a Highly Selective Luminescent Probe for Mismatched and Abasic Sites in DNA

Adapted from: Boynton, A.N.; Marcelis, L.; McConnell, A.J.; Barton, J.K. *Inorg. Chem.* **2017**, *56*, 8381-8389. L. Marcelis calculated $[Ru(bpy)_2(BNIQ)]^{2+}$ binding affinities through titration curve-fitting analysis and assisted in excited state lifetime measurements. A.J. McConnell developed the synthesis of BNIQ ligand precursor 2-chlorobenzo[c][1,7]naphthyridine.

3.1 Introduction

The design of small molecules that specifically target DNA base mismatches is a promising route in the development of therapeutic and diagnostic agents directed towards mismatch repair (MMR)-deficient cancers.[1,2] The Barton laboratory has found that octahedral rhodium complexes bearing sterically expansive aromatic ligands bind to DNA mismatches with high affinity and selectivity *via* metalloinsertion.[3,4,5] The archetypal rhodium metalloinsertor is $[Rh(bpy)_2(chrysi)]^{3+}$ (chrysi = 5,6-chrysenequinone diimine), shown in Figure 3.1. At 11.3 Å, the chrysi ligand is approximately 0.5 Å wider than a well-matched base pair, which makes intercalation a less favorable binding mode due to steric clashing between the chrysi ligand and the sugar-phosphate backbone of the DNA. A crystal structure of $[Rh(bpy)_2(chrysi)]^{3+}$ bound to an AA mismatch revealed that the chrysi ligand inserts into the DNA helix from the minor groove at the

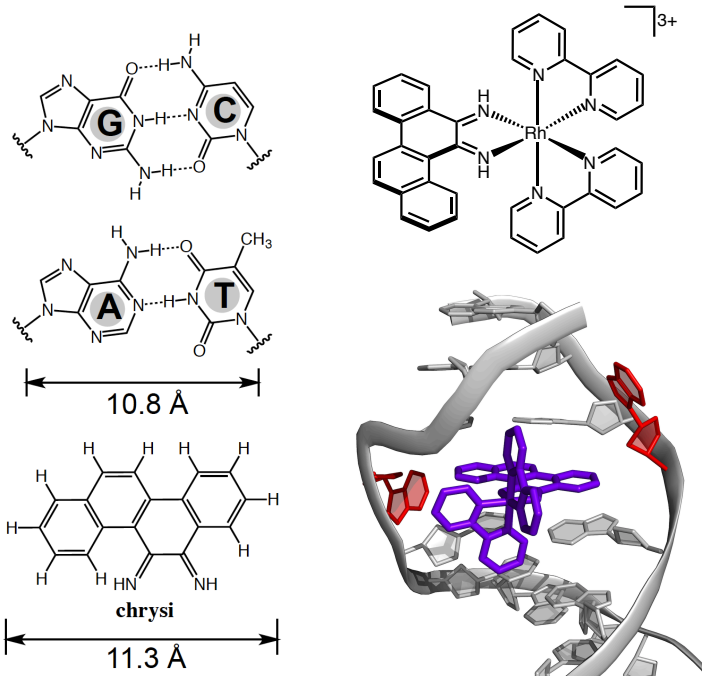

Figure 3.1. (*Left*) The chrysi ligand is 0.5 Å wider than a well-matched base pair, making intercalation unfavorable. (*Upper right)* The structure of Δ-$[Rh(bpy)_2(chrysi)]^{3+}$. (*Lower Right*) A crystal structure revealed that Δ-$Rh(bpy)_2(chrysi)]^{3+}$ (purple) binds to a mismatch *via* metalloinsertion, in which the complex inserts from the minor groove and extrudes the mismatched bases (red) (figure created from PDB structure 3GSK).

thermodynamically destabilized mismatch site by displacing the mismatched bases from the base stack (Figure 3.1),[3] a binding mode called metalloinsertion. Importantly, later generations of rhodium metalloinsertors have been shown to exhibit selective cytotoxicity towards cancer cells deficient in mismatch repair (MMR) compared to MMR-proficient cells, making these compounds promising chemotherapeutic agents for MMR-deficient cancers.[6,7]

There is also considerable interest in designing mismatch-specific luminescent small molecules to serve as diagnostic probes for the early detection of MMR-deficient cancers. While rhodium metalloinsertors are non-emissive following excitation, octahedral ruthenium(II) polypyridyl complexes have attracted significant attention as luminescent reporters of biomolecules owing to their favorable photophysical and photochemical properties.[8] Ruthenium(II) polypyridyl complexes possess an intense metal-to-ligand charge transfer (MLCT) transition which, upon excitation, yields a bright, long-lived emission in the visible region. Furthermore, these compounds exhibit high photostability and are coordinatively saturated, making them inert to ligand substitution and stable in aqueous solutions.

In addition to the ancillary ligand modification of $[Ru(phen)_2(dppz)]^{2+}$-type light switch compounds discussed in Chapter 2, another logical approach in the design of mismatch-specific luminescent ruthenium(II) polypyridyl complexes is to incorporate a sterically expansive aromatic ligand that is too large to intercalate into well-matched duplex DNA but can instead insert at destabilized sites. Several ligands that have been studied in this context include pqp (6-phenylquino[8,7-*k*][1,8]phenanthroline),[9] tpqp (7,8,13,14-tetrahydro-6-phenylquino[8,7-*k*][1,8]phenanthroline),[9] and eilatin[10] (Figure 3.2). These ligands were developed as even bulkier versions of chrysi; however, unlike diimine-containing ligands, pqp, tpqp, and eilatin were designed to coordinate directly to the ruthenium center *via* the heterocyclic nitrogen atoms.

$[Ru(bpy)_2(pqp)]^{2+}$ shows no detectable luminescence, while $[Ru(bpy)_2(tpqp)]^{2+}$ emits weakly in aqueous solution. However, $[Ru(bpy)_2(tpqp)]^{2+}$ shows no increase in emission intensity upon the addition of either well-matched or mismatched DNA. That being said, luminescence polarization and $[Fe(CN)_6]^{4-}$ quenching experiments revealed that $[Ru(bpy)_2(tpqp)]^{2+}$ binds more tightly at a

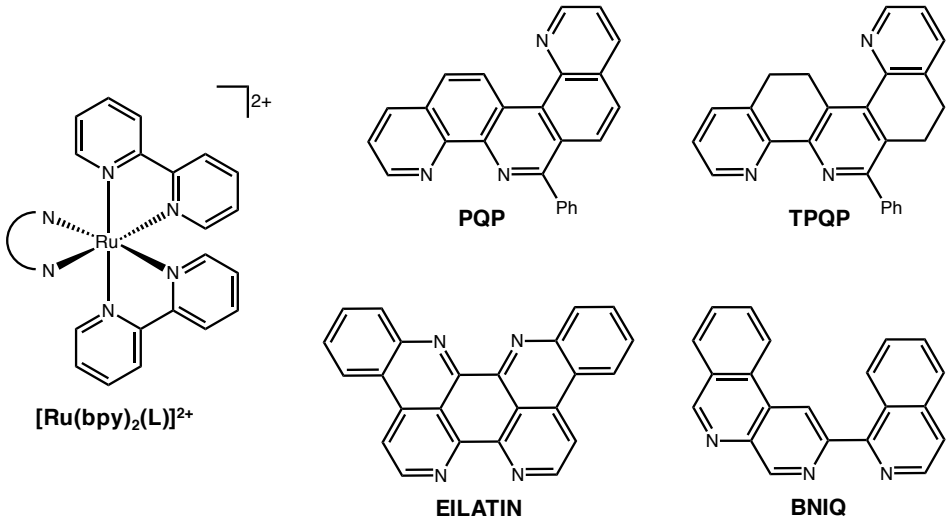

Figure 3.2. Several $[Ru(bpy)_2(L)]^{2+}$ complexes that have been investigated as luminescent reporters of DNA mismatches, incorporating sterically demanding ligands (L).

CC mismatch site compared to well-matched base pairs in the duplex. This preferential binding to the mismatch was confirmed by a $^1O_2$ sensitization assay, which showed preferential damage to the guanine adjacent to the CC mismatch compared to other guanine sites in the DNA. Another study explored the binding of $[Ru(bpy)_2(eilatin)]^{2+}$ to well-matched and mismatched DNA duplexes. Eilatin is a symmetric, aromatic ligand that is notably expansive. While competitive DNA photocleavage experiments with the metalloinsertor $[Rh(bpy)_2(chrysi)]^{3+}$ revealed some preferential binding of $[Ru(bpy)_2(eilatin)]^{2+}$ to a CC mismatch, competition experiments with the non-specific metallointercalator $[Rh(bpy)_2(phi)]^{3+}$ showed that the ruthenium complex is still readily capable of binding to well-matched sites in the duplex. These results emphasized the notion that while a planar, aromatic, bulky ligand such as chrysi can lead to high mismatch specificity,

simply increasing the steric size does not necessarily correlate with an increase in mismatch specificity.

Described in this chapter is the design and synthesis of a new sterically expansive ligand called BNIQ (Figure 3.2, BNIQ = benzo[c][1,7]naphthyridine-1-isoquinoline). The luminescent properties of the ruthenium complex bearing this ligand, $[Ru(bpy)_2(BNIQ)]^{2+}$ – both free and in the presence of well-matched and mismatched DNA duplexes – were explored using steady-state and excited-state lifetime measurements. It was found that $[Ru(bpy)_2(BNIQ)]^{2+}$ is highly selective towards destabilized sites in the DNA duplex.

3.2 Experimental Protocols

3.2.1 Materials

All chemicals and starting materials were purchased from commercial vendors and used as received. $Ru(bpy)_2Cl_2$ was prepared according to the literature.[11] UV-Visible spectra were recorded on a Beckman DU 7400 UV-Visible spectrophotometer (Beckman Coulter). Oligonucleotides were synthesized using standard phosphoramidite chemistry at Integrated DNA Technologies (Coralville, IA) and purified by HPLC using a C_{18} reverse-phase column (Varian, Inc.) on a Hewlett-Packard 1100 HPLC. The copper complex $Cu(phen)_2^{2+}$ was generated *in situ* by combining $CuCl_2$ with phen ligand in a 3:1 ratio.

3.2.2. Synthesis

*5-Amino-2-chloropyridine (**1**).* 2-Chloro-5-nitropyridine (5.49 g, 34.6 mmol) was added in portions to a solution of $SnCl_2 \bullet 2H_2O$ (39.36 g, 17.4 mmol) in 50 mL concentrated HCl at 0°C. The reaction was allowed to warm to room temperature and stirred for 4 h, followed by the addition of 5 M Na_2CO_3 (75 mL) and NH_4OH (50 mL). The mixture was extracted with CH_2Cl_2 (5 x 100

mL), dried over $MgSO_4$, filtered, and the solvent was evaporated to give **1** (3.9 g, 88%). ^{1}H NMR (500 MHz, $CDCl_3$) δ 7.88 (dd, *J* = 3.0, 0.6 Hz, 1H), 7.11 (dd, *J* = 8.5, 0.6 Hz, 1H), 7.01-6.98 (m, 1H), 3.62 (s, 2H). ESI(+)MS (*m/z*): $[M + H]^+$ calc. 129.0, found 129.3.

*Tert-butyl (6-chloro-3-pyridinyl) carbamate (**2**).* Synthesized using an adapted procedure.[12] A solution of **1** (1.83 g, 14.2 mmol) and Boc_2O (4.74 g, 21.8 mmol) in dry dioxane (15 mL) was heated under reflux under an Ar atmosphere for 45 h. During the course of the reaction, an additional 0.81 g (3.7 mmol) of Boc_2O was added to the reaction mixture. The reaction mixture was poured into H_2O (15 mL) and the product extracted with EtOAc (2 x 25 mL). The combined organic layers were washed with brine (15 mL), dried over Mg_2SO_4, filtered, and the solvent was removed. The residue was run through a plug of silica to give **2** (3.1 g, 96%). ^{1}H NMR (500 MHz, $CDCl_3$) δ 8.29 (dd, *J* = 2.9, 0.6 Hz, 1H), 7.99 (s, 1H), 7.28 (dt, *J* = 8.7, 0.6 Hz, 1H), 6.86 (s, 1H), 1.55 (s, 9H). ESI(+)MS (*m/z*): $[M + H]^+$ calc. 229.1, found 229.1.

*Tert-butyl (6-chloro-4-iodo-3-pyridinyl) carbamate (**3**).* To a solution of TMEDA (3.8 mL, 25 mmol) in dry THF (15 mL) under Ar was added *n*BuLi (10 mL, 2.5 M in hexanes) dropwise at -78°C. The solution was stirred for 30 min, and subsequently a solution of **2** (1.37 g, 6 mmol) in dry THF (5 mL) under Ar was added dropwise. The solution was stirred at -78°C for 1 h and then a solution of I_2 (3.23 g, 12.7 mmol) in 5 mL dry THF under Ar was added dropwise. The reaction was allowed to warm to room temperature and stirred overnight. The reaction was cooled to -78°C, and 20 mL of saturated NH_4Cl was added. The aqueous and organic layers were separated, and the aqueous phase was extracted with EtOAc (3 x 30 mL). The organic layers were combined, dried over $MgSO_4$, filtered, and the solvent was removed. The crude material was purified by silica gel column chromatography (9:1 hexanes/EtOAc) to give **3** (0.60 g, 28%). ^{1}H NMR (500 MHz, $CDCl_3$) δ 8.98 (s, 1H), 7.76 (s, 1H), 6.69 (s, 1H), 1.59 (s, 9H). ESI(+)MS (*m/z*): $[M + H]^+$ calc.

355.0, found 354.8.

*Tert-butyl (6-chloro-4-(2-formylphenyl)-3-pyridinyl) carbamate (**4**).* A solution of **3** (0.604 g, 1.71 mmol), 2-formylphenylboronic acid (0.384 g, 2.56 mmol), $Pd(PPh_3)_4$ (0.0986 g, 5 mol %), 2 M Na_2CO_3 (3 mL), EtOH (2 mL), and toluene (12 mL) was degassed by freeze pump thaw (4x) then heated to 90°C under Ar overnight. The reaction mixture was poured over 15 mL H_2O, the layers were separated, and the aqueous layer was extracted with EtOAc (3 x 20 mL). The organic layers were combined, dried over $MgSO_4$, filtered, and the solvent was removed. The crude material was purified by silica gel chromatography (4:1 hexanes/EtOAc) to give **4** (0.29 g, 51%). ^{1}H NMR (500 MHz, $CDCl_3$) δ 8.75 (s, 1H), 7.91-7.88 (m, 1H), 7.76 (s, 1H),7.57-7.52 (m, 3H), 7.34-7.30 (m, 1H), 6.88 (d, *J* = 5.2 Hz, 1H), 1.56 (s, 9H). ESI(+)MS (*m/z*) $[M + H]^+$ calc. 333.1, found 333.1.

*2-Chlorobenzo[c][1,7]naphthyridine (**5**).* To 0.291 g **4** (0.877 mmol) was added 5 mL CH_2Cl_2 and 0.5 mL TFA. The solution was stirred overnight, and then 5 mL 5% Na_2CO_3 was added and the solution was stirred vigorously for 1.5 h. The layers were separated, and the aqueous layer was extracted with EtOAc (2 x 20 mL). The organic layers were combined, washed with brine (1 x 25 mL), dried over $MgSO_4$, filtered, and the solvents were removed. The product was purified by column chromatography (4:1 hexanes/EtOAc) to give **5** (0.16 g, 87%). ^{1}H NMR (500 MHz, $CDCl_3$) δ 9.35 (s, 1H), 9.33 (s, 1H), 8.58 (d, *J* = 8.1 Hz, 1H), 8.39 (s, 1H), 8.15 (d, 7.9 Hz, 1H), 7.99 (ddd, *J* = 8.3 Hz, 7.2 Hz, 1.4 Hz, 1H), 7.92 (ddd, *J* = 8.1 Hz, 7.1 Hz, 1.1 Hz, 1H). ESI(+)MS (*m/z*) $[M + H]^+$ calc. 215.0, 217.0; found 215.2, 217.0.

*2-Bromobenzo[c][1,7]naphthyridine (**6**).* To a 5 mL microwave vial was added 0.010 g of **5** (0.047 mmol), 1 mL HBr, and 2 mL AcOH. The contents were heated at 130°C for 2 h. The reaction mixture was then diluted with 50 mL H_2O and the solution was neutralized to pH 7 with

$NaHCO_3$. The aqueous mixture was then washed with CH_2Cl_2 (3 x 25 mL), dried over $MgSO_4$, and filtered to give **6** (0.0090 g, 75%). ^{1}H NMR (500 MHz, $CDCl_3$) δ 9.39 (s, 1H), 9.32 (s, 1H), 8.61 (dq, *J* = 8.5, 1.0 Hz, 1H), 8.59 (s, 1H), 8.18 (ddd, *J* = 7.9 Hz, 1.4 Hz, 0.7 Hz, 1H), 8.03 (ddd, *J* = 8.3 Hz, 7.1 Hz, 1.4 Hz, 1H), 7.95 (ddd, *J* = 8.2, 7.2, 1.1 Hz, 1H). ESI(+)MS (*m/z*) $[M + H]^+$: calc. 259.0, 261.0, found 259.0, 261.0.

BNIQ ligand (7). To a flame-dried Schlenk flask under Ar was added 0.096 g 1-iodoisoquinoline (0.37 mmol) and 0.016 g LiCl (0.38 mmol). The flask was evacuated for 2 h, and anhydrous THF (1 mL) was added. The contents were stirred and 190 μL *i*-PrMgCl (2 M solution in THF) was added dropwise. The solution was stirred for 1 h, during which the reaction turned a dark purple. The contents were cooled to 0°C, and 755 μL $ZnCl_2$ in THF (0.5 M) was added and stirred for 15 min at 0°C. A solution of $Pd_2(dba)_3$ (0.009 g, 4 mol %) and PCy_3 (0.011 g, 15 mol %) in THF (3 mL) under Ar was then added to the reaction, followed by a solution of **6** (0.065 g, 0.25 mmol) in THF (3 mL). The dark red-orange solution was stirred for 17 h at 65°C. The solvent was removed *in vacuo*, and the contents were re-dissolved in EtOAc/H_2O (25:20 mL). The layers were separated and the EtOAc was washed with H_2O (2 x 20 mL). The EtOAc was evaporated and the crude material was purified by silica gel column chromatography with a solvent gradient (6:1 hexanes/EtOAc to 100% EtOAc) to obtain BNIQ ligand **7** (0.040 g, 52%). ^{1}H NMR (500 MHz, $CDCl_3$) δ 9.71 (s, 1H), 9.45 (s, 1H), 9.14 (s, 1H), 8.82-8.76 (m, 2H), 8.72 (d, *J* = 5.6 Hz, 1H), 8.18 (d, *J* = 7.9 Hz, 1H), 7.99 (ddd, *J* = 8.3 Hz, 7.1 Hz, 1.4 Hz, 1H), 7.95 (dt, *J* = 8.3 Hz, 1.0 Hz, 1H), 7.91 (ddd, *J* = 8.0 Hz, 7.1 Hz, 1.1 Hz, 1H), 7.80 (d, *J* = 5.7 Hz, 1H), 7.75 (ddd, *J* = 8.2 Hz, 6.8 Hz, 1.2 Hz, 1H), 7.66 (ddd, *J* = 8.3 Hz, 6.8 Hz, 1.3 Hz, 1H). ESI(+)MS (*m/z*) $[M + H]^+$ calc. 308.1, found 308.4.

*[Ru(bpy)$_2$(BNIQ)]X$_2$ (**8**, X = PF$_6$ or Cl).* BNIQ ligand (**7**) (0.015 g, 0.049 mmol) and Ru(bpy)$_2$Cl$_2$ (0.025 g, 0.048 mmol) were combined in 4 mL ethylene glycol and heated at 130°C for 17 h. The solution was cooled to room temperature, diluted with 5 mL H_2O, and excess NH_4PF_6 was added to precipitate the product. The precipitate was collected *via* vacuum filtration, washed with H_2O (2 x 5 mL), and dried (0.041 g, 82%). The complex was converted to the water-soluble Cl salt by anion exchange chromatography (Sephadex QAE) and further purified by preparative HPLC using a gradient of H_2O (with 0.1% TFA) to CH_3CN over 1 h. ^{1}H NMR (500 MHz, DMSO-d_6) δ 9.99 (s, 1H), 9.59 (s, 1H), 9.20-9.15 (m, 2H), 8.97 (d, *J* = 8.2 Hz, 1H), 8.94-8.86 (m, 3H), 8.45 (s, 1H), 8.44 (d, *J* = 8.2 Hz, 1H), 8.30-8.20 (m, 4H), 8.15-8.08 (m, 4H), 8.03 (td, *J* = 7.0, 1.1 Hz, 2H), 7.95 (ddd, *J* = 5.7, 1.4, 0.7 Hz, 1H), 7.85 (dddd, *J* = 5.4, 4.6, 1.5, 0.7 Hz, 2H), 7.79 (ddd, *J* = 5.6, 1.5, 0.7 Hz), 7.69 (d, *J* = 6.2 Hz, 1H), 7.64 (ddd, *J* = 7.6, 5.6, 1.3 Hz, 1H), 7.59 (ddd, *J* = 7.6, 5.6, 1.3 Hz, 1H), 7.45 (ddd, 7.2, 5.6, 1.3 Hz, 1H), 7.40 (ddd, *J* = 7.3, 5.7, 1.3 Hz, 1H). ESI(+)MS (*m/z*) $[M/2]^+$ calc. 360.6, found 360.6. UV-Vis in H_2O, λ/nm (ε x 10^4/M^{-1} cm^{-1}): 287 (8.0), 366 (3.0), 431 (1.7).

*1,1'-biisoquinoline (**9**).* **9** was synthesized according to a reported procedure.[13,14] ^{1}H NMR (500 MHz, $CDCl_3$) δ 8.69 (d, *J* = 5.7 Hz, 2H), 8.10 (dt, *J* = 8.3, 0.9 Hz, 2H), 7.98 (dd, *J* = 5.7, 0.9 Hz, 2H), 7.80 (ddd, *J* = 8.2, 6.8, 1.2 Hz, 2H), 7.74 (dq, *J* = 8.6, 1.0 Hz, 2H), 7.56 (ddd, *J* = 8.3, 6.8, 1.2 Hz, 2H). ESI(+)MS (*m/z*) $[M + H]^+$ calc. 257.1, found 257.4.

*[Ru(bpy)$_2$(1,1'-biisoq)]X$_2$ (**10**, X = PF$_6$ or Cl).* 1,1'-biisoquinoline (0.030 g, 0.12 mmol) and Ru(bpy)$_2$Cl$_2$ (0.067 g, 0.13 mmol) were combined in 15 mL ethylene glycol and heated at 130°C for 5 h. The reaction was cooled to room temperature, diluted with H_2O (15 mL), and excess NH_4PF_6 was added to precipitate the product. The precipitate was collected *via* vacuum filtration, washed with H_2O (15 mL), and dried (0.110 g, 87%). The complex was converted to the water-

soluble Cl salt by anion exchange chromatography (Sephadex QAE) and further purified by preparative HPLC using a gradient of H_2O (with 0.1% TFA) to CH_3CN over 1 h. ^1H NMR (500 MHz, D_2O) δ 8.40 (m), 8.33 (dt, J = 8.4, 1.0 Hz) 8.17 (ddd, J = 5.6, 1.5, 0.7 Hz) 8.03 (d, J = 8.3 Hz) 7.97 (m), 7.92 (m), 7.88 (d, J = 8.3 Hz) 7.84 (m), 7.79 (m), 7.74 (m), 7.69 (m), 7.64 (m), 7.52 (ddd, J = 8.5, 6.9, 1.3 Hz), 7.48 (J = 8.5, 6.9, 1.3 Hz) 7.24 (m), 7.04 (ddd, J = 7.6, 5.7, 1.3 Hz), 6.97 (ddd, J = 7.4, 5.7, 1.3 Hz), 6.62 (d, J = 5.7 Hz). ESI(+)MS (m/z) $[M/2]^+$ calc. 335.1, found 335.1. UV-Vis in H_2O, λ/nm (ε x $10^4/M^{-1}cm^{-1}$): 287 (5.8), 446 (0.96), 516 (1.0).

3.2.3 Luminescence Measurements

Steady-State Luminescence. Luminescence spectra were recorded on an ISS-K2 spectrofluorometer at 25°C. $[Ru(bpy)_2(BNIQ)]^{2+}$ was excited at 440 nm, and emission spectra were integrated from 590-850 nm. The chloride salt of the complex was used for all DNA experiments. In appropriate figures, [DNA] is defined as the concentration of the full sequence oligonucleotide.

Time-Resolved Luminescence. Time-resolved spectroscopic measurements were carried out at the Beckman Institute Laser Resource Center, and were conducted using instrumentation that has been described.[15] Briefly, a 460 nm light produced by OPO pumped with a 10 Hz, Qswitched Nd:YAG laser (Spectra-Physics Quanta-Ray PRO-Series) was used as an excitation source (pump pulse duration ≈ 8 ns). The emitted light was detected at 700 nm with a photomultiplier tube (Hamamatsu R928) following wavelength selection by a double monochromator (Instruments SA DH-10). Scattered laser light was removed from the detectors using suitable filters. The samples were held in 1 cm path length quartz cuvettes (Starna) equipped with stir bars and irradiated at 460 nm with 500−1000 laser pulses at 3 mJ/pulse. Kinetic traces were fit to exponential equations of the form $I(t) = a_0 + \Sigma\, a_n \exp(-t/\tau_n)$, where $I(t)$ is the signal

intensity as a function of time, a_0 is the intensity at long time, a_n is a pre-exponential factor that represents the relative contribution from the *n*th component to the trace, and τ_n is the lifetime of the *n*th component, convoluted with a Gaussian function to take into account the Instrument Response Function (fwmh = 8 ns). The errors are evaluated to be equal to 5%.

3.3 Results and Discussion

3.3.1 BNIQ Ligand Design and Synthesis

In this work, we designed a new sterically expansive polypyridyl ligand that possesses a similar width to the mismatch-specific chrysi ligand but lacks imine protons characteristic of chrysi. We have proposed that exchangeable imine protons are responsible for quenching any ambient temperature luminescence of compounds like $[Ru(bpy)_2(chrysi)]^{2+}$.[16] As such, BNIQ was designed to contain heterocyclic nitrogen atoms that coordinate directly to the ruthenium core, analogously to bpy or phen, and an additional non-chelating nitrogen atom that could enhance the sensitivity of the complex to its environment. BNIQ also possesses similar structural features to the tpqp ligand, which has been shown to exhibit some degree of mismatch specificity in binding.[9]

BNIQ was synthesized in seven steps (Scheme 3.1) from the starting material 2-chloro-5-nitropyridine. A key step in the ligand synthesis is the conversion of the chloride intermediate **5** into its bromide analogue **6**, a transformation that was executed in order to generate a more reactive substrate in the subsequent Negishi coupling. Using an adapted literature procedure for a related 2-chloropyridine derivative,[17] **5** was heated in a 2:1 (v/v) mixture of acetic acid/aqueous HBr at 130°C in a microwave reactor to yield **6**. Negishi coupling conditions were adapted from the literature[18,19] to synthesize the BNIQ ligand (**7**) from **6** and 1-iodoisoquinoline.

3.3.2 Synthesis and Characterization of the $[Ru(bpy)_2(BNIQ)]^{2+}$ Complex

Coordination of BNIQ to ruthenium (Scheme 3.1) is a facile synthesis, achieved by heating the ligand in a 1:1 ratio with $Ru(bpy)_2Cl_2$ in ethylene glycol at 130°C. $[Ru(bpy)_2(BNIQ)]^{2+}$ was isolated from the reaction mixture as its PF_6^- salt before conversion to its water-soluble chloride salt by anion exchange chromatography and further purification by preparative HPLC.

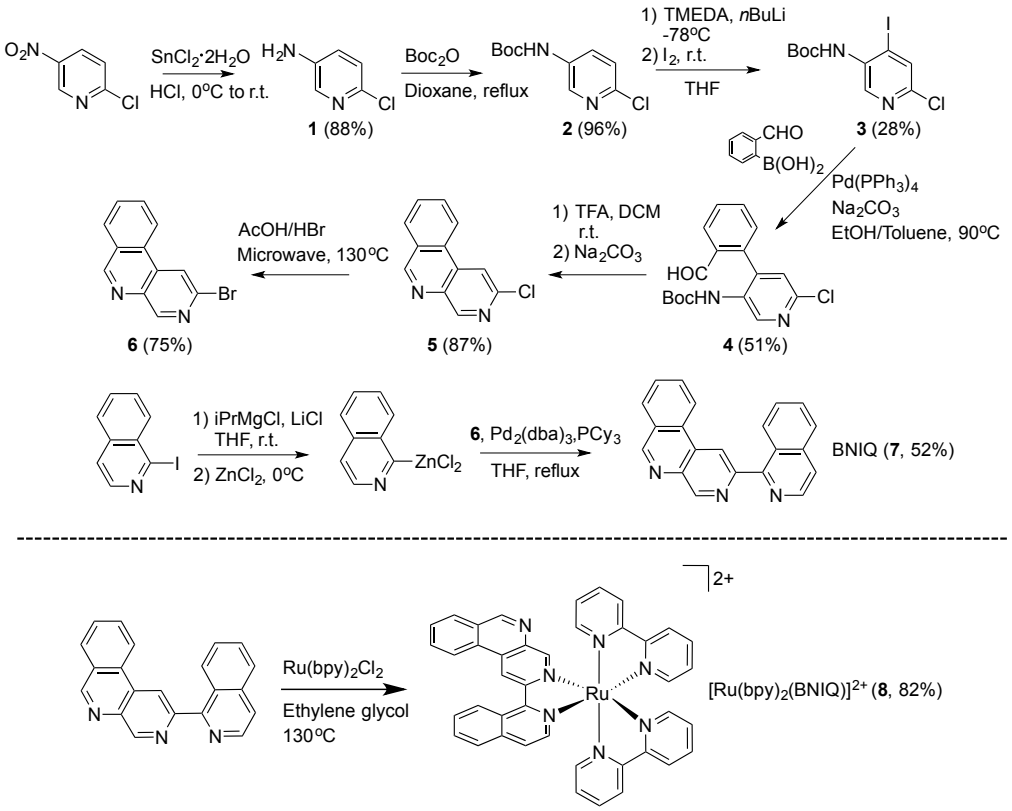

Scheme 3.1. *(Top)* Synthesis of the BNIQ ligand. (*Bottom*) Synthesis of $[Ru(bpy)_2(BNIQ)]^{2+}$.

The UV-Visible spectrum of $[Ru(bpy)_2(BNIQ)]^{2+}$ shows a characteristic MLCT transition in the visible region at 430-440 nm (Figure 3.3). Upon excitation at 440 nm in aqueous solution, $[Ru(bpy)_2(BNIQ)]^{2+}$ exhibits a broad emission centered at 700 nm that is nearly insensitive to the presence of oxygen in solution (Figure 3.3).

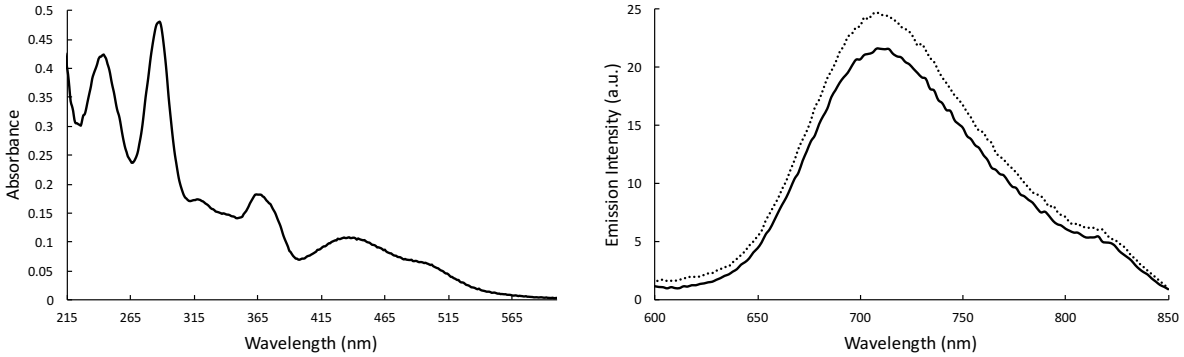

Figure 3.3. UV-Visible (*left*) and steady-state emission spectra (*right*) of $[Ru(bpy)_2(BNIQ)]^{2+}$ in aerated (solid line) and de-gassed (dotted line) solutions (6 μM in H_2O, λ_{ex} = 440 nm).

3.3.3. Steady-State Luminescence of $[Ru(bpy)_2(BNIQ)]^{2+}$ in the Presence of DNA

We investigated the steady-state emission of $[Ru(bpy)_2(BNIQ)]^{2+}$ in the presence of three different 27-mer DNA duplexes: one that is completely well-matched, one that contains a single

5'-GAC CAG CTT ATC A***C***C CCT AGA TAA GCG-3'
WM: 3'-CTG GTC GAA TAG T***G***G GGA TCT ATT CGC-5'
MM: 3'-CTG GTC GAA TAG T***C***G GGA TCT ATT CGC-5'
AB: 3'-CTG GTC GAA TAG T_G GGA TCT ATT CGC-5'

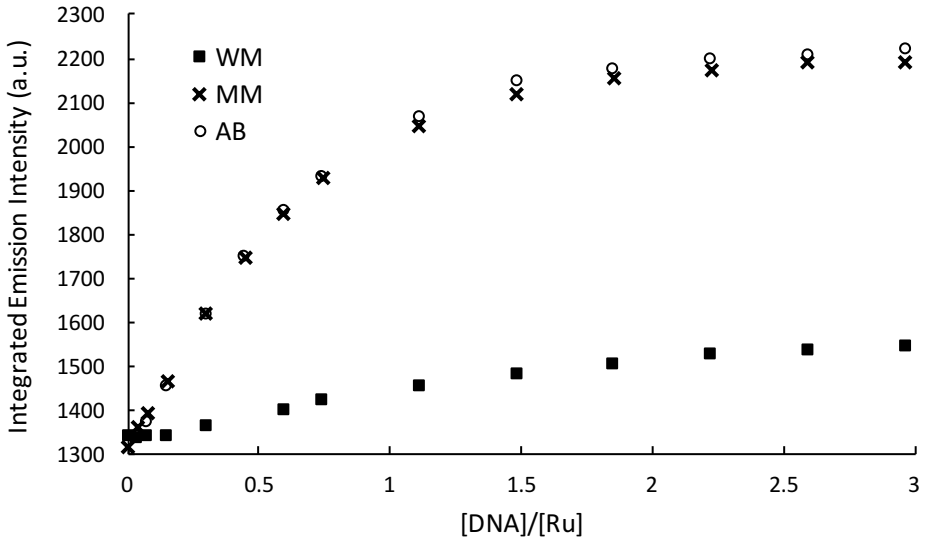

Figure 3.4. Steady-state emission titrations of $[Ru(bpy)_2(BNIQ)]^{2+}$ with well-matched, mismatched, and abasic DNA duplexes at 25°C. λ_{ex} = 440 nm, [Ru] = 4 μM. [DNA] reflects the concentration of full sequence. Samples were prepared in 5 mM Tris, 200 mM NaCl, pH 7.5. DNA sequences are provided at the top of the figure; the underscore represents the absence of a base in the abasic (AB) sequence. Emission spectra were integrated from 590-850 nm.

CC mismatch, and one containing an abasic site (sequences provided in Figure 3.4). Titrations (Figure 3.4) reveal that the emission intensity of the complex increases upon the addition of each duplex; however, the emission intensity is brighter for samples containing the CC and abasic sites compared to the well-matched DNA. The maximum ruthenium emission intensities reached for the CC mismatch and abasic DNA samples are approximately 1.7-fold larger than the emission intensity of free ruthenium complex, and 1.5-fold greater than the well-matched DNA sample.

The binding affinities evaluated by a global analysis of the titration curves (Table 3.1, Appendix A.2) reveal that $[Ru(bpy)_2(BNIQ)]^{2+}$ has a ~500-fold higher affinity for oligomers containing CC mismatched or abasic sites (3.5×10^6 and 3.8×10^6 M^{-1} respectively) compared to oligomers with fully well-matched sites (7.3×10^3 M^{-1}). Thus, the titrations demonstrate that this new ruthenium complex is very specific for the thermodynamically destabilized sites in DNA.

Table 3.1. Binding Affinities of $[Ru(bpy)_2(BNIQ)]^{2+}$ with Well-Matched, Mismatched, and Abasic DNA Duplexes

	Well-matched	Mismatched	Abasic
K_a (M^{-1})[a]	7.3×10^3	3.5×10^6	3.8×10^6

[a] Titrations were performed with DNA sequences shown in Figure 3.4. Samples were prepared in 5 mM Tris, 200 mM NaCl, pH 7.5. [Ru] = 4 μM, λ_{ex} = 440 nm. The binding affinity is expressed per binding site and not per DNA sequence.

Interestingly, analysis of the titrations indicates that the differences in emission intensities observed in Figure 3.4 are mainly related to the higher affinity of the complex towards mismatched and abasic sites. From the analysis of the steady-state titration curves, we evaluated that $[Ru(bpy)_2(BNIQ)]^{2+}$ has similar intrinsic emissivity when bound to a well-matched or mismatched site (1.36, 1.42, and 1.46 for well-matched, CC, and abasic sequences, respectively) relative to free complex. Thus, the inherent brightness of a complex bound to a mismatch site or a well-matched site are rather similar, and the dramatic differences in steady-state emission intensities observed are correlated with the higher affinity of the compound towards the destabilized base pairs.

3.3.4 Time-Resolved Luminescence of $[Ru(bpy)_2(BNIQ)]^{2+}$ with and Without DNA

In order to confirm the steady-state behavior, we studied the luminescence lifetimes of $[Ru(bpy)_2(BNIQ)]^{2+}$ in the presence of the three DNA duplexes (Table 3.2). The 700 nm emission of free complex decays as a monoexponential function with a lifetime of 215 ns in water. In the presence of 2 equivalents of the well-matched sequence, this emission decays as a biexponential with short (235 ns) and long (487 ns) components. The shorter component, which contributes approximately 75% to the overall decay, we assign to free complex in solution. The longer component, responsible for the other 25% of the decay, is thus attributed to the complex bound to DNA. In the presence of 2 equivalents of the mismatched sequence, the emission decays mono-exponentially with a lifetime of 416 ns. A comparable single lifetime of 421 ns is found in the presence of 2 equivalents of the abasic duplex.

Table 3.2. $[Ru(bpy)_2(BNIQ)]^{2+}$ Emission Lifetimes in Various Solvents and in the Presence of Well-Matched, Mismatched, and Abasic DNA Duplexes[a]

	Lifetime (ns)
Milli-Q H_2O	215
Buffer[b]	217
D_2O	389
CH_3CN (anhydrous)	265
Well-matched	235 (75%) 487 (25%)
Mismatched	416
Abasic	421

[a] λ_{ex} = 460 nm, λ_{em} = 700 nm. For studies with DNA, samples containing 6 μM Ru and 12 μM DNA were prepared in 5 mM Tris, 200 mM NaCl, pH 7.5 using DNA sequences shown in Figure 3.4. Percentages reflect the relative contributions of each lifetime to the overall decay. [b] 5 mM Tris, 200 mM NaCl, pH 7.5.

Two important conclusions can be drawn from these measurements. First, the absence of a short lifetime component with the mismatched or abasic sequences indicates that the complex is fully bound to the DNA duplex, which is in agreement with the evaluated binding affinities, based on which only 3% of the complex remains free in solution. Second, the lifetimes seen with the

mismatched and abasic sequence are close to the long component observed with the well-matched sequence. As expected from the analysis of the steady-state titrations, the lifetimes associated with complex bound to DNA for well-matched, mismatched, and abasic sites are similar. Thus, the mono-exponential decay in the 416 and 421 ns lifetimes should correspond to an average de-excitation process of complexes bound to DNA (well-matched and mismatched/abasic) and the small population of free complex in solution. These data support the conclusion that the brighter steady-state emission spectra observed with the mismatched and abasic duplexes (Figure 3.4) are due primarily to a higher binding affinity towards the destabilized sites compared to well-matched base pairs.

To elucidate the mechanism that gives rise to the enhanced luminescence observed with the duplexes, the emission lifetimes of $[Ru(bpy)_2(BNIQ)]^{2+}$ were further characterized in several solvent systems (Table 3.2). Interestingly, in anhydrous acetonitrile, the emission lifetime (265 ns) is only 50 ns longer than the lifetime in water. Thus, water itself does not dramatically quench the luminescence of $[Ru(bpy)_2(BNIQ)]^{2+}$. Nevertheless, upon interacting with DNA, the solvation sphere around the complex is greatly altered; in the restricted environment bound to DNA there is reduced dissipation of energy from the excited complex to solvent through vibrational modes. The importance of the non-radiative decay *via* vibrational relaxation can be probed using deuterated solvent. The effect of solvent deuteration on the emission of $[Ru(bpy)_3]^{2+}$ was first investigated by Watts and Van Houten, and it was found that deuteration of H_2O leads to a doubling of the $[Ru(bpy)_3]^{2+}$ emission lifetime (0.58 to 1.02 μs at 25°C).[20,21] It was proposed that the ability of the solvent vibrational modes to deactivate the ruthenium excited state was attenuated upon solvent deuteration. For $[Ru(bpy)_2(BNIQ)]^{2+}$, a similar phenomenon is occurring, since a significantly longer lifetime for the complex in D_2O (389 ns, Table 3.2) compared to water is detected. This

longer component is more consistent with the longer lifetime detected for complexes bound to DNA. One could also argue that the increase in luminescence lifetime for $[Ru(bpy)_2(BNIQ)]^{2+}$ when bound to DNA is due to greater rigidity and lower frequency of collisions compared to free complex in solution.[22] A combination of these factors could give rise to the enhanced luminescence observed upon DNA binding.

3.3.5 $[Ru(bpy)_2(BNIQ)]^{2+}$ Luminescence with Different Base Mismatches

Owing to the large size of the BNIQ ligand and the observation that $[Ru(bpy)_2(BNIQ)]^{2+}$ preferentially targets mismatched and abasic sites in DNA, we hypothesize that the complex binds to these defects by metalloinsertion. To test this hypothesis, we investigated whether $[Ru(bpy)_2(BNIQ)]^{2+}$ is capable of targeting other types of mismatches in addition to the CC mismatch. An important characteristic of metalloinsertors is that the extent of mismatch binding correlates with the thermodynamic destabilization associated with the mismatch; the more destabilized the mismatch, the easier it is to displace the mismatched bases by the inserted ligand.[5] Thus for luminescent metalloinsertors, we anticipate that the more destabilized the mismatch, the tighter the binding of the complex and the larger the observed emission enhancement.[23,24,25]

Luminescence titrations were performed with $[Ru(bpy)_2(BNIQ)]^{2+}$ and hairpin oligonucleotides containing the variable base pair XY (Figure 3.5). Indeed, we detect the greatest emission in the presence of the most destabilized mismatch, CC. Additionally, little emission enhancements are seen for the well-matched GC and GG mismatched hairpins. This small change is to be expected, given that G-containing mismatches are similar in stability to well-matched base pairs.[26,27] However, we note a few variations with respect to the predicted trend of mismatch instability and luminescence enhancement. $[Ru(bpy)_2(BNIQ)]^{2+}$ exhibits a brighter emission in the

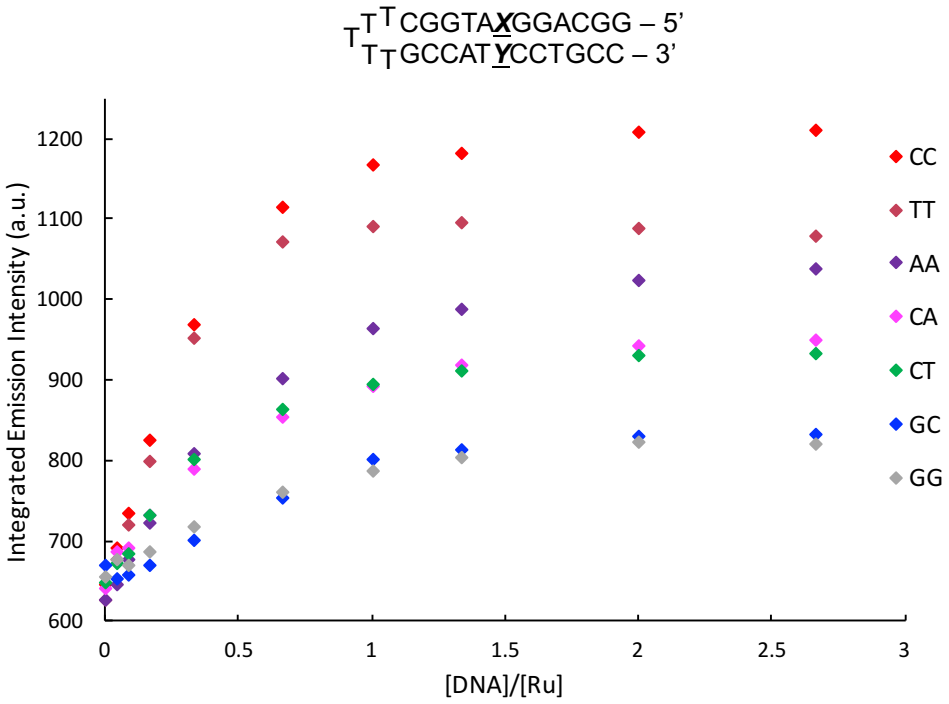

Figure 3.5. Steady-state emission titrations of $[Ru(bpy)_2(BNIQ)]^{2+}$ with DNA hairpins containing a variable XY base pair at 25°C. λ_{ex} = 440 nm, [Ru] = 4 μM. [DNA] reflects concentration of full sequence. Samples were prepared in 5 mM Tris, 50 mM NaCl, pH 7.5. Emission spectra were integrated from 590-850 nm.

presence of the "like-with-like" base mismatches AA and TT relative to CT and CA, even though we expect CT and CA to be more destabilized compared to AA and TT.[26] Nonetheless, the emission of $[Ru(bpy)_2(BNIQ)]^{2+}$ is clearly sensitive to the identity of the single base mismatch, consistent with binding through metalloinsertion.

3.3.6 Luminescence Quenching with $Cu(phen)_2^{2+}$

To further elucidate the binding mode of $[Ru(bpy)_2(BNIQ)]^{2+}$ at the mismatch site, we employed the quencher $Cu(phen)_2^{2+}$, which binds in the DNA minor groove[28,29,30] and has been used to selectively quench the luminescence of ruthenium complexes bound to a mismatch in the minor groove.[23,31] We applied the $Cu(phen)_2^{2+}$ quencher to samples containing $[Ru(bpy)_2(BNIQ)]^{2+}$ with the well-matched and mismatched duplexes (Figure 3.6). For the mismatched sample, as the concentration of $Cu(phen)_2^{2+}$ is increased, we observe quenching of the

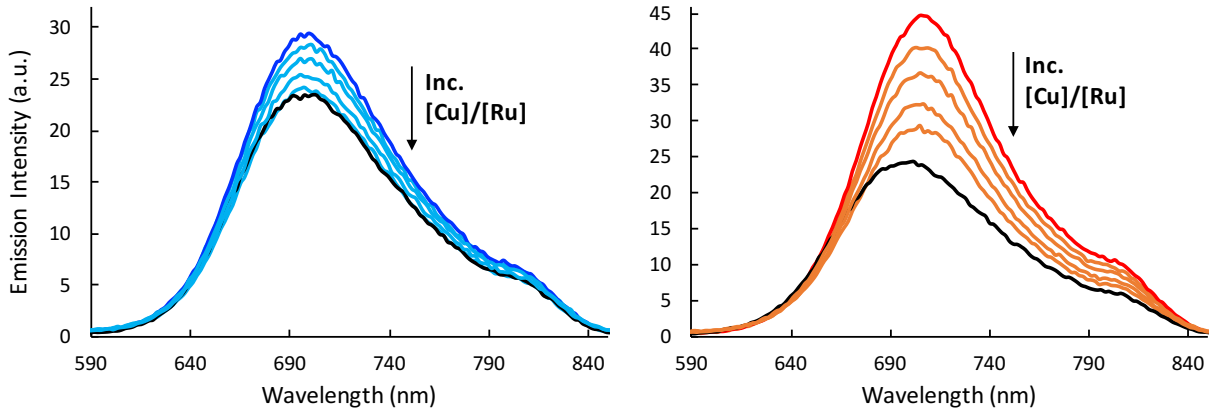

Figure 3.6. Steady-state emission spectra of $[Ru(bpy)_2(BNIQ)]^{2+}$ (4 μM) with well-matched (blue) and mismatched (red) DNA duplexes (12 μM) at 25°C. $Cu(phen)_2^{2+}$ was added to the samples such that [Cu]/[Ru] = 6, 12, 24, and 36 (indicated in light blue for well-matched and orange for mismatched samples). Black lines represent samples of Ru in the absence of DNA or Cu. λ_{ex} = 440 nm. Samples were prepared in 5 mM Tris, 200 mM NaCl, pH 7.5. DNA sequences shown in Figure 3.4 were used.

luminescence of the ruthenium complex. This quenching suggests that the complex binds to the mismatch in the minor groove, consistent with metalloinsertion. Interestingly, the enhanced emission associated with binding to the well-matched duplex also decreases as $Cu(phen)_2^{2+}$ is added. In fact, one can see that at the highest [Cu]/[Ru] for the well-matched DNA sample, the emission spectrum overlays precisely with the spectrum corresponding to free ruthenium (Figure 3.6). Given the very low binding affinity of $[Ru(bpy)_2(BNIQ)]^{2+}$ towards well-matched base pairs ($7.3 \times 10^3\ M^{-1}$) compared to the CC mismatch ($3.5 \times 10^6\ M^{-1}$), the observed decrease in emission intensity with the well-matched sample is likely a reflection of excess $Cu(phen)_2^{2+}$ displacing the weakly associated ruthenium complex from well-matched sites in the duplex to yield free ruthenium complex in solution. This result suggests that $[Ru(bpy)_2(BNIQ)]^{2+}$ interacts with well-matched sites from the minor groove.

3.3.7 Luminescence Quenching with $[Fe(CN)_6]^{3-}$

We have proposed that $[Ru(bpy)_2(BNIQ)]^{2+}$ binds to the mismatch site *via* metalloinsertion. Therefore, we predict that at the mismatch, the complex is bound deeper and

more tightly compared to well-matched sites. We used $[Fe(CN)_6]^{3-}$ to quench the emission of $[Ru(bpy)_2(BNIQ)]^{2+}$ when bound to the well-matched and mismatched duplexes (Table 3.3, Figure 3.7). $[Fe(CN)_6]^{3-}$, an anionic quencher, is repelled by the negatively charged phosphate backbone of the DNA.[32] As such, its ability to quench $[Ru(bpy)_2(BNIQ)]^{2+}$ will be dictated by how well the ruthenium complex is protected by the DNA duplex.

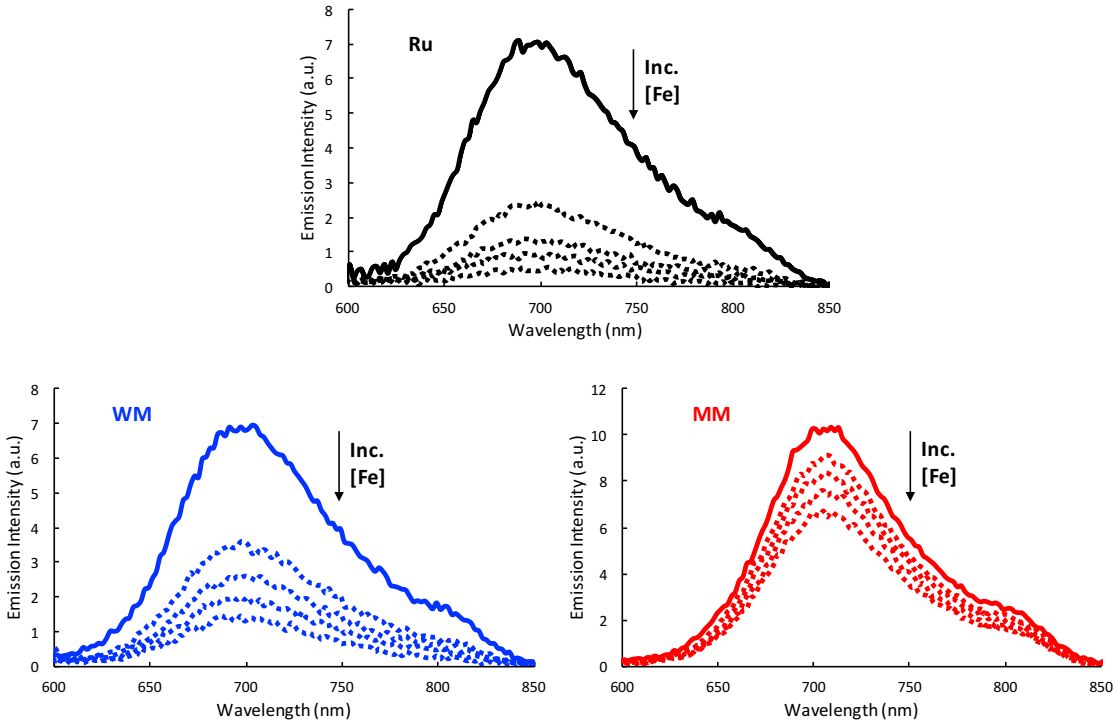

Figure 3.7. Ferricyanide quenching of free $[Ru(bpy)_2(BNIQ)]^{2+}$ (black) and in the presence of well-matched DNA (blue) and mismatched DNA (red). Ferricyanide was added (dotted lines) to concentrations of 1.2, 2.3, 3.5, and 5.6 mM. [Ru] = 2 μM, [DNA] = 4 μM, λ_{ex} = 440 nm. Samples were prepared in 5 mM Tris, 200 mM NaCl, pH 7.5 at 25°C.

As expected, $[Fe(CN)_6]^{3-}$ dramatically quenches the emission lifetime of free $[Ru(bpy)_2(BNIQ)]^{2+}$ in solution (Table 3.3); we also observe quenching in the steady-state spectra (Figure 3.7). In the presence of the well-matched duplex, the shorter lifetime component is nearly eliminated, consistent with quenching of free ruthenium. We also see that the steady-state emission intensity for the well-matched sample is significantly quenched (Figure 3.7). Conversely, the

longer component is quenched by over 50%. This differential quenching of the two lifetime components reveals that binding to well-matched sites does in fact protect the complex from quenching and likely occurs through intercalation.

Table 3.3. $[Ru(bpy)_2(BNIQ)]^{2+}$ Emission Lifetimes in the Presence and Absence of $[Fe(CN)_6]^{3-}$ Quencher[a]

	[Fe] = 0 mM	[Fe] = 8 mM
Free Ru	215	9
Well-matched	235 (75%), 487 (25%)	24 (40%), 215 (60%)
Mismatched	416	335

[a]Samples containing 6 μM Ru and 12 μM DNA were prepared in 5 mM Tris, 200 mM NaCl, pH 7.5 using DNA sequences shown in Figure 3.4. λ_{ex} = 460 nm, λ_{em} = 700 nm. Percentages reflect the relative contributions of each lifetime to the overall decay. $K_3[Fe(CN)_6]_{(aq)}$ was added to a final concentration of 8 mM.

Importantly, we observe that the emission lifetime associated with binding to the mismatched site is quenched to a much lesser extent compared to well-matched binding, which is also evident from the steady-state $[Fe(CN)_6]^{3-}$ quenching. This observation illustrates that the complex is bound deeply at the mismatched site and is less accessible to the quencher. This result supports the notion that compared to well-matched sites, the complex binds to destabilized sites through an alternate binding mode, ostensibly metalloinsertion.

3.3.8 Model for $[Ru(bpy)_2(BNIQ)]^{2+}$ Binding to the Destabilized DNA Mismatch

Figure 3.8 illustrates our model for binding by $[Ru(bpy)_2(BNIQ)]^{2+}$ to a destabilized mismatch site. We propose that the complex binds by metalloinsertion. Based upon the increase in excited state lifetime, the BNIQ ligand is deeply inserted into the helix, and the Cu titrations suggest binding occurs from the minor groove side. Consistent with the relative thermodynamics in binding different mismatches, binding of the complex is by metalloinsertion with extrusion of the destabilized mismatched bases.

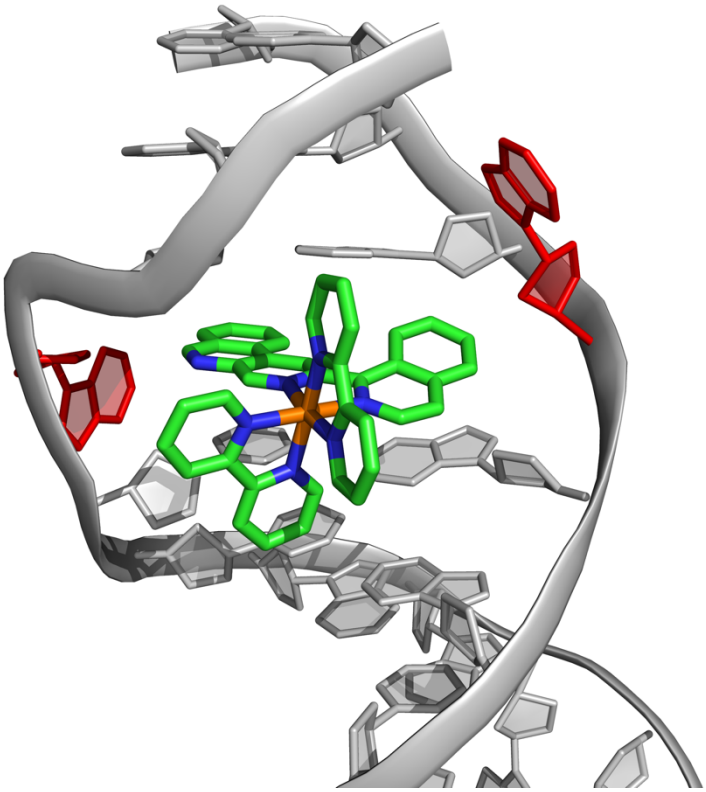

Figure 3.8. Model of $[Ru(bpy)_2(BNIQ)]^{2+}$ bound to a mismatch *via* metalloinsertion. Consistent with other metalloinsertors, we propose that the large BNIQ ligand is capable of extruding the destabilized bases (red) from the DNA π-stack and inserting deeply into the helix. The $[Ru(bpy)_2(BNIQ)]^{2+}$ structure was generated in Spartan 14 (Wavefunction, Inc.) and modeled into the X-ray crystal structure of $[Rh(bpy)_2(chrysi)]^{3+}$ bound to an AA mismatch (PDB: 3GSK) using PyMOL.

The structure for the $[Ru(bpy)_2(BNIQ)]^{2+}$ complex illustrated in Figure 3.8 was generated in Spartan 14 (Wavefunction, Inc.), since a crystal structure of the compound was not obtained. This model of the $[Ru(bpy)_2(BNIQ)]^{2+}$ complex revealed that the BNIQ ligand is not entirely planar, owing to steric clashing between hydrogen atoms of the 2- and 3-ring systems of the ligand. The close proximity of these hydrogen atoms can be easily visualized in a space-filling model of the complex (Figure 3.9), in which the ligand must buckle in order to alleviate interactions between these hydrogen atoms. This phenomenon is consistent with a complex previously reported in the literature, $[Ru(bpy)_2(1,1'\text{-biisoq})]^{2+}$ (Figure 3.9).[33,34] A crystal structure of this compound established that the 1,1'-biisoquinoline ligand is nonplanar due to steric interactions between

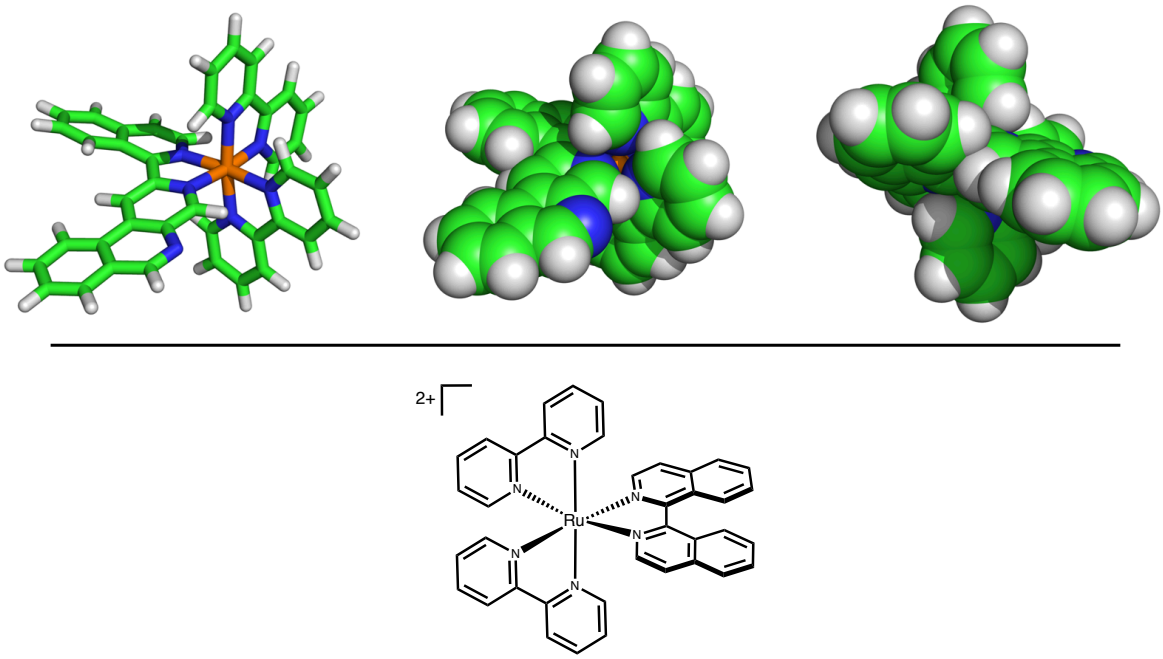

Figure 3.9. (*Top*) $[Ru(bpy)_2(BNIQ)]^{2+}$ model (Spartan 14). Space-filling representations of the complex reveal that hydrogen atoms on the 2- and 3-ring systems of the BNIQ ligand lie in very close proximity, and thus the ligand must buckle to alleviate steric strain. (*Bottom*) A previously reported crystal structure of $[Ru(bpy)_2(1,1'\text{-biisoq})]^{2+}$ showed that the 1,1'-biisoquinoline ligand is not planar due to steric clashing between hydrogen atoms on both sides of the ligand, as depicted in the drawing above.

hydrogens on neighboring ring systems.[34] Owing to the similarities between this ligand and BNIQ, $[Ru(bpy)_2(1,1'\text{-biisoq})]^{2+}$ was synthesized and its luminescent properties with DNA were investigated. The 1,1'-biisoquinoline ligand was synthesized *via* the Ni-catalyzed homocoupling of 1-iodoisoquinoline as reported previously,[13,14] and coordinated to ruthenium in an analogous fashion to BNIQ (Scheme 3.2).

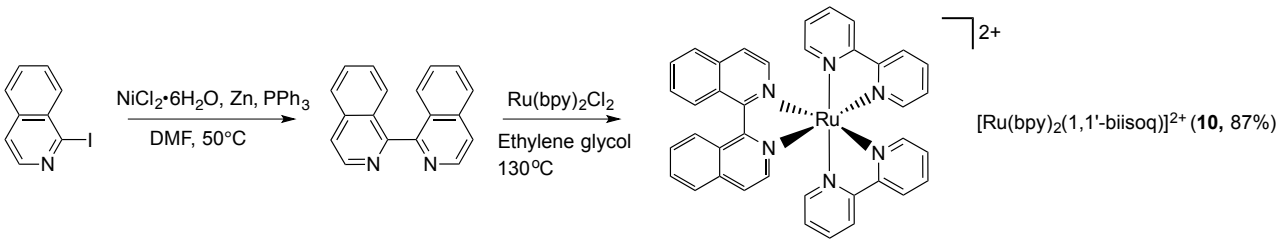

Scheme 3.2. Synthesis of $[Ru(bpy)_2(1,1'\text{-biisoq})]^{2+}$ (**10**) from 1-iodoisoquinoline.

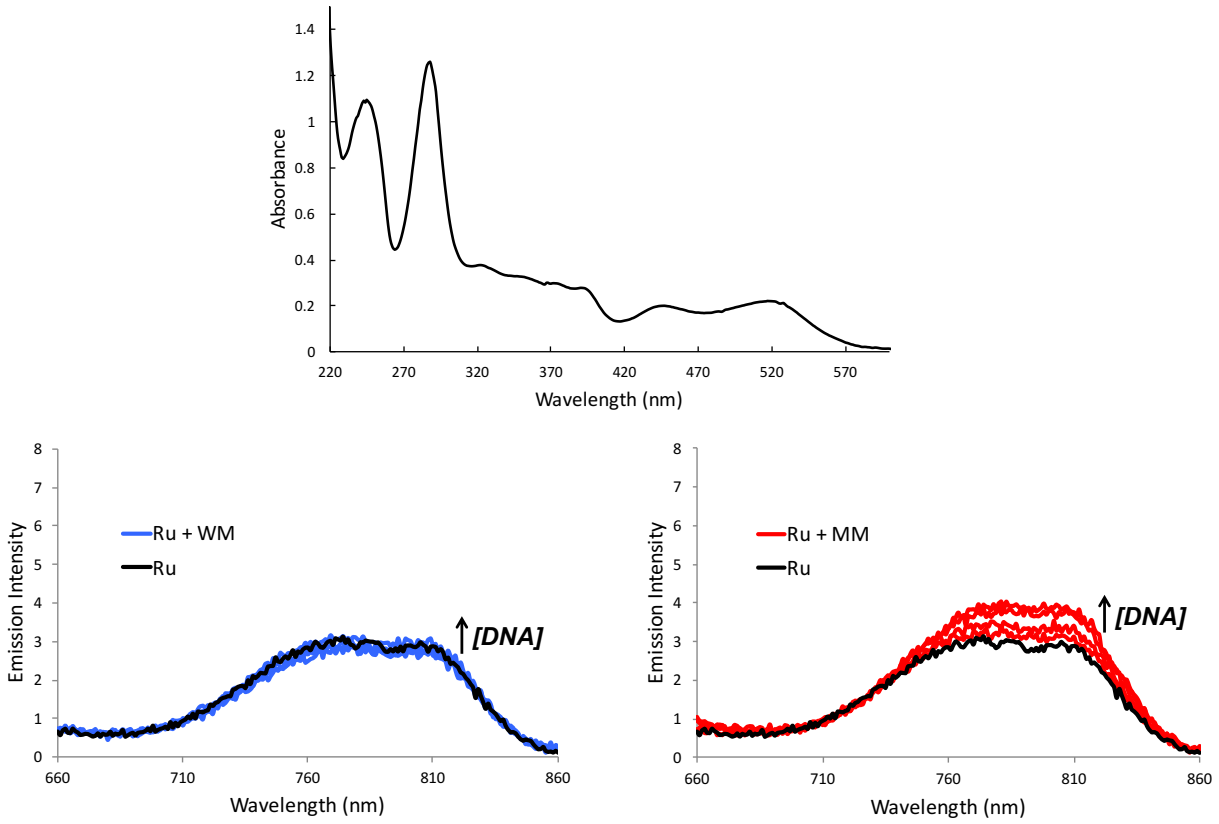

Figure 3.10. (*Top*) UV-Visible spectrum of $[Ru(bpy)_2(1,1'\text{-biisoq})]^{2+}$ (H_2O). (*Bottom*) Steady-state emission of $[Ru(bpy)_2(1,1'\text{-biisoq})]^{2+}$ with increasing concentrations of well-matched (blue) and mismatched (red) DNA duplexes at 25°C. λ_{ex} = 460 nm. [DNA] reflects increasing concentration of full sequence from 0 to 6 μM. Samples were prepared in 5 mM Tris, 50 mM NaCl, pH 7.5. DNA sequences shown in Figure 3.4 were used.

The UV-Visible spectrum of $[Ru(bpy)_2(1,1'\text{-biisoq})]^{2+}$ is presented in Figure 3.10, and shows a significantly red-shifted absorption profile relative to $[Ru(bpy)_2(BNIQ)]^{2+}$. Upon excitation at either 445 nm or 517 nm, the complex exhibits a very weak, low-energy emission centered at 780 nm. Upon addition of the well-matched 27-mer DNA duplex, there is no change in the emission intensity; however, in the presence of the 27-mer duplex containing the single CC mismatch, a small increase in emission intensity is observed. This trend was confirmed in excited-state lifetime measurements (Table 3.4), in which the lifetime essentially doesn't change with the well-matched sequence but increases by ca. 30 ns with the mismatch. The severe non-planarity of

Table 3.4. $[Ru(bpy)_2(1,1'\text{-biisoq})]^{2+}$ Emission Lifetimes in the Absence and Presence of Well-Matched and Mismatched 27-mer DNA Duplexes[a]

	Ru alone	Ru + WM	Ru + MM
Lifetime (ns)	54	60	88

[a]Samples containing 7 μM Ru, 7 μM DNA (5 mM Tris, 50 mM NaCl, pH 7.4) were prepared (λ_{ex} = 355 nm, λ_{em} = 785 nm). Emission decays were fit to a monoexponential function.

1,1'-biisoquinoline must break the aromaticity of its core bipyridine, resulting in an extremely weak emission intensity relative to, say, $[Ru(bpy)_3]^{2+}$ or even $[Ru(bpy)_2(BNIQ)]^{2+}$. This buckling of the 1,1'-biisoquinoline ligand may also disfavor intercalation at well-matched sites because the ligand cannot stack well between base pairs. However, the observation that the excited state lifetime of $[Ru(bpy)_2(1,1'\text{-biisoq})]^{2+}$ is enhanced with the mismatched sequence implies that the compound is capable of binding to the mismatch; this binding must stabilize the complex in a more rigid orientation, enhancing its emission lifetime. These observations can be taken to gain a firmer understanding of $[Ru(bpy)_2(BNIQ)]^{2+}$ binding to DNA. The non-planarity of BNIQ must play a role in disfavoring intercalation between well-matched base pairs, yet still allow for $[Ru(bpy)_2(BNIQ)]^{2+}$ to undergo metalloinsertion at a mismatch.

3.4 Conclusions

$[Ru(bpy)_2(BNIQ)]^{2+}$ is a novel luminescent complex that exhibits an enhanced emission in the presence of a DNA mismatch or abasic site relative to well-matched base pairs. Owing to the sterically expansive BNIQ ligand, $[Ru(bpy)_2(BNIQ)]^{2+}$ is highly selective in binding towards these defect sites, and we propose that the complex binds to these regions *via* metalloinsertion. Remarkably, the binding is highly specific for the mismatched site given the 500-fold increase in binding affinity versus well-matched duplex DNA. This work illustrates that the design of novel sterically demanding ligands is a valid approach in the development of mismatch-specific coordination complexes.

References

1. Boyle, K.M; Barton, J.K. *Inorg. Chim. Acta.* **2016**, *452*, 3-11.

2. Granzhan, A.; Kotera, N.; Teulade-Fichou, M.-P. *Chem. Soc. Rev.* **2014**, *43*, 3630-3665.

3. Zeglis, B.M.; Pierre, V.C.; Kaiser, J.T.; Barton, J.K. *Biochemistry* **2009**, *48*, 4247-4253.

4. Pierre, V.C.; Kaiser, J.T.; Barton, J.K. *Proc. Natl. Acad. Sci. U.S.A.* **2007**, *104*, 429-434.

5. Jackson, B.A.; Barton, J.K. *Biochemistry* **2000**, *39*, 6176-6182.

6. Komor, A.C.; Schneider, C.J.; Weidmann, A.G.; Barton, J.K. *J. Am. Chem. Soc.* **2012**, *134*, 19223-19233.

7. Komor, A.C.; Barton, J.K. *J. Am. Chem. Soc.* **2014**, *136*, 14160-14172.

8. Juris, A. et al. *Coord. Chem. Rev.* **1988**, *84*, 85-277.

9. Ruba, E.; Hart, J. R.; Barton, J. K. *Inorg. Chem.* **2004**, *43*, 4570–4578.

10. Zeglis, B. M.; Barton, J. K. *Inorg. Chem.* **2008**, *47*, 6452–6457.

11. Sullivan, B.P.; Salmon, D.J.; Meyer, T.J. *Inorg. Chem.* **1978**, *17*, 3334-33341.

12. Hughes, R. O. et al. *J. Med. Chem.* **2010**, *53*, 2656-2600.

13. Dai, L. et al. *J. Chem. Soc., Chem. Commun.* **1987**, 1760-1762.

14. Tiecco, M. et al. *Synthesis* **1984**, 736-738.

15. Dempsey, J. L.; Winkler, J. R.; Gray, H. B. *J. Am. Chem. Soc.* **2010**, *132*, 1060−1065.

16. McConnell, A.J.; Lim, M.H.; Olmon, E.D.; Song, H.; Dervan, E.E.; Barton, J.K. *Inorg. Chem.* **2012**, *51*, 12511-12520.

17. Qiujiang, D. *Chemical Industry Times* **2005**, *2*, 39-40.

18. Luzung, M.R.; Patel, J.S.; Yin, J. A. *J. Org. Chem.* **2010**, *75*, 8330-8332.

19. Milne, J.E.; Buchwald, S.L. *J. Am. Chem. Soc.* **2004**, *126*, 13028-13032.

20. Van Houten, J.; Watts, R.J. *J. Am. Chem. Soc.* **1975**, *97*, 3843-3844.

21. Van Houten, J.; Watts, R.J. *J. Am. Chem. Soc.* **1976**, *98*, 4853-4858.

22. Barton, J.K.; Danishefsky, A.T.; Goldberg, J.M. *J. Am. Chem. Soc.* **1984**, *106*, 2172-2176.

23. Boynton, A.N.; Marcelis, L.; Barton, J.K. *J. Am. Chem. Soc.* **2016**, *138*, 5020-5023.

24. Lim, M.H.; Song, H.; Olmon, E.D.; Dervan, E.E.; Barton, J.K. *Inorg. Chem.* **2009**, *48*, 5392-5397.

25. Fung, S.K. et al. *Nature Comm. 7*, **2016**, 1-9.

26. Peyret, N.; Senevirante, A.; Allawi, H.T.; SantaLucia, J. *Biochemistry* **1999**, *38,* 3468-3477.

27. SantaLucia, J.; Hicks, D. *Annu. Rev. Biophys. Biomol. Struct.* **2004**, *33*, 415-440.

28. Sigman, D.S.; Chen, C.-H.B. *Annu. Rev. Biochem.* **1990**, *59,* 207-236.

29. Sigman, D.S.; Mazumder, A.; Perrin, D.M. *Chem. Rev.* **1993**, *93*, 2295-2316.

30. Lim, M.H.; Lau, I. H.; Barton, J.K. *Inorg. Chem.* **2007**, *46*, 9528-9530.

31. Song, H.; Kaiser, J.T.; Barton, J.K. *Nat. Chem.* **2012**, *4*, 615-620.

32. Kumar, C.V.; Barton, J.K.; Turro, N.J. *J. Am. Chem. Soc.* **1985**, *107*, 5518-5523.

33. Glazer, E.C.; Tor, Y. *Angew. Chem. Int. Ed.* **2002**, *41*, 4022-4026.

34. Ashby, M.T; Govindan, G.N.; Grafton, A.K. *J. Am. Chem. Soc.* **1994**, *116*, 4801-4809.

Chapter 4

Pursuing Mismatch Specificity with Dppz Ligand Modification

4.1 Introduction

The $[Ru(Me_4phen)_2(dppz)]^{2+}$ and $[Ru(bpy)_2(BNIQ)]^{2+}$ complexes discussed in Chapters 2 and 3 represent successful efforts in the development of luminescent ruthenium(II) compounds that are mismatch-specific. $[Ru(Me_4phen)_2(dppz)]^{2+}$ makes use of its bulky Me_4phen ligands to discriminate against intercalation at well-matched sites and allow for selective metalloinsertion at a mismatch. Conversely, $[Ru(bpy)_2(BNIQ)]^{2+}$ achieves its mismatch specificity by way of the sterically expansive BNIQ ligand. Two other approaches for obtaining a mismatch-selective ruthenium complex have been explored in the Barton laboratory.[1] A series of $[Ru(bpy)_2(L)]^{2+}$ complexes were synthesized bearing the known inserting ligands chrysi, phzi, acri, or naphthi (Figure 4.1). However, it was found that these derivatives were not luminescent at ambient

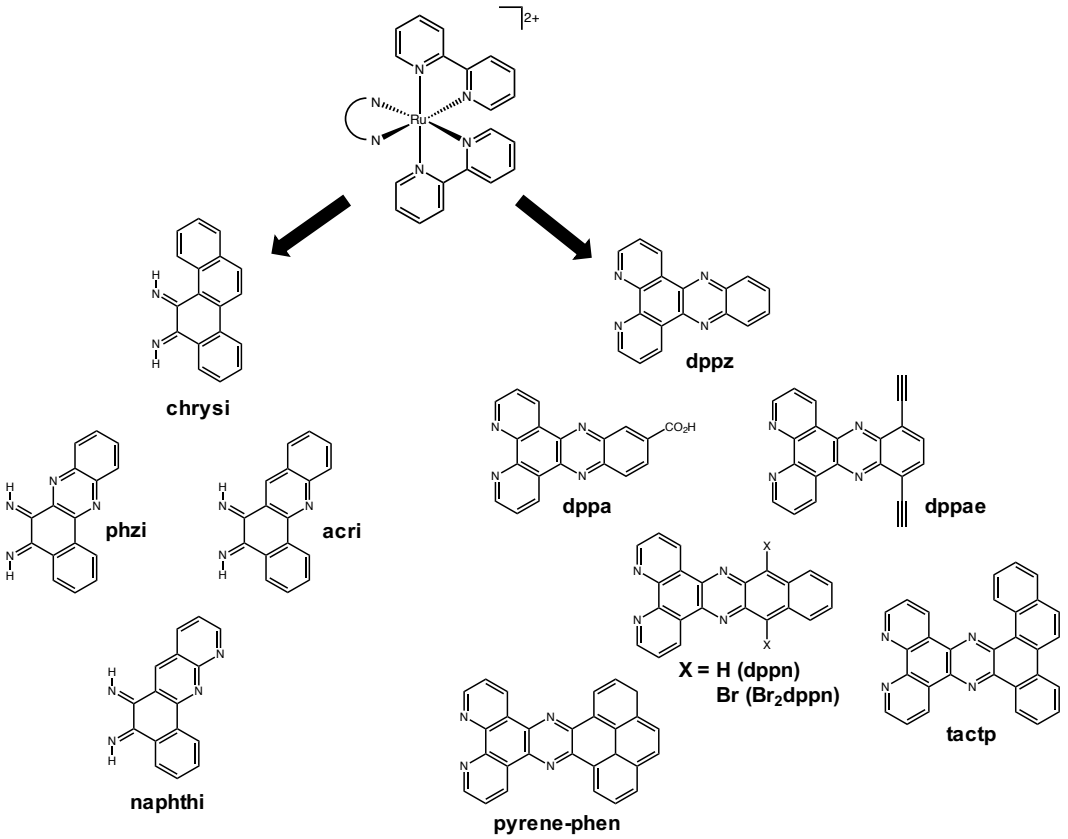

Figure 4.1. A series of $[Ru(bpy)_2(L)]^{2+}$ complexes were previously investigated as potential luminescent probes for DNA mismatches. The ligand L was either chrysi and related derivatives or a functionalized dppz.

temperature in aqueous solution – emission was only observed at 77 K. This quenching was ostensibly the result of interactions between the aqueous solvent and ligand imine protons, leading to vibrational relaxation. Another family of Ru complexes was synthesized in which the intercalating dppz ligand was modified with various functional groups (Figure 4.1). These derivatives were designed to achieve mismatch specificity by making the dppz ligand too bulky to intercalate between well-matched base pairs in DNA. However, no improvement in the luminescence differential between mismatched and well-matched DNA was met with these derivatives compared to the parent $[Ru(bpy)_2(dppz)]^{2+}$ complex. Additionally, complexes possessing extended aromatic ligands such as pyrene-phen and tactp were found to aggregate in aqueous solution. These results demonstrated that appending modifications to the distal ring of the phenazine moiety were not sufficient to prevent deep intercalation of the dppz ligand.

We hypothesized that adding functional groups to the phenanthroline portion of dppz might introduce unfavorable steric interactions with the DNA bases upon intercalating at well-matched sites in the duplex, but still allow for metalloinsertion at a mismatch. This chapter describes the synthesis and steady-state luminescence characterization of $[Ru(bpy)_2(tmdppz)]^{2+}$ (tmdppz = 3,4,7,8-tetramethyl dipyridophenazine), which incorporates methyl groups into the phenanthroline moiety of dppz in an effort to generate a mismatch-specific complex.

4.2 Experimental Protocols

4.2.1 Materials

All chemicals and starting materials were purchased from commercial vendors and used as received. $Ru(bpy)_2Cl_2$ was prepared according to the literature.[2] UV-Visible spectra were recorded on a Beckman DU 7400 UV-Visible spectrophotometer (Beckman Coulter). Oligonucleotides

were synthesized using standard phosphoramidite chemistry at Integrated DNA Technologies (Coralville, IA) and purified by HPLC using a C_{18} reverse-phase column (Varian, Inc.) on a Hewlett-Packard 1100 HPLC.

4.2.2 Synthesis

3,4,7,8-Tetramethyl-1,10-phenanthroline-5,6-dione. To a small round bottom flask was added 50 mg 3,4,7,8-tetramethyl-1,10-phenanthroline (0.21 mmol) and 10 equivalents of potassium bromide. The flask was chilled with an ice bath and ice-cold sulfuric acid (2 mL) was added slowly (dropwise) along the inner wall of the flask (*this detail is critical*). Subsequently, ice-cold nitric acid (1 mL) was also added dropwise to the mixture. The dark red-brown solution was stirred and heated to 85°C. The reaction was run for 2 h, cooled to room temperature, poured into 50 mL ice-cold DI H_2O, and neutralized to pH 6-7 with $NaHCO_3$. The aqueous layer was extracted three times with 50 mL aliquots of dichloromethane (DCM). The DCM extracts were combined and washed once with 125 mL brine and evaporated, leaving crude product. The mass of the desired product was confirmed by LC-MS (267 m/z, $[M+H]^+$).

Tetramethyl-dppz (tmdppz): To 80 mg of crude 3,4,7,8-tetramethyl-1,10-phenanthroline-5,6-dione was added 19 mg 1,2-phenylenediamine in 3 mL ethanol. The contents were brought to 80°C and stirred for 1.5 h. The reaction was removed and the ethanol was evaporated. The crude mixture was re-dissolved in 15 mL DCM, and the DCM was extracted three times with 15 mL of 0.1 M HCl. The aqueous extract, a deep red-brown, was made basic (pH ~10) with NaOH. Upon becoming basic the solution turned a cloudy yellow. The yellow precipitate was filtered through a fine glass frit. The precipitate was re-dissolved in ethanol, and the mass of the tmdppz product was confirmed by LC-MS (339 m/z, $[M+H]^+$).

[Ru(bpy)$_2$(tmdppz)]Cl$_2$. 14 mg of crude tmdppz ligand was combined with 22 mg $Ru(bpy)_2Cl_2$ in 3 mL ethylene glycol and refluxed at 130°C for 4 h. The reaction was cooled to room temperature, diluted with 3 mL H_2O, and excess NH_4PF_6 was added to crash out red-orange precipitate. The precipitate was collected in a fine glass frit and washed with 15 mL cold H_2O. The crude complex was subjected to Cl anion exchange on a Sephadex QAE resin, and subsequently purified using a Sep Pak C18 cartridge. The complex was further purified by preparatory HPLC using a gradient of 85% H_2O (containing 0.1% TFA)/15% acetonitrile to 35% H_2O/65% acetonitrile over 50 minutes. The purified complex was once again converted to its Cl salt. ESI-MS: 376 m/z $[M/2]^+$. ^{1}H NMR (500 MHz, DMSO-d_6): δ 8.84 (dd, 4 H), 8.46 (dd, 2H), 8.15 (m, 6 H), 7.87 (s, 2H), 7.73 (t, 4H), 7.55 (t, 2H), 7.37 (m, 2H), 3.37 (s, 6H), 2.38 (s, 6H).

4.2.3 Luminescence Measurements

Steady-State Luminescence. Luminescence spectra were recorded on an ISS-K2 spectrofluorometer at 25°C. $[Ru(bpy)_2(tmdppz)]^{2+}$ was excited at 440 nm. The Cl salt of the complex was used for all DNA experiments.

4.3 Results and Discussion

The goal of this work was to investigate whether appending extra steric bulk on the phenanthroline portion of the dppz ligand would help discriminate against intercalation at well-matched sites in the DNA duplex and thus favor binding to a destabilized mismatch. The ligand tmdppz (tetramethyl dipyridophenazine, Scheme 4.1) was synthesized with the intention that the added methyl groups would prevent deep intercalation of the dppz ligand. Tmdppz was synthesized from the commercially-available 3,4,7,8-tetramethyl-1,10-phenanthroline as depicted in Scheme 4.1 Following oxidation of the starting material to 3,4,7,8-tetramethyl-1,10-

phenanthroline-5,6-dione, a final condensation with 1,2-phenylenediamine yielded the desired product. The complex $[Ru(bpy)_2(tmdppz)]^{2+}$ was synthesized *via* coordination of tmdppz to

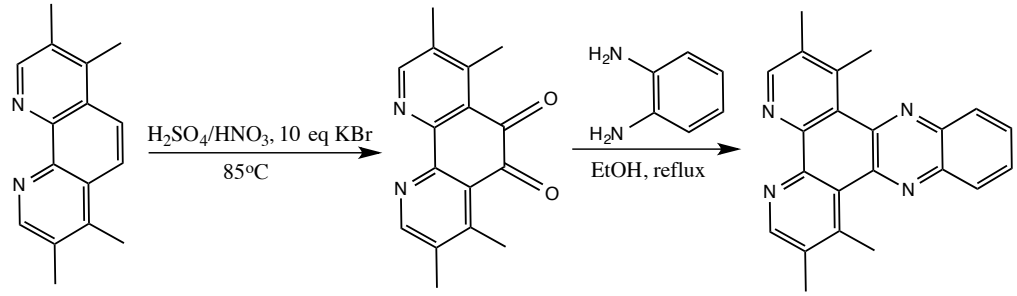

Scheme 4.1. Synthesis of tmdppz from the commercially-available 3,4,7,8-tetramethyl-1,10-phenanthroline.

$Ru(bpy)_2Cl_2$ and purified by HPLC.

$[Ru(bpy)_2(tmdppz)]^{2+}$ possesses a UV-Visible spectrum typical of $[Ru(bpy)_2(dppz)]^{2+}$ complexes (Figure 4.2): a bpy π-π* transition at 280 nm, the dppz π-π* absorption at 360-370 nm, and an MLCT transition at 440-450 nm. Interestingly, this complex is not a true "light switch" like its parent $[Ru(bpy)_2(dppz)]^{2+}$. Upon excitation in aqueous solution it does exhibit a weak emission spectrum centered at 620 nm (Figure 4.2). This observation is actually not surprising based on prior literature. R.M. Hartshorn and J.K. Barton reported a series of $[Ru(phen)_2(dppz)]^{2+}$

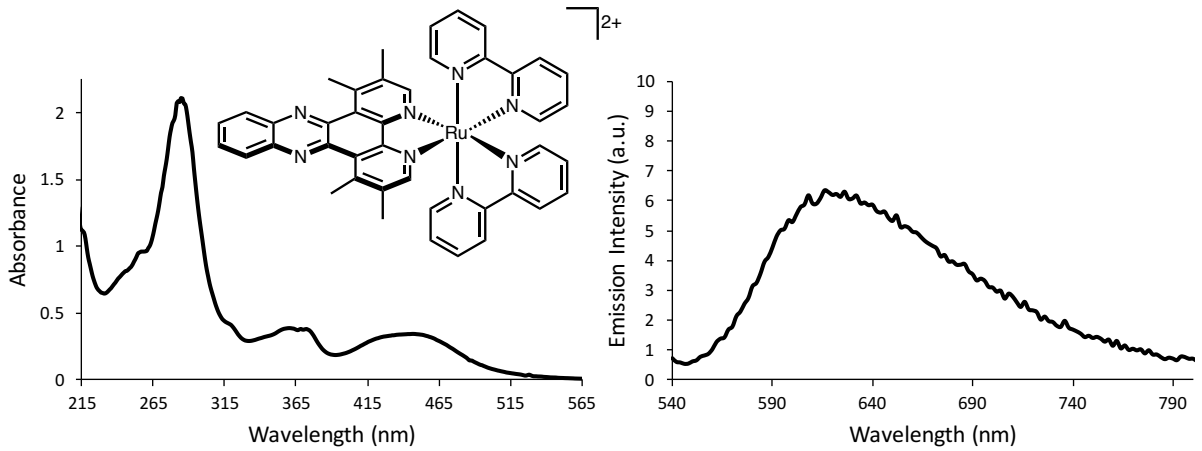

Figure 4.2. (*Left*) UV-Visible spectrum of $[Ru(bpy)_2(tmdppz)]Cl_2$ (H_2O). (*Right*) Steady-state emission spectrum of $[Ru(bpy)_2(tmdppz)]Cl_2$ (8 μM in H_2O).

derivatives bearing modifications to the dppz ligand.[3] One complex in particular, $[Ru(phen)_2(dppm2)]^{2+}$ (Figure 4.3), exhibited a weak emission in aqueous solution in the absence of DNA, albeit with a very short (~10 ns) lifetime. This observation was attributed to the methyl group on the dppm2 ligand creating a more "hydrophobic" micro-environment in the vicinity of the adjacent phenazine nitrogen atom, which likely attenuates the interactions between water and the phenazine nitrogen atom necessary for complete quenching of the excited state. N. Komatsuzaki et al.[4] reported the synthesis and characterization of the dimethyl complex $[Ru(bpy)_2(dmdppz)]^{2+}$ (Figure 4.3), which is closely related to $[Ru(bpy)_2(tmdppz)]^{2+}$. A crystal structure of $[Ru(bpy)_2(dmdppz)]^{2+}$ revealed that the methyl substituents are in close proximity to the phenazine nitrogen atoms, and the methyl carbon atoms lie very much within the same plane as the dppz framework. Interestingly, the lifetime of $[Ru(bpy)_2(dmdppz)]^{2+}$ is 27 times longer than that of $[Ru(bpy)_2(dppz)]^{2+}$ in methanol, illustrating that the increased steric environment resulting from the dmdppz methyl groups attenuates solvent interactions with the phenazine nitrogen atoms. Amazingly, the emission of $[Ru(phen)_2(dppm2)]^{2+}$ is enhanced ca. 300-fold in the presence of DNA.[3] Furthermore, it was reported that the steady-state emission intensity of

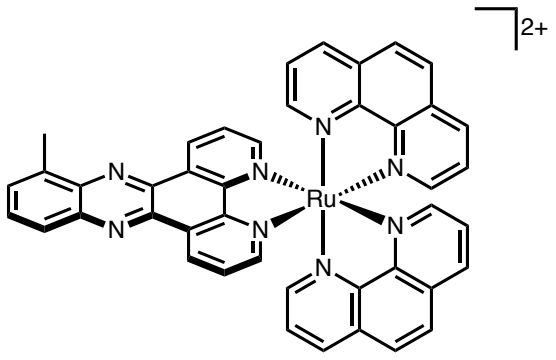

$[Ru(phen)_2(dppm2)]^{2+}$

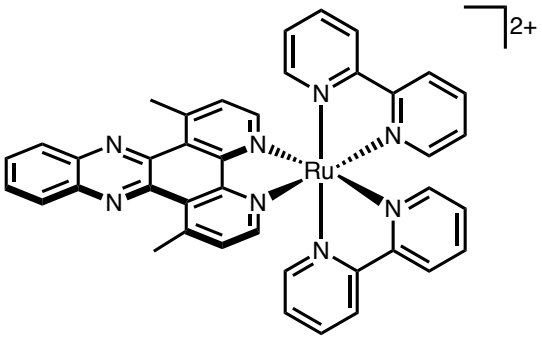

$[Ru(bpy)_2(dmdppz)]^{2+}$

Figure 4.3. Chemical structures of $[Ru(phen)_2(dppm2)]^{2+}$ (*left*) and $[Ru(bpy)_2(dmdppz)]^{2+}$ (*right*).

$[Ru(phen)_2(dppm2)]^{2+}$ with DNA was approximately 5-fold brighter than $[Ru(phen)_2(dppz)]^{2+}$ with DNA. This is attributed to the extra methyl group on dppm2 further protecting the ligand from quenching by water upon intercalation.

We thus investigated the steady-state emission of $[Ru(bpy)_2(tmdppz)]^{2+}$ in the presence of the well-matched and mismatched 27-mer DNA sequences (Figure 4.4). Remarkably, the emission intensity of the complex is enhanced almost 500-fold in the presence of the DNA duplexes. However, unlike the parent complex $[Ru(bpy)_2(dppz)]^{2+}$, which exhibits a 1.5- to 2-fold emission

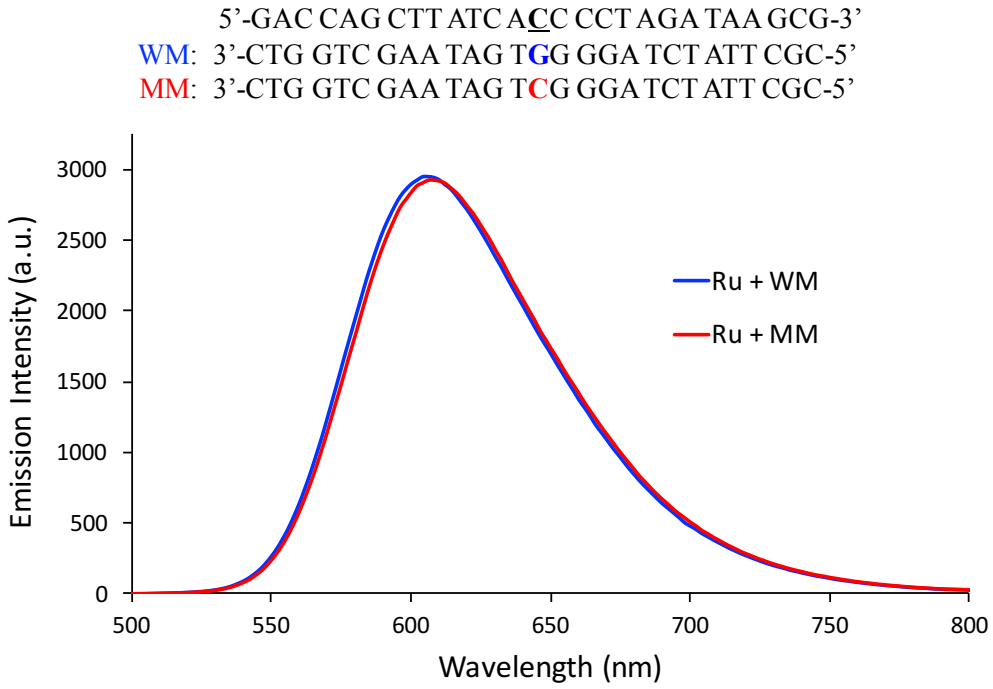

Figure 4.4. Steady-state emission spectra of $[Ru(bpy)_2(tmdppz)]Cl_2$ (8 μM) in the presence of the well-matched and mismatched DNA duplexes (8 μM, full sequence). Samples were prepared in 5 mM tris, 50 mM NaCl, pH 7.5, and excited at 440 nm.

enhancement in the presence of a CC mismatch compared to well-matched DNA, $[Ru(bpy)_2(tmdppz)]^{2+}$ exhibits comparable emission intensities in the presence of both duplexes. Two conclusions can be drawn from these observations. First, it is evident that introducing the methyl groups into the phenanthroline moiety of dppz does not inhibit intercalation into well-

matched base pairs. Second, the dramatic emission enhancement seen with the well-matched sequence suggests that once intercalated, the methyl groups of tmdppz provide substantial protection of the ligand from quenching by water. We might anticipate that the compound would bind to the mismatch through metalloinsertion, based on the evidence that $[Ru(bpy)_2(dppz)]^{2+}$ undergoes metalloinsertion at mismatched sites.[5,6] However, even if $[Ru(bpy)_2(tmdppz)]^{2+}$ does undergo metalloinsertion at the mismatch, it is evident that this binding mode does not equate to luminescence discrimination compared to intercalation at well-matched base pairs.

4.4 Conclusions

The aim of this work was to introduce steric bulk into the phenanthroline portion of the dppz ligand to discriminate against intercalation at well-matched sites in the DNA duplex. Interestingly, $[Ru(bpy)_2(tmdppz)]^{2+}$ exhibits nearly the opposite effect than what was intended, namely that any luminescence discrimination between mismatched and well-matched DNA appears to be lost. This is likely the result of the methyl substituents providing a shielding effect that attenuates the interactions between water and the phenazine nitrogen atoms. This less-efficient ability of water to quench the excited state of $[Ru(bpy)_2(tmdppz)]^{2+}$ results in dramatic emission enhancement in the presence of the DNA. Even bolder modifications to dppz might be needed to discriminate against intercalation. However, the evidence that even small changes to the dppz ligand framework can result in unfavorable alterations in the excited-state properties (such as loss of the light-switch effect) points to the conclusion that in the pursuit of mismatch selectivity, perhaps the dppz ligand is best left alone.

References

1. McConnell, A.J.; Lim, M.H.; Olmon, E.D.; Song, H.; Dervan, E.E.; Barton, J.K. *Inorg. Chem.* **2012**, *51*, 12511-12520.

2. Sullivan, B.P.; Salmon, D.J.; Meyer, T.J. *Inorg. Chem.* **1978**, *17*, 3334-33341.

3. Hartshorn, R.M.; Barton, J.K. *J. Am. Chem. Soc.* **1992**, *114*, 5919-5925.

4. Komatsuzaki, N.; Katoh, R.; Himeda, Y.; Sugihara, H.; Arakawa, H.; Kasuga, K. *J. Chem. Soc., Dalton Trans.* **2000**, 3053-3054.

5. Lim, M. H.; Song, H.; Olmon, E. D.; Dervan, E. E.; Barton, J. K. *Inorg. Chem.* **2009**, *48*, 5392–5397.

6. Song, H.; Kaiser, J. T.; Barton, J. K. *Nat. Chem.* **2012**, *4*, 615–620.

Chapter 5

Investigating the Biological Activity of Mismatch-Specific Ruthenium Metalloinsertors

Performed in collaboration with Julie Bailis and Natalie Mariano (Dept. Oncology Research, Amgen, Inc., South San Francisco).

5.1 Introduction

As discussed in Chapter 1, the Barton laboratory has developed rhodium metalloinsertors capable of targeting mismatch repair (MMR)-deficient cancers.[1,2] $[Rh(chrysi)(phen)(PPO)]^{2+}$ is highly potent towards the MMR-deficient cell line HCT116O compared to the MMR-proficient HCT116N line (EC_{50} < 500 nM, Figure 5.1). This compound inhibits DNA synthesis and induces cell death by necrosis in HCT116O cells.[3] Our research group has collaborated with Julie Bailis (Dept. Oncology Research, Amgen, Inc., South San Francisco) to investigate the mechanism of action of $[Rh(chrysi)(phen)(PPO)]^{2+}$ in the HCT116O cell line. Recent work has shown that $[Rh(chrysi)(phen)(PPO)]^{2+}$ activates a DNA damage response that leads to cell death.[4] It is proposed that upon binding to a DNA mismatch *in cellulo* through metalloinsertion, a novel lesion is created that is recognized by the cellular DNA damage response but is incapable of being repaired, thus resulting in cell death. It is possible that $[Rh(chrysi)(phen)(PPO)]^{2+}$ inserted at a

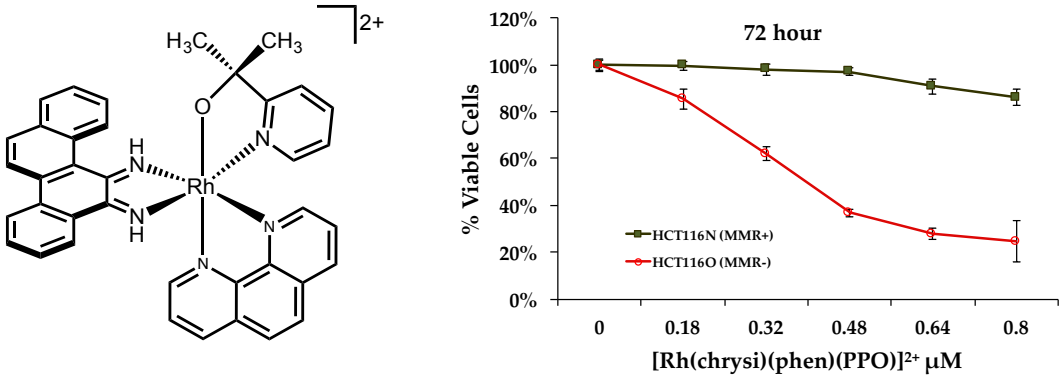

Figure 5.1. *(Left)* Structure of $[Rh(chrysi)(phen)(PPO)]^{2+}$. *(Right)* Differential cytotoxicity (as measured by the MTT assay) of the metalloinsertor towards MMR-proficient HCT116N and MMR-deficient HCT116O cell lines.

mismatch interferes with mismatch processing by repair enzymes. Interestingly, unlike cisplatin, $[Rh(chrysi)(phen)(PPO)]^{2+}$ does not appear to activate apoptosis, and instead leads to irreversible cell death likely through a necrotic pathway.[3,4]

While these metalloinsertors are promising chemotherapeutic agents directed towards MMR-deficient cancers, a complete understanding of their mechanism of action is hindered by their inability to be visualized within cells, owing to the fact that they are non-luminescent. Thus, we must rely on developing fluorescently-tagged metalloinsertors or mismatch-specific luminescent analogues. Such derivatives could serve as tools for co-localization experiments of DNA damage checkpoint and repair proteins with sites of DNA mismatches. Current work in our group is focusing on generating a fluorescently-tagged $[Rh(chrysi)(phen)(PPO)]^{2+}$ conjugate. Additionally, mismatch-specific ruthenium complexes may be useful in this context. Luminescent ruthenium polypyridyl complexes, along with other transition metal centers such as iridium, platinum, and rhenium, have seen great utility as cellular imaging agents owing to their water solubility, chemical inertness, and photostability.[5,6]

In this work, we explored the mismatch-specific ruthenium complexes discussed in Chapters 2 and 3 in a biological context. In particular, we investigated the cytotoxic activity of $[Ru(Me_4phen)_2(dppz)]^{2+}$, $[Ru(Me_2bpy)_2(dppz)]^{2+}$, and $[Ru(bpy)_2(BNIQ)]^{2+}$ in the HCT116N and HCT116O cell lines to determine whether the *in vitro* mismatch-specificity of these complexes translated to cell-selective cytotoxicity comparable to rhodium metalloinsertors. Furthermore, in a collaboration with Julie Bailis, we have conducted live- and fixed-cell imaging experiments to visualize the localization of $[Ru(Me_4phen)_2(dppz)]^{2+}$ in the HCT116N and HCT116O lines. Information gained from such experiments will be critical to see whether this compound can be a useful probe in co-localization experiments with proteins involved in the DNA damage response to mismatch binding, such as phosphorylated H2AX.

5.2 Experimental Protocols

5.2.1 Materials

Cell media and culture supplements, trypsin-EDTA (0.05%), and phosphate-buffered saline were purchased from Invitrogen (Carlsbad, CA). 24 well plates (sterilized and tissue culture-treated) for confocal microscopy were purchased from Ibidi. Reagents for cell proliferation ELISA and the MTT assay were purchased in kit format from Roche Molecular biochemical (Mannheim, Germany). Formaldehyde (for cell fixing experiments) was purchased as 16% solutions (w/v, methanol-free) in glass-sealed ampules from Thermo Scientific Pierce. Triton X-100 was purchased from Sigma. DRAQ5 was purchased as a 5 mM solution from Thermo Scientific. Ruthenium complexes (as Cl salts) were synthesized as described in Chapters 2 and 3.

5.2.2 Cell Culture

HCT116N and HCT116O cells were grown in RPMI medium 1640 with the following supplementation: 10% FBS, 2 mM L-glutamine, 0.1 mM non-essential amino acids, 1 mM sodium pyruvate, 100 units/mL penicillin, 100 μg/mL streptomycin, and 400 μg/mL Geneticin G418. Cells were grown in tissue culture flasks (Corning Costar) at 37°C under a 5% CO_2 humidified atmosphere.

5.2.3 MTT Cytotoxicity Assay

HCT116N and HCT116O cells were plated in 96-well plates (50,000 cells/well) and treated with a range of ruthenium concentrations (5 wells, or replicates, per concentration per cell line) for the desired time duration (24 to 72 hours) at 37°C humidified 5% CO_2 atmosphere. After the incubation period, MTT was added to the cells (Roche Cell Proliferation Kit I) and the cells were incubated for an additional 4 hours. Insoluble formazan crystals were dissolved in solubilizing reagent (Roche) over 24 hours (37°C, 5% CO_2, humidified atmosphere). The solubilized formazan

was quantified at 570 nm with 690 nm as the reference wavelength. Percent cell viability was calculated as a function of formazan formed in the ruthenium-treated cells relative to untreated cells.

5.2.4 Cellular Proliferation ELISA

HCT116N and HCT116O cells were plated on a 96-well plate at 2,000 cells per well and incubated at 37°C under 5% CO_2 overnight to adhere. Cells were then treated with a range of ruthenium concentrations for 72 hours. Ruthenium-containing media was removed and replaced with fresh media, and labeled with BrdU for 24 hours. BrdU incorporation was quantified by an antibody assay kit. The quantified BrdU incorporation into treated cells was normalized to untreated controls to determine the cellular proliferation at each treatment concentration.

5.2.5 Nuclear Count Assay for Cell Viability (performed at Amgen, Inc.)

Cells were plated to Perkin Elmer 96-well View Plates at 5,000 cells per well and incubated overnight. Cells were then treated with *rac*- or Δ-$[Ru(Me_4phen)_2(dppz)]^{2+}$ in a dose response fashion for 3 days. Cells were fixed in 4% formaldehyde, permeabilized with 0.5% Triton X-100 in PBS, and then stained with DAPI. The number of nuclei per well was counted using a Cellomics ArrayScan (Thermo Fisher) and used to calculate the percent viable cells relative to the number of cells from untreated samples.

5.2.6 Confocal Microscopy

For live-cell imaging, HCT116N and HCT116O cells were seeded at ca. 30,000 cells/well in 24 well confocal imaging plates from Ibidi (1.9 cm^2 growth area per well) in 1 mL media and allowed to adhere for at least several hours. Cells were then treated with a given ruthenium concentration for the desired time period. Following this incubation period, the media was removed, and each well was washed three times with 1 mL PBS. Cells were then imaged in 1 mL

PBS on a Zeiss LSM 710 Inverted NLO 33A microscope using a 20x objective and exciting the ruthenium complex with 460 nm light (Beckman Imaging Facility, Caltech).

For fixed-cell experiments, cells were seeded as described above in 24 well plates and allowed to adhere for at least several hours. Media was then removed, and cells were washed once with 1 mL PBS. The cells were then treated with 1 mL 4% formaldehyde for 10 min and washed twice with PBS, followed by treatment with 0.5% (v/v in PBS) Triton X-100 for 10 min (**note**: it is important to warm the 0.5% Triton solution to 37°C to allow Triton to fully solubilize in PBS). Cells were again washed with PBS and incubated with a 1 mL solution of ruthenium in PBS at the desired concentration for 15-20 min. For co-staining experiments with DRAQ5, cells were incubated with 5 μM DRAQ5 in PBS for 15 min.

5.3 Results and Discussion

5.3.1 Biological Activity of Ruthenium Complexes

We initially investigated whether the ruthenium complexes that exhibit mismatch specificity (as demonstrated from the *in vitro* steady-state and time-resolved luminescence experiments discussed in Chapters 2 and 3) also function as cell-selective cytotoxic agents directed towards the MMR-deficient HCT116O cells. This was first performed using the MTT assay (Figure 5.1), which assesses cell viability following treatment with a range of metal concentrations. This assay reports on cell metabolic activity based on the reduction of the MTT reagent (3-(4,5-dimethylthiazol-2-yl)-2,5-diphenyltetrazolium bromide) by mitochondrial enzymes. HCT116N and HCT116O cells were treated with *rac*-$[Ru(Me_4phen)_2(dppz)]^{2+}$, *rac*-$[Ru(Me_2bpy)_2(dppz)]^{2+}$, and *rac*-$[Ru(bpy)_2(BNIQ)]^{2+}$ for 72 hours at the concentrations indicated in Figure 5.2 below.

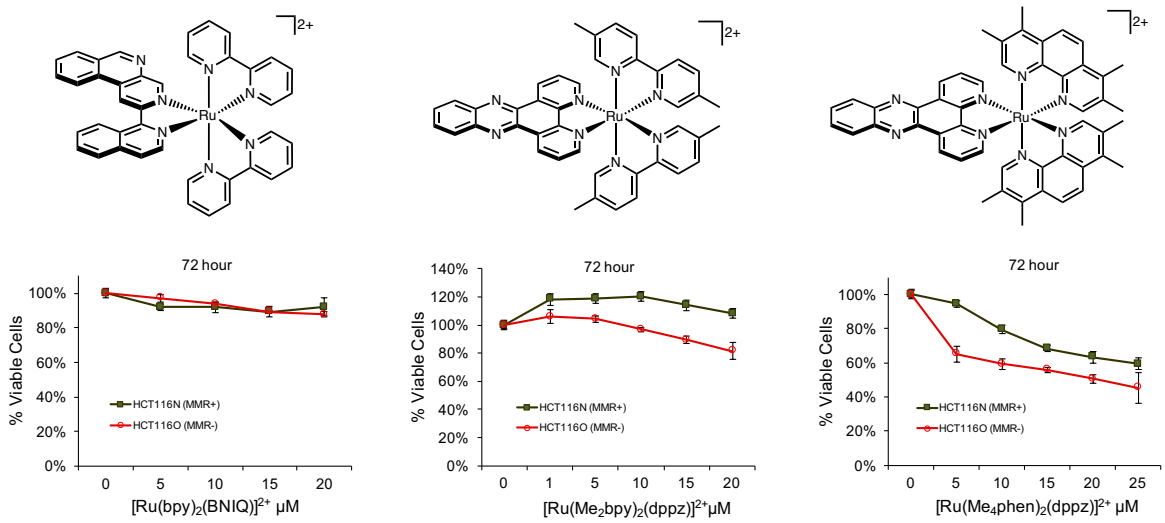

Figure 5.2. MTT assays of ruthenium complexes with HCT116N (green) and HCT116O (red) cell lines. Cells were plated in a 96-well format (5 x 10^4 cells/well) and treated with the indicated metal concentrations for 72 hours. Following this incubation period, the cells were labeled with MTT for 4 hours.

The BNIQ complex exhibits no cytotoxicity towards either cell line, and the Me_2bpy compound also shows minimal activity. The Me_4phen complex does show activity across a 5-25 μM range, and maintains some cell selectivity at concentrations below 10 μM. Compared to the other two complexes, $[Ru(Me_4phen)_2(dppz)]^{2+}$ likely benefits from increased cellular uptake. An interesting observation is that as concentrations are increased above 10 μM, the percentage of viable cells gradually levels off, which is uncharacteristic of cell-selective rhodium metalloinsertors.[1-3] Other MTT assays were performed after 24 and 48 hours of $[Ru(Me_4phen)_2(dppz)]^{2+}$ incubation, but no activity was seen compared to the 72 hour MTT shown in Figure 5.2.

Intrigued by the MTT assay results, we repeated the assay with Δ- and Λ-$[Ru(Me_4phen)_2(dppz)]^{2+}$ alongside the racemic complex (Figure 5.3). As discussed in Chapter 2, the Δ enantiomer of this complex is the isomer which imparts all mismatch selectivity. Thus, we would expect the Δ enantiomer to preferentially bind mismatches in cells and induce cell-selective

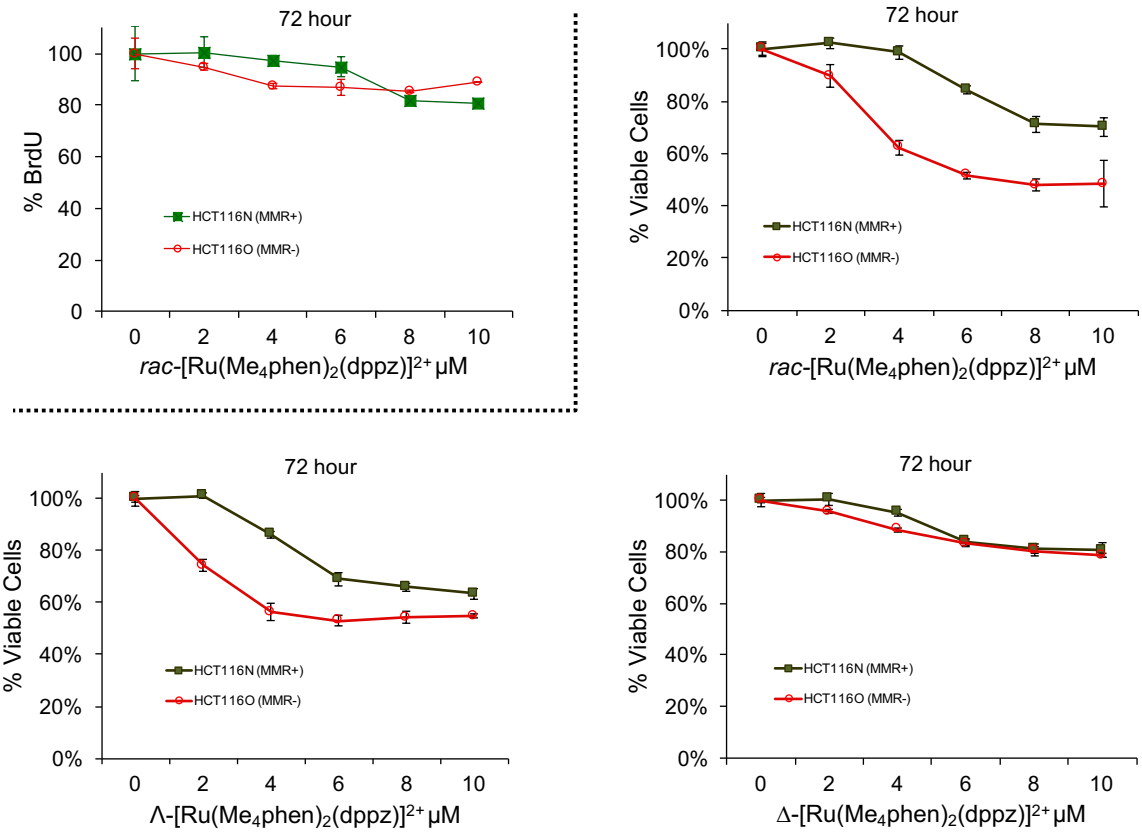

Figure 5.3. (*Top left*) Cellular proliferation assay (ELISA) for HCT116N (green) and HCT116O (red) cells treated with *rac*-$[Ru(Me_4phen)_2(dppz)]^{2+}$ with the indicated concentrations for 72 hours. Cell proliferation was quantified by BrdU incorporation during cell replication. (*Top right, bottom)* MTT assay results of *rac*-, Δ,- and Λ-$[Ru(Me_4phen)_2(dppz)]^{2+}$. Cells were plated in a 96-well format (5 x 10^4 cells/well) and treated with the indicated metal concentrations for 72 hours. Following this incubation period, the cells were labeled with MTT for 4 hours.

cytotoxicity. Interestingly, the MTT results presented in Figure 5.3 imply that the opposite is true: the Δ isomer exhibits negligible activity toward either cell line, but the Λ isomer shows some degree of cell-selective activity comparable to the racemic mixture. This is surprising, because the Λ isomer demonstrates little selectivity for mismatched DNA *in vitro* (Chapter 2). However, as discussed above, instead of the cell viability continually decreasing down to under 20% (as seen for $[Rh(chrysi)(phen)(PPO)]^{2+}$, Figure 5.1), the cell viability plateaus when treated with *rac*-$[Ru(Me_4phen)_2(dppz)]^{2+}$. Furthermore, rhodium metalloinsertors have been shown to selectively

inhibit DNA synthesis in the MMR-deficient HCT116O cell line, as measured by the ELISA assay for DNA synthesis.[1-3] This assay quantifies the effects on proliferation of the cell lines, as expressed by BrdU incorporation. For cell-selective rhodium metalloinsertors, the results of the MTT assay typically mirror those of the ELISA – that is, cell-selective inhibition of DNA synthesis correlates with cell-selective cytotoxicity.[2,3] For *rac*-$[Ru(Me_4phen)_2(dppz)]^{2+}$, we see negligible activity in the ELISA assay (Figure 5.3). This result implies that neither enantiomer is capable of cell-selective inhibition of DNA synthesis.

Given that Δ-$[Ru(Me_4phen)_2(dppz)]^{2+}$ is capable of selectively binding a mismatch *in vitro* (Chapter 2) with comparable affinity to biologically-active rhodium metalloinsertors (~10^6 M^{-1}), the lack of any activity for Δ-$[Ru(Me_4phen)_2(dppz)]^{2+}$ as measured by the ELISA or MTT assays must result from the compound's uptake and/or sub-cellular localization properties. For example, preferential localization to the mitochondria could explain the lack of cell selectivity.[2] It is also possible that the MTT assay is not the best readout for cell viability upon treatment with $[Ru(Me_4phen)_2(dppz)]^{2+}$. This point is supported by the peculiar result that Λ-$[Ru(Me_4phen)_2(dppz)]^{2+}$ does exhibit some selectivity towards HCT116O cells in the MTT assay (Figure 5.3), which is an unexpected observation because this isomer does not show any specificity for mismatched DNA *in vitro* (Chapter 2). Thus, it is unlikely that the differential activity seen for Λ-$[Ru(Me_4phen)_2(dppz)]^{2+}$ in the MTT assay actually results from the complex preferentially targeting mismatched DNA in HCT116O cells. Instead, this isomer too probably localizes to mitochondria. Perhaps Λ-$[Ru(Me_4phen)_2(dppz)]^{2+}$ partakes in non-specific binding in mitochondria and induces an altered metabolic response, giving rise to the diminished cell viability seen in Figure 5.3 upon treatment with this isomer.

An alternative assay for viability was performed with Julie Bailis (Amgen, Inc.), in which HCT116N and HCT116O cells were treated in a dose-response fashion with *rac*- and Δ-$[Ru(Me_4phen)_2(dppz)]^{2+}$ for 72 hours. Cells were then fixed with 4% formaldehyde, permeabilized with 0.5% Triton X-100, and nuclei were stained with DAPI. The number of nuclei per well were counted using a Cellomics ArrayScan (Thermo Fisher) high-content system, and the percent viable

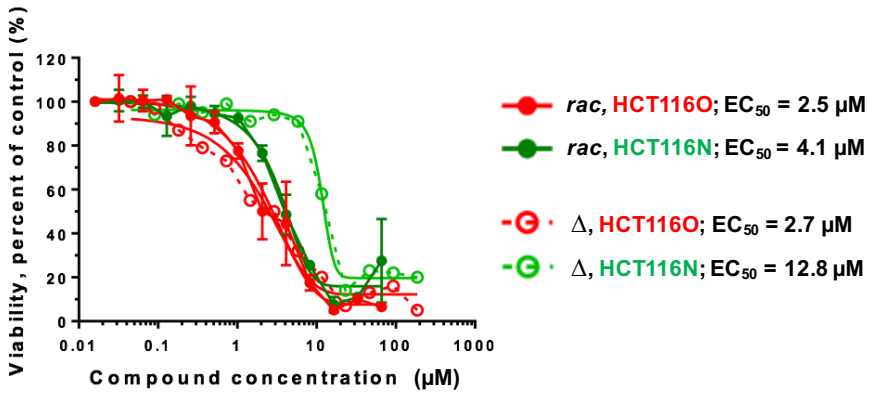

Figure 5.4. HCT116N and HCT116O cells were treated in a dose-response fashion for 72 hours with *rac*- and Δ-$[Ru(Me_4phen)_2(dppz)]^{2+}$ and cell viability was assessed by a nuclear count assay. Performed with Julie Bailis at Amgen, Inc.

cells were calculated relative to untreated cells. The results of this assay, conducted with the racemic complex and its Δ isomer, are presented in Figure 5.4. The first important observation is that in this assay, we see that cell viability is significantly diminished to <10% at the highest treatment concentrations (>50 μM), implying that this assay might be a more reliable readout of viability compared to the MTT. Second, we observe greater differential activity with the Δ isomer compared to the racemic mix. Because Δ is the isomer which exhibits mismatch specificity *in vitro* (Chapter 2), the nuclear count assay results are more consistent with mismatch-specific rhodium metalloinsertors such as $[Rh(chrysi)(phen)(PPO)]^{2+}$. However, it should be noted that the ruthenium complex is at least an order of magnitude less potent than $[Rh(chrysi)(phen)(PPO)]^{2+}$.

The discrepancy between the MTT and nuclear count assays for viability could possibly be explained in terms of $[Ru(Me_4phen)_2(dppz)]^{2+}$ localization and/or binding within the cell. C.A. Puckett studied the uptake and localization of dppz-based ruthenium complexes such as $[Ru(bpy)_2(dppz)]^{2+}$ and $[Ru(DIP)_2(dppz)]^{2+}$ (DIP = 4,7-diphenyl-1,10-phenanthroline) and found that the compounds generally exhibit uneven cytoplasmic staining with some evidence of mitochondrial localization.[7] Based on the "light switch" nature of these dppz complexes, the fact that they can be directly visualized within the cytoplasm of cells[8,9,10] signifies that they bind to cellular structures other than DNA, such as proteins or lipids. If $[Ru(Me_4phen)_2(dppz)]^{2+}$ does show significant accumulation in the mitochondria, perhaps this off-target binding could affect cellular metabolic pathways and result in a lack of selectivity in the MTT assay. The sub-cellular localization of $[Ru(Me_4phen)_2(dppz)]^{2+}$ is discussed in the following section.

5.3.2 Confocal Microscopy Imaging of $[Ru(Me_4phen)_2(dppz)]^{2+}$ in HCT116N and HCT116O Cells

Confocal imaging experiments have been conducted with $[Ru(Me_4phen)_2(dppz)]^{2+}$ in the HCT116N and HCT116O cells, both at Caltech (Beckman Imaging Facility) and with Julie Bailis and Natalie Mariano at Amgen, Inc. One could envision two potential uses for a mismatch-specific luminescent metalloinsertor. First, because Δ-$[Ru(Me_4phen)_2(dppz)]^{2+}$ exhibits a significantly brighter emission intensity when bound to a DNA mismatch compared to well-matched sites (Chapter 2), this opens up the possibility for the compound to be used as a diagnostic probe for detecting mismatches in MMR-deficient cancer cells. In theory, MMR-deficient cells accumulate a greater number of mismatches compared to MMR-proficient cells owing to a 100- to 1000-fold increase in mutation rate.[11] Second, while it has been shown that the potent, cell-selective metalloinsertor $[Rh(chrysi)(phen)(PPO)]^{2+}$ activates a DNA damage response in HCT116O cells, it is not yet known which specific proteins are involved in this response pathway. A mismatch-

specific luminescent metalloinsertor could help answer this question, because it would allow us to investigate the co-localization of the luminescent probe with fluorescently-labeled proteins that might be involved in the DNA damage response, such as phosphorylated H2AX (pH2AX), *via* fluorescence microscopy.

We first explored whether $[Ru(Me_4phen)_2(dppz)]^{2+}$ could be utilized as a diagnostic probe to preferentially detect mismatches in MMR-deficient cells by conducting microscopy imaging experiments in fixed HCT116N and HCT116O cells (Figure 5.5). DRAQ5, a nuclear co-stain (shown as red in Figure 5.5), clearly stains the nuclei of the cells. $[Ru(Me_4phen)_2(dppz)]^{2+}$ (Figure

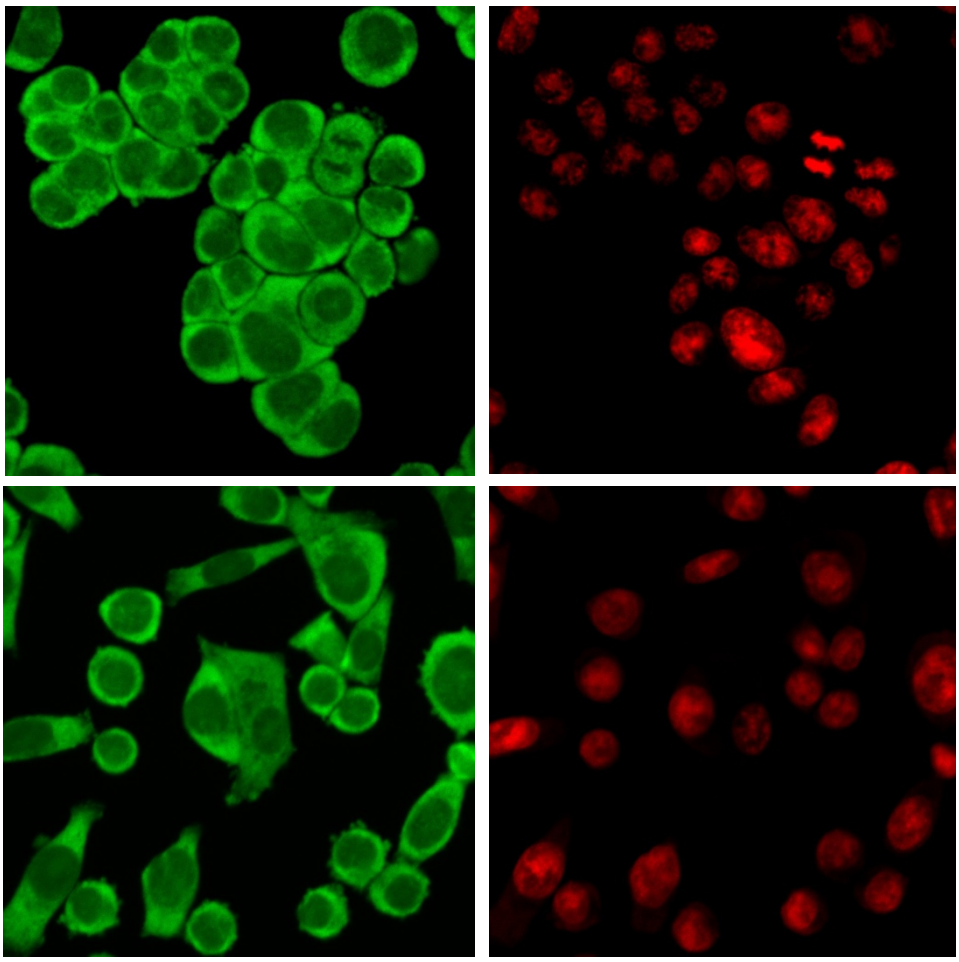

Figure 5.5. Fixed-cell images of *rac*-$[Ru(Me_4phen)_2dppz]^{2+}$ with HCT116N (top row) and HCT116O (bottom row) lines. Cells were fixed with 4% formaldehyde, permeabilized with 0.5% Triton X-100, and incubated with 10 μM Ru and 5 μM DRAQ5 for 15 min. Ru emission is shown in green, and DRAQ5 emission shown in red.

5.5, green) exhibits diffuse staining predominantly in the cytoplasmic regions surrounding the nucleus, although faint nuclear accumulation is observed. However, any difference in nuclear brightness for HCT116N *vs*. HCT116O is not obvious; qualitatively, the ruthenium staining for both cell lines appears nearly identical. Even if the HCT116O cells possess more genomic mismatches, because the complex "lights up" much of the cell (presumably as a result of binding to lipids or proteins), it will be very difficult to detect a discernible luminescence difference between the cell lines from microscopy images alone. In order for a signal-on light switch probe to achieve this objective, it would need to exhibit negligible affinity for other biomolecules, so as to eliminate the high background signal resulting from non-specific binding.

However, based on the observation that the Δ and Λ enantiomers of $[Ru(Me_4phen)_2(dppz)]^{2+}$ do exhibit differences in activity in the MTT assay, we asked the question of whether the enantiomers exhibit similar or noticeably different staining patterns in live and fixed cells. Figure 5.6 presents live-cell images obtained after incubation with the individual enantiomers. The complex is capable of entering live cells, a result that is consistent with prior reports of $[Ru(L)_2(dppz)]^{2+}$-type complexes.[7] Although a nuclear co-staining dye was not employed here, by merging the ruthenium emission with the cell brightfield images (Figure 5.6, top row), it is evident that these compounds do not exhibit staining characteristic of significant nuclear accumulation. This observation is consistent with those made by C.A. Puckett in microscopy experiments with $[Ru(DIP)_2(dppz)]^{2+}$, a complex that displays predominantly punctate cytoplasmic staining in live cells.[7] Both enantiomers of $[Ru(Me_4phen)_2(dppz)]^{2+}$ are capable of entering the cells, however, and exhibit similar perinuclear staining that appears more punctate than diffuse.

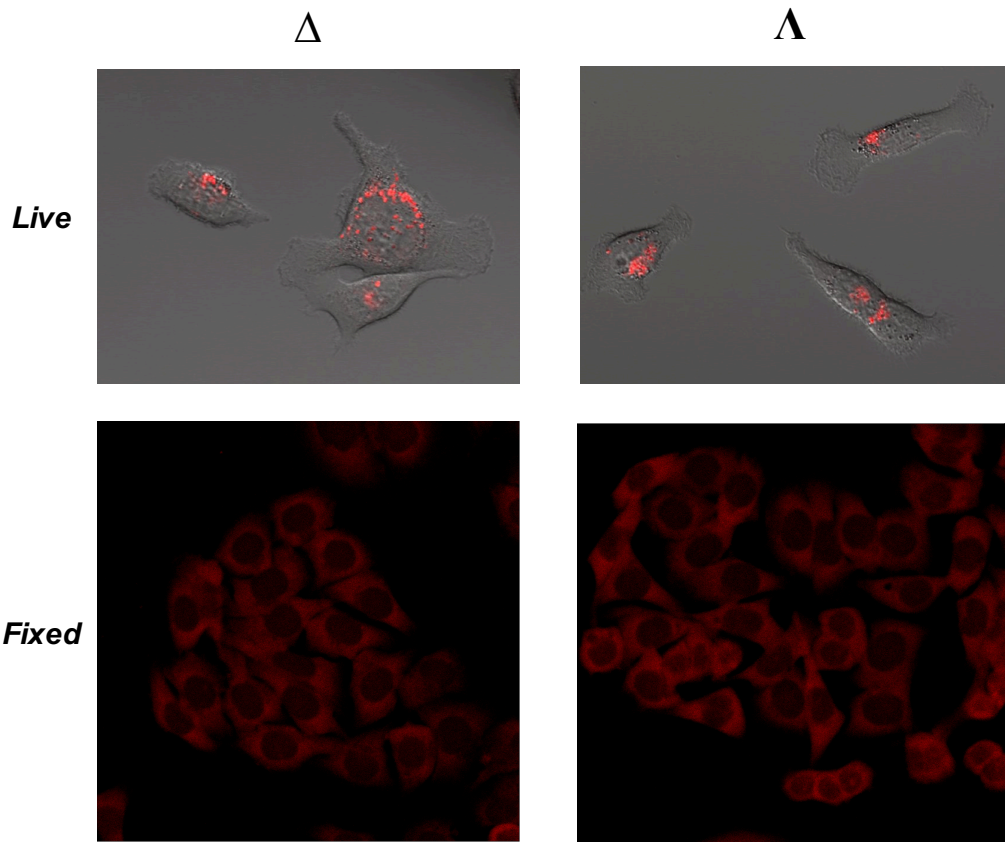

Figure 5.6. (*Top*) Live-cell images of Δ-$[Ru(Me_4phen)_2(dppz)]^{2+}$ (left) and Λ-$[Ru(Me_4phen)_2(dppz)]^{2+}$ (right) with HCT116O cells. Cells were incubated with 25 μM Ru for 20 hours and imaged in PBS. Shown are composite images of the Ru emission (red) and the cell brightfield (gray). *(Bottom)* Fixed-cell images of the enantiomers with HCT116O cells. Cells were fixed with 4% formaldehyde, followed by 0.5% Triton X-100 permeabilization, and incubated with 5 μM Ru for 10 min and imaged in HBSS.

The overall staining pattern does change noticeably when the complex is applied to fixed cells (Figures 5.5 and 5.6), in which we see a more diffuse ruthenium emission throughout the cytoplasm and faint nuclear accumulation. This is not surprising, as the membrane permeabilization during fixing ostensibly provides the complex with greater access to regions of the cell. However, as illustrated in Figure 5.6, there is no immediately obvious difference in staining when comparing the two enantiomers.

The punctate perinuclear staining in live cells seen in Figure 5.6 suggests mitochondrial localization. To confirm this observation, Natalie Mariano, a member of Julie Bailis' group at Amgen, performed live-cell imaging of *rac*-$[Ru(Me_4phen)_2(dppz)]^{2+}$ with nuclear and mitochondrial co-stains (Figure 5.7). It is very clear from Figure 5.7 that the punctate ruthenium emission co-localizes significantly with the mitochondrial dye MitoTracker, and less so with the live cell nuclear stain Hoechst. These results confirm our hypothesis that the relatively "greasy" cation $[Ru(Me_4phen)_2(dppz)]^{2+}$, similarly to lipophilic rhodium complexes,[2] preferentially localizes to the mitochondria.

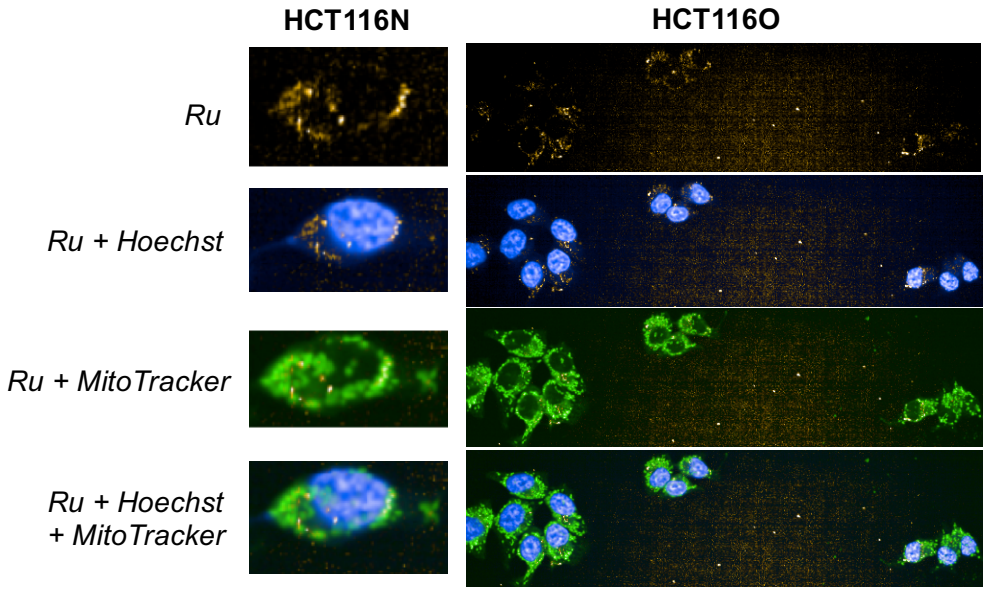

Figure 5.7. Live-cell images of *rac*-$[Ru(Me_4phen)_2(dppz)]^{2+}$ (5 μM) incubated with HCT116N (left column) and HCT116O (right column) cells for 24 hours. From top to bottom: Ru emission alone (gold), Ru + Hoechst nuclear stain (blue), Ru + Mitotracker (green), and an overlay of all three stains. Conducted by Natalie Mariano at Amgen, Inc.

Although $[Ru(Me_4phen)_2(dppz)]^{2+}$ exhibits significant mitochondrial accumulation, the fact that it is even capable of entering cells is an important result. As discussed previously, another potential use for a luminescent metalloinsertor is to investigate co-localization of the probe with proteins involved in the DNA damage response pathway that is activated upon mismatch binding

in cellulo. This is an active area of pursuit with our collaborators at Amgen. Julie Bailis and Natalie Mariano have been conducting optimization experiments to determine cell fixing conditions that will be best for $[Ru(Me_4phen)_2(dppz)]^{2+}$ visualization in future co-localization studies. Upon

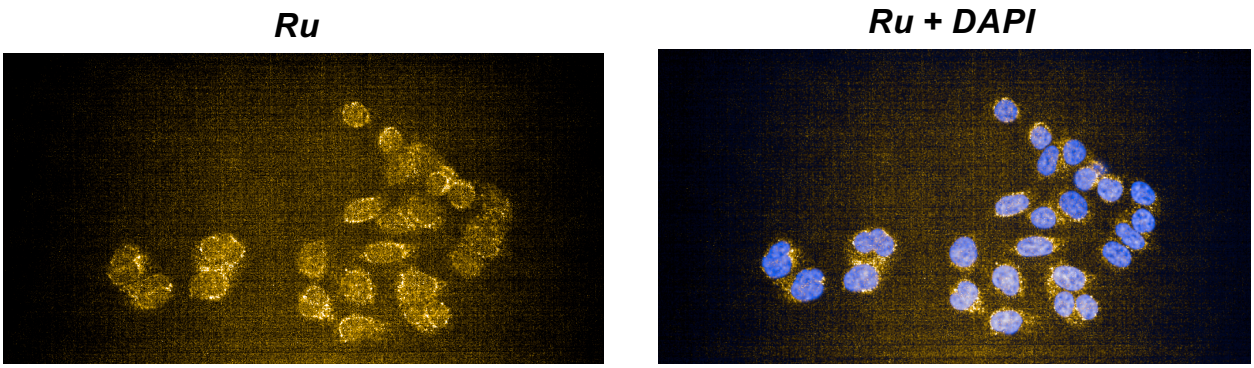

Figure 5.8. Fixed-cell images of *rac*-$[Ru(Me_4phen)_2(dppz)]^{2+}$ with HCT116N cells. Cells were plated at 5,000 cells/well and treated with 5 μM Ru for 24 hours. Cells were then fixed with 4% formaldehyde (15 min), permeabilized with 0.5% Triton (15 min), and co-stained with DAPI (15 min), followed by washing with PBS. Ru emission alone (gold) is shown at left, and Ru + DAPI is shown at right. Conducted by Natalie Mariano at Amgen, Inc.

treating live cells with the ruthenium complex for 24 hours followed by fixing, permeabilizing, and co-staining with DAPI, the ruthenium is visualized within the cells (Figure 5.8). Again, although the compound does exhibit non-specific staining throughout the cells, it can be detected in the nuclei. Importantly, with this method (first treating with the ruthenium complex followed by fixing the cells), punctate staining within the nuclei is seen – that is, ruthenium foci are maintained. This will be vital moving forward in co-localization experiments with fluorescently labeled proteins.

5.4 Conclusions

$[Ru(Me_4phen)_2(dppz)]^{2+}$ is capable of entering live cells and can be visualized in both live- and fixed-cell imaging experiments. However, the complex significantly accumulates in mitochondria and does not exhibit the same degree of activity in the MTT assay as cell-selective

rhodium metalloinsertors. However, the results of the nuclear count assay for cell viability (Figure 5.4) are promising because they do show selective activity towards the MMR-deficient HCT116O cell line, and this effect is amplified when cells are treated with the Δ enantiomer. As discussed in Chapter 2, there is strong evidence that $[Ru(Me_4phen)_2(dppz)]^{2+}$ undergoes metalloinsertion when bound to a mismatch, ostensibly flipping out the mismatched bases in an analogous fashion to rhodium metalloinsertors. Although $[Ru(Me_4phen)_2(dppz)]^{2+}$ exhibits non-specific accumulation throughout the cell, it can be detected in nuclei. Ongoing work with our collaborators at Amgen is focusing on investigating the co-localization of $[Ru(Me_4phen)_2(dppz)]^{2+}$ with phosphorylated H2AX (pH2AX), an early marker for DNA damage response activation. This is also being explored with a fluorescent conjugate of a rhodium metalloinsertor bearing a cyanine dye.[12] The goal of this work will be to determine if both compounds act by the same mechanism or a different mechanism; for example, one possible outcome is that pH2AX co-localization occurs for both compounds, but that a higher percentage of co-localization is observed for one compound compared to the other. Another potential outcome is that co-localization occurs with only one of the compounds. These experiments aim to provide a more complete picture with respect to the generality of metalloinsertion activating a particular DNA damage response in MMR-deficient cancer cells.

References

1. Ernst, R.J.; Komor, A.C.; Barton, J.K. *Biochemistry* **2011**, *50*, 10919-10928.

2. Komor, A.C.; Schneider, C.J.; Weidmann, A.G.; Barton, J.K. *J. Am. Chem. Soc.* **2012**, *134*, 19223-19233.

3. Komor, A.C.; Barton, J.K. *J. Am. Chem. Soc.* **2014**, *136*, 14160-14172.

4. Bailis, J.M.; Weidmann, A.G.; Barton, J.K. *Submitted*.

5. Gill, M.R.; Thomas, J.A. *Chem. Soc. Rev.* **2012**, *41*, 3179-3192.

6. Baggaley, E; Weinstein, J.A.; Williams, J.A. *Coord. Chem. Rev.* **2012**, *256*, 1762-1785.

7. Puckett, C.A. *The Cellular Uptake of Luminescent Ruthenium Complexes.* Ph.D. Thesis, California Institute of Technology, Pasadena, CA, **2010**.

8. Puckett, C.A.; Barton, J.K. *Bioorg. Med. Chem.* **2010**, *18*, 3564-3569.

9. Puckett, C.A.; Barton, J.K. *J. Am. Chem. Soc.* **2009**, *131*, 8738-8739.

10. Puckett, C.A.; Barton, J.K. *J. Am. Chem. Soc.* **2007**, *129*, 46-47.

11. Glaab, W.E.; Tindall, K.R. *Carcinogenesis* **1997**, *18*, 1-8.

12. Nano, A.; Barton, J.K. *Manuscript in preparation.*

Chapter 6

Amino Acid Conjugation of the Rhodium Metalloinsertor $[Rh(HDPA)_2(chrysi)]^{3+}$

6.1 Introduction

An ongoing effort in the Barton laboratory is to further improve the selectivity of rhodium metalloinsertors towards MMR-deficient cancer cells while minimizing undesired off-target effects on MMR-proficient cells. While $[Rh(phen)(chrysi)(PPO)]^{2+}$ is highly potent and exhibits cell-selective cytotoxicity towards the MMR-deficient HCT116O cells compared to MMR-proficient HCT116N cells,[1] this is only the case for a low (sub-micromolar) concentration range; at higher drug doses, the compound begins to affect the viability of the "healthy" or MMR-proficient HCT116N cells. This off-targeting is not ideal, and limits the therapeutic dose of metalloinsertor that can be employed. Thus, an active area of research is focusing on making modifications to rhodium metalloinsertors to improve their selectivity over a larger concentration range.

One potential way to achieve enhanced selectivity towards the targeted cancerous tissue is through antibody-drug conjugation (ADC). ADC utilizes the tumor cell specificity of a monoclonal antibody tethered to a cytotoxic agent to increase the fraction of drug delivered to tumor tissues and minimize possible negative side effects of systemic drug administration.[2] As shown in Figure 6.1, an ADC typically consists of a drug payload conjugated to an antibody through a linker. The ADC localizes to the cancerous tissue expressing the target antigen and is subsequently internalized into the cell. Once inside the cell, the drug is released from the antibody typically through some cleavage mechanism of the linker.[3] An example of such a conjugate is shown in Figure 6.1, in which the drug MMAE is conjugated to an antibody *via* the Val-Cit dipeptide linker; upon incorporation into the cell, it is proposed that Cathepsin B enzymatically cleaves at the site of this dipeptide, releasing free drug.[4] In one study, MMAE was conjugated to the cAC10 antibody, which is directed towards the CD30 antigen expressed on Karpas 299 tumor cells. The ADC

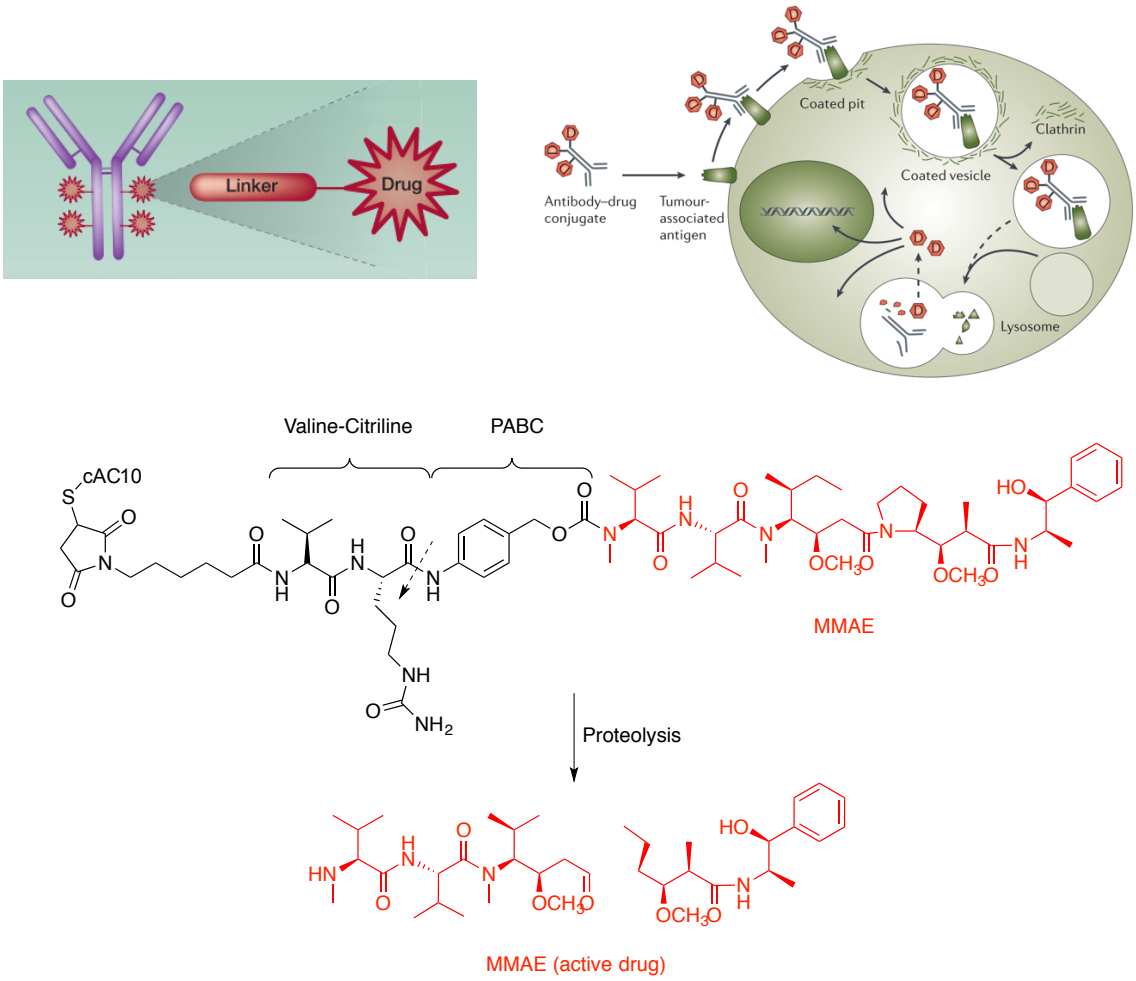

Figure 6.1. (*Top left*) General schematic of an antibody-drug conjugate. Reprinted with permission from ref. 2, © 2011 AACR. (*Top right)* Basic pathway for an ADC into a cell. Reprinted with permission from ref. 3, © 2006 Nature Publishing Group. (*Bottom*) Example of an ADC. The drug MMAE is conjugated to the cAC10 antibody through a Val-Cit peptide linker. Proteolysis by Cathepsin B at the cleavage site (dotted arrow) within the cell releases free drug payload. Adapted from ref. 4.

exhibited significant antitumor activity *in vitro* and *in vivo*.[5,6] Other similar ADCs bearing various dipeptide linkers were reported by Doronina et. al.[7]

With this amino acid conjugation idea in mind, we considered whether a similar strategy could be employed to enhance the therapeutic window of rhodium metalloinsertors. Figure 6.2 depicts a possible ADC design, illustrating a rhodium complex that is tethered to an antibody *via* some dipeptide linker. Proteolysis of the dipeptide linker releases a cleavage product bearing a

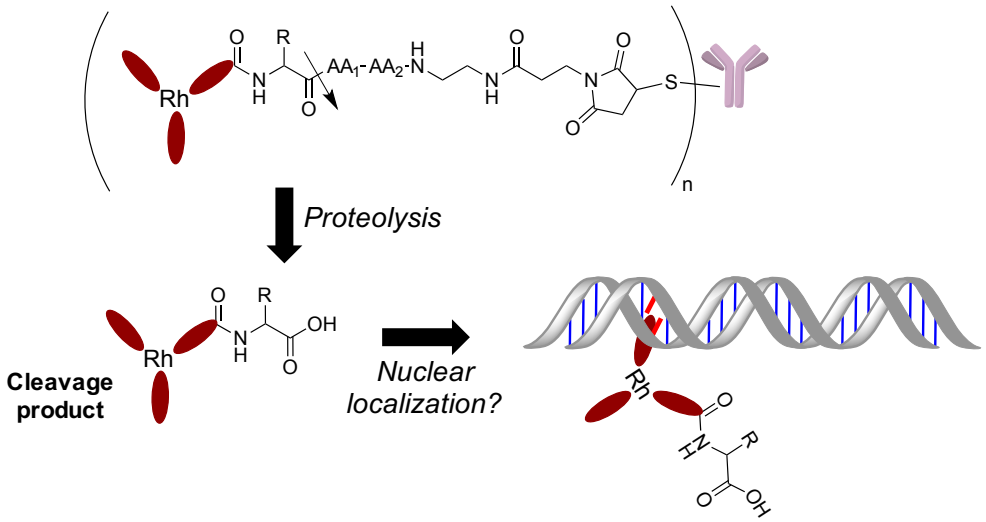

Figure 6.2. General schematic of an ADC design for a rhodium metalloinsertor. After proteolysis of a dipeptide linker AA_1-AA_2 by some enzyme such as Cathepsin B, a cleavage product bearing a single amino acid ideally localizes to the nucleus and specifically binds to a DNA mismatch.

single amino acid; ideally, this product would localize to the nucleus for mismatch binding.

The focus of this work was to synthesize rhodium complexes bearing single amino acids that would serve as the proteolytic cleavage product depicted in Figure 6.2. The goal was to synthesize an effective rhodium amino acid conjugate that 1) still demonstrated mismatch specificity, and 2) maximized nuclear and minimized mitochondrial uptake. Prior work in our group investigated appending peptides to rhodium and ruthenium complexes in an effort to improve cellular uptake and nuclear localization. A D-octaarginine appendage conjugated to a rhodium ancillary ligand (Figure 6.3) did bestow fast nuclear uptake in HeLa cells, but the complex no longer exhibited specific binding to mismatches.[8] A shorter peptide appendage, the RrRK nuclear targeting signal, was tethered to a ruthenium complex (Figure 6.3) and did impart an enhanced cellular uptake compared to free complex, but it was found that a higher concentration was required to accumulate in the nucleus compared to an octaarginine conjugate.[9] The identity of the conjugated peptide also greatly altered the nuclear uptake. For example, an SrSr sequence appended to the ruthenium complex exhibited a much lower nuclear accumulation compared to

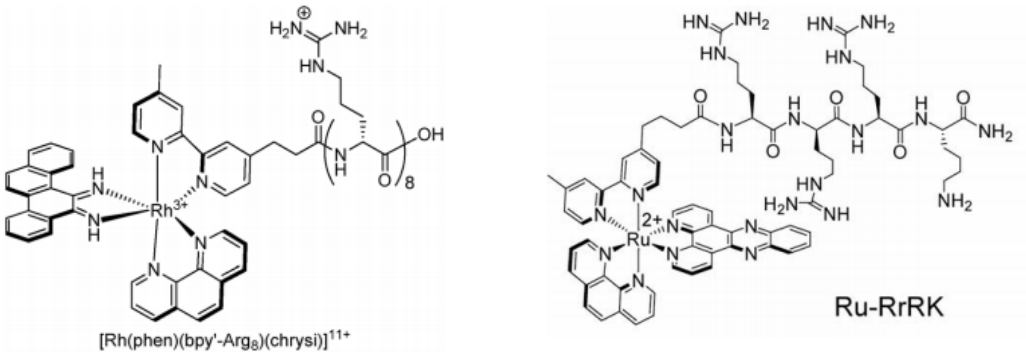

Figure 6.3: (*Left*) Rhodium metalloinsertor conjugated to D-octaarginine. Adapted from ref. 8. (*Right*) Ruthenium complex conjugated to RrRK nuclear targeting signal. Reprinted with permission from ref. 9, © 2010 Elsevier Ltd.

the RrRK tetrapeptide.

Given the variable characteristics that different peptides can impart on a compound's uptake and localization, this work involved synthesizing a small family of rhodium metalloinsertors bearing single amino acids with various R-groups, namely serine, arginine, and phenylalanine. The DNA mismatch binding affinities of these complexes were determined, and the anti-proliferative and cytotoxic activities of these conjugates were studied in the MMR-proficient HCT116N and MMR-deficient HCT116O cell lines.

6.2 Experimental Protocols

6.2.1 Materials

All reagents and solvents were purchased from commercial suppliers and used without further purification. Sep-Pak C18 solid-phase extraction (SPE) cartridges were purchased from Waters Chemical Co. (Milford, MA). Media and supplements were purchased from Invitrogen (Carlsbad, CA). BrdU, antibodies, buffers, peroxidase substrate, MTT, and acidified lysis buffer (10% SDS in 10 mM HCl) solution were purchased in kit format from Roche Molecular biochemical (Mannheim, Germany). Oligonucleotides were ordered from Integrated DNA

Technologies and purified by HPLC using a C18 reverse-phase column (Varian, Inc.) on a Hewlett-Packard 1100 HPLC. Single-stranded concentrations were quantified by measuring the absorbance at 260 nm using extinction coefficients provided from IDT. Radiolabeled [^{32}P]-ATP was purchased from MP Biomedicals (Santa Ana, CA). Chrysene-5,6-dione (chrysi) was synthesized as described.[10] The rhodium complex [Rh(HDPA)(chrysi)(DPA-AcOH)]$^{3+}$ (HDPA = 2,2'-dipyridylamine; DPA-AcOH = di(pyridine-2-yl)glycine was synthesized according to the methods described by A. Weidmann.[11,12]

6.2.2 Synthesis

[Rh(HDPA)(chrysi)(DPA-Ser-OMe)]$^{3+}$. In a scintillation vial containing 11.5 mg [Rh(HDPA)(chrysi)(DPA-AcOH)]$^{3+}$ (0.0105 mmol) was added 12.5 mg HATU (0.0329 mmol, 3.13 eq.) and 6.6 mg L-serine methyl ester hydrochloride (0.042 mmol, 4.0 eq). The vial contents were dried under vacuum (lyophilization) for 3.5 hours. The contents were then dissolved in ca. 2 mL anhydrous DMF, and subsequently 11 μL DIEA (diisopropylethylamine, 0.063 mmol, 6.0 eq.) were added. The vial was flushed with argon for 15 minutes, and the reaction was stirred under argon for 14 hours at room temperature. The solvents were evaporated *via* lyophilization, and the crude reaction product was carried directly into the next step.

[Rh(HDPA)(chrysi)(DPA-Ser)]$^{3+}$. Crude [Rh(HDPA)(chrysi)(DPA-Ser-OMe)]$^{3+}$ was dissolved in 50 mL of 4:1 water:ethanol (v/v). The orange-red solution was stirred in a 250 mL found bottom flask and basified to pH ~10 with 1 N NaOH, yielding a yellow-green color change; the reaction was then stirred for 2 hours. The reaction was neutralized to a pH of 5-6 using 1 N HCl, producing a red color change, and the solvents were evaporated, leaving a rust-orange solid. The complex was purified by preparatory HPLC using a C_{18} reverse-phase column (Varian, Inc.) on a Hewlett Packard 1100 HPLC (85:15 to 40:60 H_2O (0.1% TFA):MeCN) and then converted

to its chloride salt *via* anion exchange on a Sephadex QAE column primed with 1 M $MgCl_2$. ESI-MS m/z: calc. $[M - 2H]^+$ 844.2, obs. 843.9.

[Rh(HDPA)(chrysi)(DPA-Arg)]$^{3+}$. Synthesized analogously to [Rh(HDPA)(chrysi)(DPA-Ser)]$^{3+}$ *via* peptide coupling with L-arginine methyl ester hydrochloride followed by ester de-protection as described above. The product was purified by preparatory HPLC and converted to its chloride salt *via* anion exchange on a Sephadex QAE column. ESI-MS m/z: calc. $[M - 2H]^+$ 913.3, obs. 913.0; calc. $[(M - H)/2]^+$ 457.1, obs. 457.3.

[Rh(HDPA)(chrysi)(DPA-Phe)]$^{3+}$. Synthesized analogously to [Rh(HDPA)(chrysi)(DPA-Ser]$^{3+}$ *via* peptide coupling with L-phenylalanine methyl ester hydrochloride followed by ester de-protection as described above. The product was purified by preparatory HPLC and converted to its chloride salt *via* anion exchange on a Sephadex QAE column. ESI-MS m/z: calc. $[M - 2H]^+$ 904.2, obs. 904.0; calc. $[(M - H)/2]^+$ 452.6, obs. 452.8.

6.2.3 Photocleavage Competition Titrations and Binding Constant Determination

Photocleavage competition titrations with the amino acid metalloinsertor conjugates and $[Rh(bpy)_2(chrysi)]^{3+}$ were performed using ^{32}P-labeled oligonucleotides and polyacrylamide gel electrophoresis (PAGE) as described previously.[1,11,13] Briefly, the single-stranded 29-mer DNA hairpin sequence 5'-GGCAGGCATGGCTTTTTGCCATCCCTGCC-3' (underline denotes a CC mismatch) was labeled at the 5'-end with ^{32}P by incubating the DNA with ^{32}P-ATP and polynucleotide kinase (PNK) at 37°C for 2 hours and purified using gel electrophoresis. A small portion of the labeled DNA (<1% total DNA) was added to 2 μM unlabeled oligonucleotide in 100 mM NaCl, 20 mM NaP_i, pH 7.1 buffer. The hairpin was annealed by heating to 90°C and slowly cooling back to room temperature over 1.5 hours. Stock solutions of each amino acid rhodium conjugate ranging from 0.1 μM (or 0.5 μM) to 50 μM were prepared in Milli-Q water. A 4 μM

rac-$[Rh(bpy)_2(chrysi)]Cl_3$ sample was also prepared. Working samples were prepared by combining 2 μM annealed DNA (10 μL), 4 μM $[Rh(bpy)_2(chrysi)]^{3+}$ (5 μL), and 5 μL of a given rhodium conjugate stock in a microcentrifuge tube at 37°C for 10 min to give 1 μM $[Rh(bpy)_2(chrysi)]^{3+}$ and 1 μM DNA as final concentrations. Control samples were also prepared: light control (DNA only) and dark control (highest conjugate concentration with DNA and no irradiation). Samples were irradiated on an Oriel (Darmstadt, Germany) 1000-W Hg/Xe solar simulator (340-440 nm) for 15 min. Samples were subsequently dried on a SpeedVac concentrator and electrophoresed in a 20% denaturing polyacrylamide gel. The gel was exposed to a phosphor screen, and the amount of DNA in each band was analyzed *via* autoradiography and quantified by phosphorimagery (ImageQuant). The fraction of cleaved DNA in each lane of a gel (corresponding to cleavage by $[Rh(bpy)_2(chrysi)]^{3+}$) was quantified and expressed as a percentage of the total DNA in that lane. The percent cleaved was plotted against the log of the rhodium conjugate concentration. OriginPro 8.5 was used to fit the plots to a sigmoidal curve, and the midpoint value (log of rhodium conjugate concentration at the plot inflection point) was converted to concentration. The binding constant of the conjugate was determined in Mathematica 6.0 by solving simultaneous equilibria of DNA, $[Rh(bpy)_2(chrysi)]^{3+}$, and the conjugate.

6.2.4 Cell Culture and MTT Cytotoxicity Assay

Basic cell culture of the HCT116N and HCT11O cell lines, as well as the MTT cytotoxicity assay, were performed as discussed in Chapter 5.

6.2.5 Cellular Proliferation ELISA

HCT116N and HCT116O cells were plated on a 96-well plate at 2,000 cells/well and incubated at 37°C under 5% CO_2 overnight to adhere. Cells were then treated with a range of rhodium conjugate concentrations (0-10 μM) for 24 or 48 hours. At the end of these respective

time points, rhodium-containing media was removed and replaced with fresh media. Cells were grown for the remainder of the 72 hour growth period. 24 hours prior to analysis, cells were labeled with BrdU, and BrdU incorporation was quantified by an antibody assay kit. The quantified BrdU incorporation into treated cells was normalized to untreated controls to determine the cellular proliferation at each rhodium treatment concentration.

6.2.6 ICP-MS Analysis for Whole-Cell Uptake

The whole-cell uptake of the Rh(DPA-Arg) and Rh(DPA-Phe) metalloinsertor conjugates was performed as described.[13] Briefly, HCT116O cells were plated at 1 x 10^6 cells/well in 6-well plates (3 mL media per well). The cells were incubated overnight to adhere. The following day, cells were treated with 10 μM rhodium complex. Following incubation for the indicated time points (6, 12, and 24 hours), the media in each well was carefully removed, and the cell monolayer was washed with 3 mL PBS. 800 μL of 1% SDS was then added to lyse the cells. The cell lysates were collected and sonicated on a Qsonica Ultrasonic processor for 10 seconds at 20% amplitude. For ICP-MS analysis, 750 μL of each cell lysate was combined with 750 μL 2% HNO_3 (v/v). The remaining lysate was quantified for total protein content using a bicinchoninic assay (BCA). The lysate/HNO_3 solutions were subjected to ICP-MS analysis to determine ^{103}Rh counts in each sample. The rhodium counts were normalized to the amount of protein as determined from the BCA, which gives ng Rh/mg protein values that can be compared amongst the different time point samples and Rh(DPA-Arg) and Rh(DPA-Phe) complexes. Three replicates per time point were recorded for each complex.

6.3 Results and Discussion

6.3.1 General Design Considerations

The goal of this work was to generate metalloinsertor conjugates bearing single amino acid moieties. While the prospect of applying metalloinsertor amino acid conjugates towards antibody-drug conjugation was being considered at the inception of this project, our initial investigations focused on exploring how modifying a metalloinsertor with single amino acids affected 1) mismatch binding affinity, and 2) cell-selective anti-proliferation and cytotoxicity. The aim was to screen several conjugates containing different amino acids to see whether any exhibited favorable cell-selective activity by minimizing mitochondrial localization and maximizing nuclear uptake. Work on this project began prior to the more recently-developed metalloinsertors bearing a unique Rh-O coordination such as $[Rh(phen)(chrysi)(PPO)]^{2+}$ (Chapter 5, Figure 5.1), which exhibit high cell selectivity and potency. As such, this work focused on conjugating the metalloinsertor scaffold which, at the time, exhibited the best combination of cell selectivity and potency: $[Rh(HDPA)_2(chrysi)]^{3+}$ (Figure 6.4).[14]

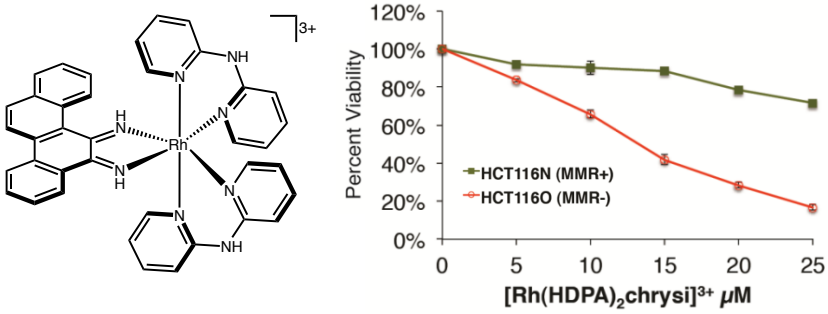

Figure 6.4. (*Left*) Structure of the rhodium metalloinsertor $[Rh(HDPA)_2(chrysi)]^{3+}$. (*Right*) Selective cytotoxicity of the metalloinsertor towards MMR-deficient HCT116O cells as measured by the MTT assay. HCT116N and HCT116O cells were plated in a 96-well format at 50,000 cells/well and treated with 0-25 μM $[Rh(HDPA)_2(chrysi)]^{3+}$. After 72 hours, the cells were labeled with MTT for 4 hours.

Conjugation of the $[Rh(HDPA)_2(chrysi)]^{3+}$ scaffold can be achieved by substituting one of the HDPA ligands with DPA-AcOH (di(pyridine-2-yl)glycine, Figure 6.5). The free carboxylic acid group on DPA-AcOH is very amenable to amide-bond coupling, thus making this site ideal for peptide conjugation. The complex $[Rh(HDPA)(chrysi)(DPA\text{-}AcOH)]^{3+}$ has previously been used as a precursor for a bimetallic rhodium-oxaliplatin conjugate.[11]

In this work, three conjugates of $[Rh(HDPA)(chrysi)(DPA\text{-}AcOH)]^{3+}$ were generated, each bearing a different amino acid (arginine, serine, and phenylalanine, Figure 6.5). These derivatives were synthesized *via* peptide coupling between the free carboxylic acid group on $[Rh(HDPA)(chrysi)(DPA\text{-}AcOH)]^{3+}$ and methyl ester-protected amino acids, followed by ester de-protection (see Experimental Protocols).

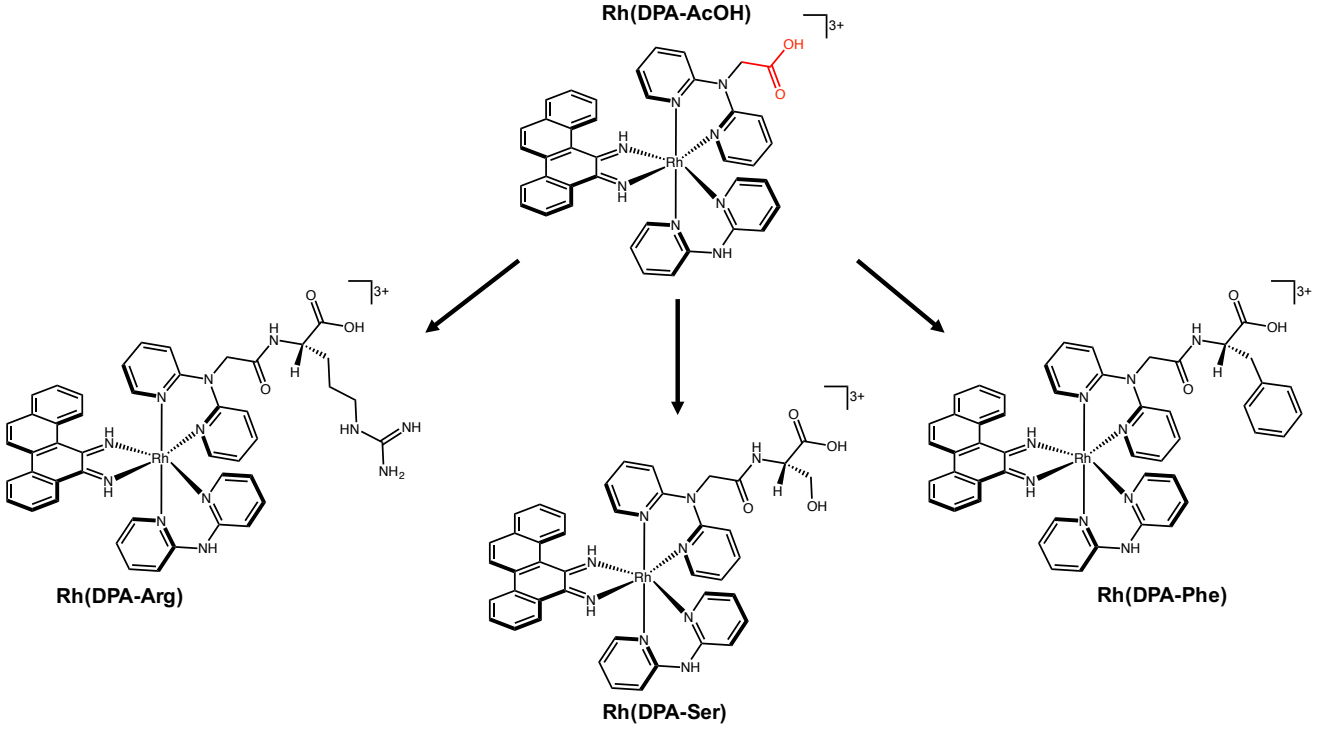

Figure 6.5. Amino acid conjugates investigated in this study. The precursor $[Rh(HDPA)(chrysi)(DPA\text{-}AcOH)]^{3+}$ (referred to as Rh(DPA-AcOH), top) is amenable to peptide conjugation through amide coupling with its free carboxylic acid group (red).

6.3.2 Characterizing the CC Mismatch Binding Affinity of Amino Acid Conjugates

Whenever a new rhodium metalloinsertor conjugate is generated, it is imperative to characterize the binding affinity for a DNA mismatch to ensure that the added functionalities have not hindered the ability to bind to DNA. This is achieved using a photocleavage competition titration between the metalloinsertor conjugate and $[Rh(bpy)_2(chrysi)]^{3+}$ as described.[13] While $[Rh(bpy)_2(chrysi)]^{3+}$ promotes DNA strand cleavage upon irradiation, newer generations of metalloinsertors, including $[Rh(HDPA)_2(chrysi)]^{3+}$ and its derivatives, do not. As described in the Experimental Protocols, samples are prepared containing constant concentrations of ^{32}P-labeled CC hairpin DNA and mismatch-specific $[Rh(bpy)_2(chrysi)]^{3+}$, but varying concentrations of the metalloinsertor conjugate. The extent of DNA photocleavage by $[Rh(bpy)_2(chrysi)]^{3+}$ as a function of increasing conjugate concentration can be determined from gel electrophoresis and phosphorimaging. If the metalloinsertor conjugate binds mismatches, it is expected that as its concentration is increased, it will compete with $[Rh(bpy)_2(chrysi)]^{3+}$ for the CC binding site.

A representative photocleavage gel from a competition assay with $[Rh(bpy)_2(chrysi)]^{3+}$ and the serine metalloinsertor conjugate Rh(DPA-Ser) is presented in Figure 6.6. As expected, as the concentration of Rh(DPA-Ser) is increased relative to $[Rh(bpy)_2(chrysi)]^{3+}$, the observed photocleavage by $[Rh(bpy)_2(chrysi)]^{3+}$ decreases, indicating that the conjugate is competing for binding at the mismatch. This can be quantified by plotting the percentage of DNA photocleaved as a function of conjugate concentration (Figure 6.6). By fitting the points to a sigmoidal curve, the concentration of rhodium complex at the midpoint (inflection point) of each plot can be calculated in OriginPro. From this concentration, the binding constant of the conjugate for the CC mismatch is calculated in Mathematica 6.0 by solving simultaneous equilibria involving the DNA, $[Rh(bpy)_2(chrysi)]^{3+}$, and the conjugate.

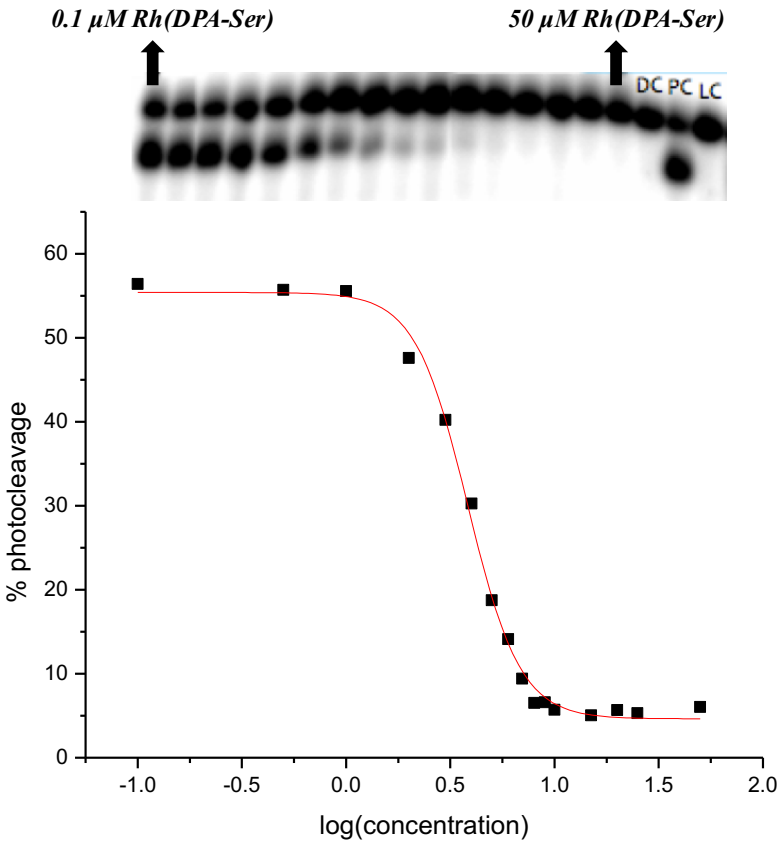

Figure 6.6. Binding affinities determined through DNA photocleavage. (*Top*) Samples containing 1 μM $[Rh(bpy)_2(chrysi)]^{3+}$, 1 μM radiolabeled CC hairpin DNA, and varying concentrations of Rh(DPA-Ser) conjugate (0.1 to 50 μM) were irradiated and electrophoresed through a 20% denaturing PAGE gel. Several control samples were included: a light control (LC, DNA only with irradiation), a dark control (DC, $[Rh(bpy)_2(chrysi)]^{3+}$ + conjugate + DNA with no irradiation), and a positive control (PC, DNA + $[Rh(bpy)_2(chrysi)]^{3+}$ + irradiation, no conjugate). (*Bottom*) Representative sigmoidal curve fit of data from photocleavage competition titration between $[Rh(bpy)_2(chrysi)]^{3+}$ and 0.1-50 μM Rh(DPA-Ser).

All three amino acid conjugates compete for mismatch site binding with $[Rh(bpy)_2(chrysi)]^{3+}$. From the photocleavage competition titrations, binding affinities for the CC mismatch were determined for each complex: $K_B(CC) = 5.8 \times 10^6\ M^{-1}$ for Rh(DPA-Ser), $2.0 \times 10^6\ M^{-1}$ for Rh(DPA-Phe), and $4.2 \times 10^6\ M^{-1}$ for Rh(DPA-Arg). These values, all on the order of 10^6, are consistent with other HDPA-based metalloinsertors.[13] Thus, these data reveal that the amino acid conjugates are capable of binding to the mismatch.

6.3.3 Biological Activity of Amino Acid Conjugates

We next investigated the anti-proliferative and cytotoxic activity of these conjugates in the MMR-proficient HCT116N and MMR-deficient HCT11O cell lines. The ELISA for DNA synthesis was employed to quantify the relative effects of the metalloinsertors on cell proliferation. HCT116N and HCT116O cells were incubated with a range of conjugate concentrations (Figure 6.7) for 24 or 48 hours; after each incubation time point, rhodium-containing media was removed and replaced with fresh media and the cells were allowed to grow for the remainder of the 72-hour growth period. The cellular proliferation is represented by the percentage of BrdU incorporated into the cells treated with conjugate relative to untreated cells. $[Rh(HDPA)_2(chrysi)]^{3+}$ was included as a control.

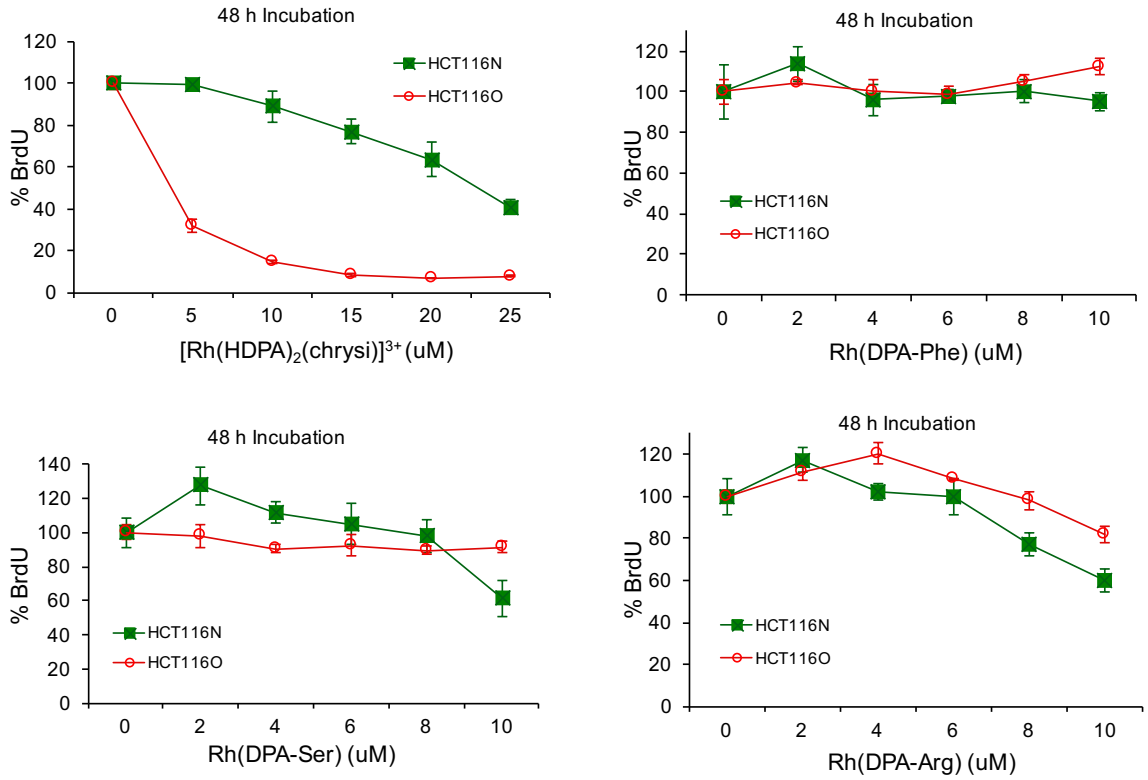

Figure 6.7. Inhibitory effects of $[Rh(HDPA)_2(chrysi)]^{3+}$ and amino acid conjugates on cellular proliferation as determined by the ELISA. Cells were treated with rhodium for 48 hours.

As expected, the control complex, $[Rh(HDPA)_2(chrysi)]^{3+}$, exhibits cell-selective anti-proliferative activity towards the MMR-deficient HCT116O line. However, none of the amino acid conjugates demonstrate this cell-selective activity after 24 hours (not shown) or 48 hours of rhodium treatment. In fact, the conjugates display very little activity at all, in either cell line. This phenomenon has been reported before for the metalloinsertor $[Rh(chrysi)(phen)(MeDPA)]^{3+}$, which after 24 hours does not display significant inhibition of DNA synthesis toward either cell line over a 0-25 μM concentration range.[13]

Although the conjugates do not demonstrate cell-selective inhibition of DNA synthesis, we pursued their cytotoxic effects in the cell lines by the MTT assay. Metalloinsertors that exhibit cell selectivity in the ELISA typically also exhibit cell-selective cytotoxicity.[1,13] Over a 0-25 μM concentration range, none of the amino acid conjugates exhibit significant cytotoxicity towards

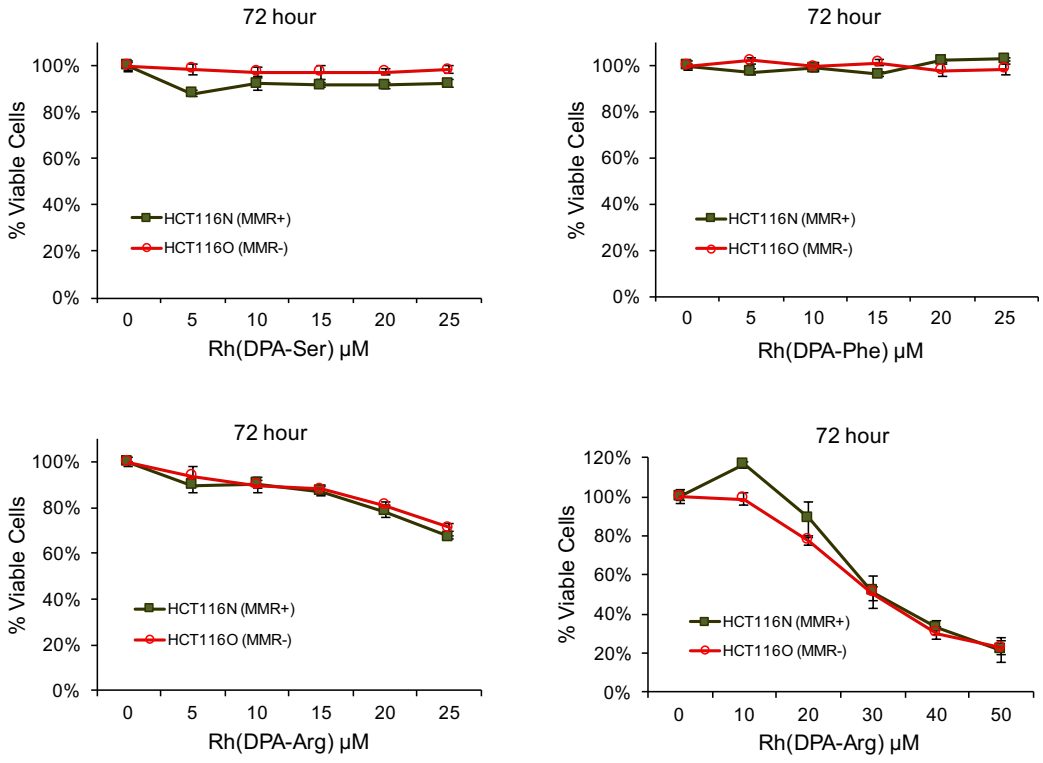

Figure 6.8. Cytotoxicity of rhodium amino acid conjugates as measured by the MTT assay. Cells were treated with the concentration range of rhodium indicated for 72 hours.

either cell line, although the Rh(DPA-Arg) complex slowly decreases cell viability with increasing concentration (Figure 6.8). We tested the Rh(DPA-Arg) complex at even higher MTT assay concentrations (0-50 μM, Figure 6.8), and indeed we see that the conjugate displays comparable cytotoxicity towards both cell lines, down to ca. 20% viability. Increasing the cell treatment concentration of Rh(DPA-Ser) and Rh(DPA-Phe) to 50 μM does not induce any cytotoxicity (not shown).

Given that these conjugates are capable of binding to a mismatch *in vitro* with comparable affinity to other biologically-active metalloinsertors, the lack of any activity (as for Rh(DPA-Phe) and Rh(DPA-Ser)) or lack of cell-selective activity (as for Rh(DPA-Arg)) must lie in uptake and/or sub-cellular localization properties. To investigate whether the differences in MTT activity observed for the Rh(DPA-Arg) and Rh(DPA-Phe) conjugates was related to differences in whole-cell uptake, an ICP-MS assay for whole-cell rhodium was conducted. HCT116O cells were treated with complex for 6, 12, and 24 hours, and subsequently lysed with 1% SDS and sonication. A portion of the cell lysate was combined with 2% HNO_3 for ICP-MS analysis and the remainder of the lysate was quantified for protein content *via* the BCA assay. ICP-MS rhodium counts were normalized to the protein content calculated in the BCA assay to express the rhodium uptake levels as 'ng Rh/mg protein' (Figure 6.9).

As illustrated in Figure 6.9, the Rh(DPA-Arg) and Rh(DPA-Phe) conjugates do not demonstrate significant differences in whole-cell uptake over 24 hours. Thus, the fact that MTT activity is observed for Rh(DPA-Arg) (albeit not cell-selective) but not for Rh(DPA-Phe) suggests that Rh(DPA-Arg) localizes to the mitochondria; in general, metalloinsertors that demonstrate cell-selective biological activity accumulate less in the mitochondria, while those that show greater

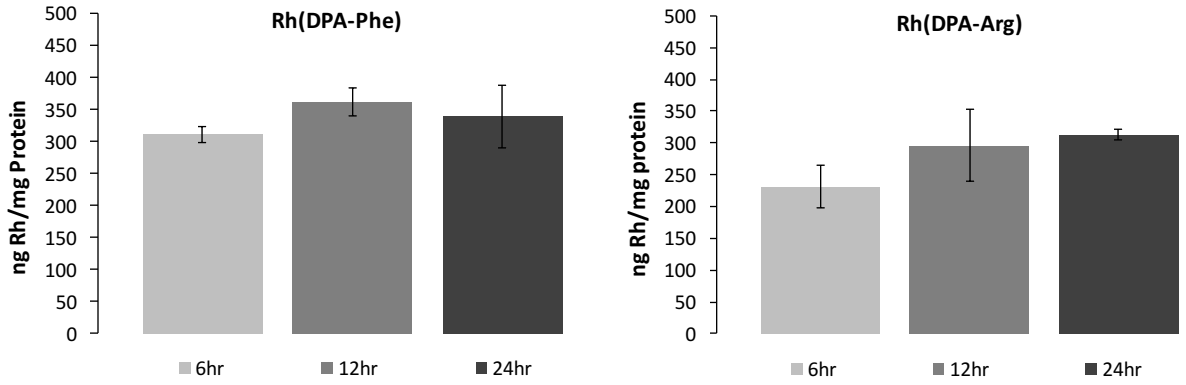

Figure 6.9. ICP-MS assay for whole-cell rhodium accumulation. HCT116O cells were treated with 10 μM conjugate for 6, 12, and 24 hours, and following cell lysis, the rhodium content was analyzed by ICP-MS. Error bars represent three replicates per time point.

mitochondrial accumulation lose cell selectivity.[13] A key structural difference amongst the amino acid conjugates studied here is the presence of the guanidinium group in Rh(DPA-Arg), which is expected to carry a positive charge at physiological pH. This might influence its localization properties relative to the other two complexes. Furthermore, it should be noted that the carboxylic acid group (drawn protonated in Figure 6.5) likely carries a negative charge at physiological pH. Other metalloinsertors do not carry a negatively charged carboxyl group, so perhaps this is also involved in the lack of activity. Performing sub-cellular localization ICP-MS assays for nuclear and mitochondrial rhodium content would paint a clearer picture as to whether the lack of any biological activity for Rh(DPA-Ser) and Rh(DPA-Phe) lies within their specific accumulation in organelles. The lack of any activity for these two derivatives at high concentrations (>25 μM) is surprising. At these concentrations, we'd expect at least some accumulation in the nucleus or mitochondria and the triggering of a biological response. We could hypothesize that the bulky amino acid, together with its negatively-charged carboxyl group, plays a role in altering the protein recognition of the mismatch-bound metalloinsertor lesion. Alternatively, perhaps there are other unseen mechanisms at play such as endosomal or lysosomal trapping.[15,16]

6.4 Conclusions

The goal of this work was to generate amino acid-conjugated metalloinsertors based off the $[Rh(HDPA)_2(chrysi)]^{3+}$ scaffold. The hope was that these conjugates would exhibit selective activity toward the MMR-deficient cells, thus rendering them potential candidates for antibody-drug conjugation. While all three conjugates investigated here demonstrate mismatch binding affinities comparable to other metalloinsertors, cell-selective biological activity is non-existent. Only the Rh(DPA-Arg) complex demonstrates any activity in the MTT assay, but it is not selective for either cell line, possibly due to mitochondrial accumulation. Since conducting these experiments, a newer generation of metalloinsertors ($[Rh(chrysi)(phen)(L)]^{2+}$, L = PPO, DPE, PyOctanol, PPE)[1] bearing a Rh-O coordination have been more fully characterized and exhibit significant cell selectivity with high potency. Current work in the lab is focusing on synthesizing antibody-drug conjugates based off this new generation of compounds with the ultimate goal of improving specificity towards mismatch repair-deficient tumors.

References

1. Komor, A.C.; Barton, J.K. *J. Am. Chem. Soc.* **2014**, *136*, 14160-14172.

2. Teicher, B.A.; Chari, R.V. *Clin. Cancer Res*., **2011**, *17*, 6389-6397.

3. Schrama, D.; Reisfeld, R.; Becker, J. C. *Nat. Rev. Drug Discov.* **2006**, *5*, 147–159.

4. Ducry, L.; Stump, B. *Bioconj. Chem*. **2010**, *21*, 5-13.

5. Doronina, S.O. et al. *Nat. Biotech.* **2003**, *21*, 778-784.

6. Senter, P.D. *Curr. Op. in Chem. Biol*. **2009**, *13*, 1-10.

7. Doronina, S.O. et. al. *Bioconj. Chem*. **2008**, *19*, 1960-1963.

8. Brunner, J.; Barton, J.K. *Biochemistry* **2006**, *45*, 12295-12302.

9. Puckett, C.A.; Barton, J.K. *Bioorg. Med. Chem*. **2010**, *18*, 3564–3569.

10. Zeglis, B.M.; Barton, J.K. *Nat. Prot.* **2007**, *2*, 357-371.

11. Wiedmann, A.G.; Barton, J.K. *Inorg. Chem.* **2014**, *53*, 7812-7814.

12. Weidmann, A.G. *Biological Activity of Rhodium Metalloinsertors and the Design of Bifunctional Conjugates.* Ph.D. Thesis, California Institute of Technology, Pasadena, CA, **2015**.

13. Komor, A.C.; Schneider, C.J.; Weidmann, A.G.; Barton, J.K. *J. Am. Chem. Soc.* **2012**, *134*, 19223-19233.

14. Komor, A.C. *Design, Synthesis, and Biological Activity of Rhodium Metalloinsertors*. Ph.D. Thesis, California Institute of Technology, Pasadena, CA, **2014**.

15. Puckett, C.A. *The Cellular Uptake of Luminescent Ruthenium Complexes.* Ph.D. Thesis, California Institute of Technology, Pasadena, CA, **2010**.

16. De Duve, C. et al. *Biochem. Pharmacol.* **1974**, *23*, 2495-2531.

Chapter 7

Investigating Rhenium and Ruthenium Complexes as Probes for DNA-Mediated Charge Transport

Performed in collaboration with A. Vlcek, Queen Mary University of London, School of Biological and Chemical Sciences.

7.1 Introduction

While most of the work described in this thesis relates to developing rhodium and ruthenium complexes that target DNA mismatches, the Barton laboratory has also focused on the study of transition metal complexes as probes for DNA-mediated charge transport (CT).[1,2] Consecutive base pairs in the DNA helix are packed closely with one another, creating a continuous aromatic π system through which charge can be transmitted, much like stacked sheets of graphite.[3] In 1993, C. Murphy et al. demonstrated DNA-mediated CT between two transition metal complexes (Figure 7.1).[4] The ruthenium intercalator $[Ru(phen)_2(dppz)]^{2+}$ was covalently tethered to one end of a DNA duplex, and as expected, yielded a bright steady-state emission when bound (Figure 7.1). However, when the rhodium intercalator $[Rh(phi)_2(bpy)]^{3+}$ was covalently tethered to the opposite end of the same duplex, complete quenching of the ruthenium emission was observed, due to electron transfer through the DNA helix from the ruthenium donor to the rhodium acceptor.

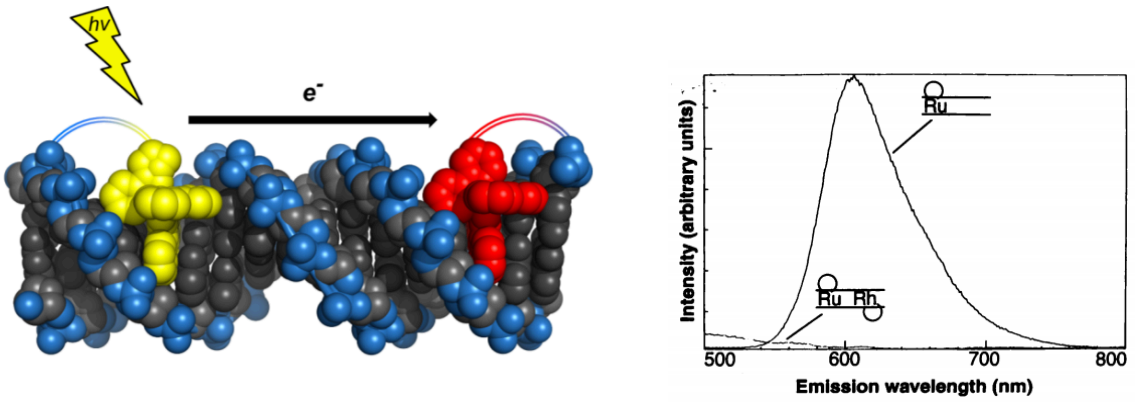

Figure 7.1. DNA-mediated CT between transition metal intercalators. (*Left*) Following excitation, electron transfer from the Ru donor to the Rh acceptor occurs through the base stack. Reprinted with permission from ref. 2, © 2015 American Chemical Society. (*Right*) The Ru complex exhibits an intense steady-state emission when covalently tethered to a DNA duplex in the absence of the Rh acceptor. However, when the Rh intercalator is tethered to the opposite end of the same duplex, quenching of the Ru emission occurs. Reprinted with permission from ref. 4, © 1993 American Association for the Advancement of Science.

DNA-mediated CT has been investigated with a number of different donor-acceptor pairs[5,6] and in the context of long-range guanine oxidation.[7] Typically, these experiments rely on indirect biochemical assays and techniques that monitor rate of quenching of the donor. However, the ability to directly monitor the rate of charge arrival at the acceptor has remained elusive. If we wish to gain a deeper kinetic understanding of the excited-state species involved these systems, we must turn to other spectroscopic methods. UV-Visible transient absorption (TA) spectroscopy is one of the most common techniques for probing solution excited states. However, TA spectra are often broad and featureless with overlapping bands that might not yield much structural information on the excited states.[8,9] Time-resolved vibrational spectroscopy – in particular time-resolved infrared spectroscopy (TRIR) – produces well-resolved, high resolution transient IR bands following excitation that can distinguish individual molecular species and provide insight into the structure and electronic distribution of excited-state intermediates.[9]

Perhaps the most widely-studied molecules in the context of TRIR are rhenium tricarbonyls of the type $[Re(CO)_3(N,N)(L)]^n$, where *N,N* is generally a bipyridine-type ligand and L is a monodentate axial ligand.[10] These complexes have garnered much attention owing to the strongly IR-active nature of the CO ligands. Another family of complexes that has been studied by TRIR include those with the general structure $[M(N,N)_2(L)_2]$, in which M is typically Ru, *N,N* is some type of bipyridine, and L is NCS^- or CN^-.[11,12]

TRIR has also been used to study $[Re(CO)_3(dppz)(py'\text{-}OR)]^+$ and $[Re(CO)_3(F_2dppz)Cl]$ (F_2dppz = 11,12-difluorodipyrido[3,2-*a*:2',3'-*c*]phenazine). These complexes intercalate into DNA *via* their phenazine ligands and are capable of oxidizing guanine upon photoexcitation.[13,14] $Re(CO)_3$ complexes are thus attractive candidates owing to their ability to trigger electron transfer (ET) and the IR sensitivity of their CO ligands. A prior investigation found that the dppz-

containing complex $[Re(CO)_3(dppz)(py'\text{-}OR)]^+$ preferentially populates a long-lived intraligand (^{3}IL) excited state, and this ^{3}IL state bears a very close TRIR spectral resemblance to the bands corresponding to the reduced-state Re complex. This overlap between the $Re(CO)_3$ reduced state and ^{3}IL excited state bands made TRIR spectra difficult to interpret. In the work presented in this chapter, two intercalating complexes were developed with the goal of using them as a donor-acceptor pair to study ET through DNA by TRIR spectroscopy.

7.2 Experimental Protocols

7.2.1 Materials

All chemicals and starting materials were purchased from commercial vendors and used as received. Dipyrido[3,2-*a*:2',3'-*c*]phenazine (dppz) was prepared according to the literature.[15] $Ru(DMSO)_4Cl_2$ was synthesized according to the literature[16] (also commercially available, Sigma). UV-Visible spectra were recorded on a Beckman DU 7400 UV-Visible spectrophotometer (Beckman Coulter). Oligonucleotides were synthesized using standard phosphoramidite chemistry at Integrated DNA Technologies (Coralville, IA) and purified by HPLC using a C_{18} reverse-phase column (Varian, Inc.) on a Hewlett-Packard 1100 HPLC.

7.2.2 Synthesis

$[Re(CO)_3(phendione)Cl]$. 253 mg of $Re(CO)_5Cl$ (0.70 mmol) and 147 mg of phendione (0.70 mmol) were dissolved in 30 mL of anhydrous toluene. The reaction was stirred and refluxed for 4.5 h under argon. The orange precipitate was filtered out and purified by silica gel chromatography (THF). 260 mg of product were obtained (72%).

$[Re(CO)_3(dppn)Cl]$. 98 mg of $[Re(CO)_3(phendione)Cl]$ (0.19 mmol) and 60 mg of 2,3-diaminonaphtalene (0.34 mmol) were suspended in 10 mL ethanol. The solution was refluxed for

2 h. After cooling down to room temperature, the orange precipitate was filtered and washed with water, diethyl ether, and cold ethanol. The product did not require any a further purification. 105 mg of product were obtained (87%). ^{1}H NMR (500 MHz, CD_3CN) δ 9.91 (dd, J = 8.2, 1.4 Hz, 2H), 9.51 (dd, J = 5.2, 1.4 Hz, 2H), 9.19 (s, 2H), 8.44 (dd, J = 6.4, 3.3 Hz, 2H), 8.19 (dd, J = 8.2, 5.2 Hz, 2H), 7.83 (dd, J = 6.7, 3.1 Hz, 2H).

PyOEt (ethyl 3-(pyridine-4-yl)propanoate). This ligand was synthesized by the esterification of 4-pyridinepropionic acid: 250 mg of 4-pyridineproprionic acid (1.65 mmol) and 1.93 mL of ethanol (1.52 g, 33 mmol) were mixed in 28 mL of toluene. One drop of concentrated HCl was added and the mixture was refluxed for 5 h using a Dean Stark apparatus. After cooling, the reaction mixture was evaporated to dryness, yielding an oil.

[Re(CO)$_3$(pyOEt)(dppn)]X (X = PF$_6$ or Cl). 105 mg of [Re(dppn)(CO)$_3$Cl] (0.16 mmol) were dissolved in 16 mL anhydrous DMF under argon. The solution was stirred and heated to 50°C, then solid $AgPF_6$ (166 mg, 0.66 mmol) was added, and the solution was heated at 50°C under argon for 5 minutes. Meanwhile, 186 mg of pyOEt (1.0 mmol) was added dropwise to the solution, and the reaction was heated at 70°C for 6 h. The reaction was then cooled and filtered to remove AgCl. The crude product was purified on a silica column first using 1:9 MeCN:$CHCl_3$, followed by a second silica column utilizing a gradient of 1% to 8% MeOH in $CHCl_3$. The orange product was re-crystallized *via* vapor diffusion from 1:1 DCM:MeCN with Et_2O. ^{1}H NMR (500 MHz, CD_3CN) δ 9.89 (dd, J = 8.2, 1.4 Hz, 2H), 9.67 (dd, J = 5.2, 1.4 Hz, 2H), 9.09 (s, 2H), 8.35 (dd, J = 6.5, 3.2 Hz, 2H), 8.33 – 8.24 (m, 4H), 7.79 – 7.72 (m, 2H), 7.19 – 7.13 (m, 2H), 3.91 (q, J = 7.1 Hz, 2H), 2.79 (t, J = 7.3 Hz, 2H), 2.49 (t, J = 7.3 Hz, 2H), 1.02 (t, J = 7.1 Hz, 3H). ESI(+)MS (*m/z*): $[M]^+$ calc. 782.14, found 782.14. The PF_6 counter-ion was exchanged to Cl using Sephadex QAE anion exchange resin. (**Note**: the final complex is susceptible to decomposition by

substitution of the pyOEt ligand by Cl in the presence of excess Cl. Anion exchanges of the final product should be conducted quickly, and at low $MgCl_2$ concentrations (e.g. 0.05 M). It is not known whether performing anion exchanges in the dark will help).

[Ru(tpy)(DMSO)(Cl_2)]. A mixture of ethanol (95%, 20 mL) and methanol (6 mL) was slowly stirred as $Ru(DMSO)_4Cl_2$ (1.26 g, 2.2 mmol) was added. The mixture was stirred and refluxed under an inert argon atmosphere for 15 min. A separate mixture of ethanol (95%, 10 mL) and terpyridine (tpy, 0.600 g, 2.6 mmol) was prepared and added dropwise under argon. The resulting brown mixture was refluxed and stirred under argon for another 8.5 h. The precipitate was collected by vacuum filtration. The solid was washed with cold water, cold ethanol, and ether. 800 mg of red solid were obtained (75% yield).

[Ru(tpy)(dppz)(Cl)]Cl. A mixture of 0.30 g (0.65 mmol) [Ru(tpy)(DMSO)$(Cl)_2$] and 0.485 g (1.6 mmol) dppz was added to dry DMF (30 mL). The resulting solution was stirred and heated for 30 h at 130°C under argon. After the reaction was cooled to room temperature, the dark purple mixture was brought to dryness under vacuum, and directly engaged in the next reaction step.

[Ru(tpy)(dppz)(CN)]PF_6. The solid obtained from the previous reaction was dissolved in 50 mL of Milli-Q water containing 0.2 g NaOH and 420 mg KCN (10 eq). The mixture was refluxed for 8 h. After cooling, the complex was precipitated by addition of 1.2 equivalents of KPF_6 and the solid was washed with water. The product, contaminated with dppz ligand, can be purified by HPLC using an isocratic eluent of 45% MeCN 55% Water (with 1%TFA) on a Zorbax SB-C18 column. ^{1}H NMR (300 MHz, CD_3CN) δ 10.48 (d, *J* = 5.3 Hz, 1H), 9.84 (d, *J* = 8.1 Hz, 1H), 9.44 (d, *J* = 8.0 Hz, 1H), 8.58 (d, *J* = 8.1 Hz, 2H), 8.53 – 8.36 (m, 5H), 8.25 (t, *J* = 8.1 Hz, 1H), 8.13 (dt, *J* = 6.5, 2.8 Hz, 2H), 7.93 (t, *J* = 7.8 Hz, 2H), 7.75 (t, *J* = 5.6 Hz, 3H), 7.59 (dd, *J* = 8.1, 5.2 Hz, 1H), 7.22 (t, *J* = 6.5 Hz, 2H). ESI(+)MS (*m/z*): $[M]^+$ calc. 643.09, found 643.19. The

purified complex was converted to its Cl salt by Sephadex QAE anion exchange.

7.2.3 Luminescence Measurements

Steady-State Luminescence. Luminescence spectra were recorded on an ISS-K2 spectrofluorometer at 25°C. The Re complex was excited at 398 nm, and the Ru complex at 460 nm. The Cl salts of the complexes were used for all experiments with DNA. Stock solutions of the complexes were prepared in water with a small portion (less than 10%) of methanol added to assist in solubility.

7.3 Results and Discussion

7.3.1 Designing the Donor-Acceptor System for TRIR Analysis of DNA-Mediated CT

The goal of this work was to use TRIR to study a DNA-mediated electron transfer reaction between donor and acceptor metal complexes intercalated into DNA. The chemical structures of the compounds investigated here are provided in Figure 7.2. $[Ru(tpy)(CN)(dppz)]^+$ (tpy = terpyridine) was developed to serve as a charge donor in a DNA-mediated CT reaction with the charge acceptor $[Re(CO)_3(pyOEt)(dppn)]^+$ (pyOEt = ethyl 3-(pyridine-4-yl)propanoate; dppn = benzodipyridophenazine). In theory, by monitoring time-dependent changes in the TRIR spectra of the IR-active CN and CO ligands, one can measure rates of charge injection by the donor and charge arrival at the acceptor.

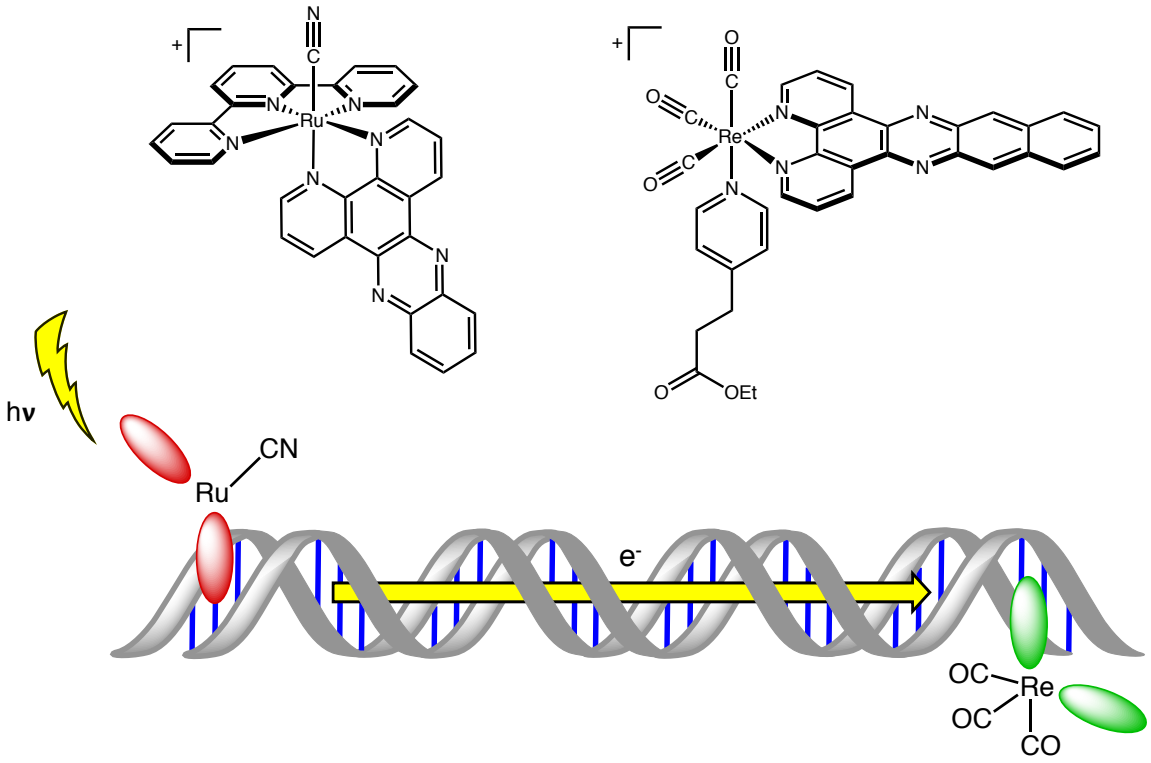

Figure 7.2. (*Top*) Chemical structures of TRIR probes investigated in this work, $[Ru(tpy)(CN)(dppz)]^+$ and $[Re(CO)_3(pyOEt)(dppn)]^+$. (*Bottom*) Following intercalation of the IR-active probes into DNA, excitation of the ruthenium donor will result in electron transfer through the base stack to the rhenium acceptor. TRIR can be used to monitor the changes in CN and CO stretching frequencies corresponding to charge injection and charge arrival, respectively.

In previous investigations it was found that observing the reduced state of $[Re(CO)_3(pyOEt)(dppz)]^+$ by TRIR is hindered by the persistence of lowest excited state ^{3}IL dppz bands, which overlap with the reduced $Re(CO)_3$ bands.[13] Thus, optimizations of the Re structure must be made with the intent of generating a complex which possesses an MLCT lowest excited state; from a TRIR perspective, a $Re(CO)_3$ complex with an MLCT lowest excited state would be a more useful probe owing to more spectrally-distinct TRIR bands compared to ^{3}IL-dominant species.[13] It has been reported that incorporating dppn into $Re(CO)_3$ systems lowers the energy of the MLCT and IL absorption bands owing to the more extended π–conjugation of the dppn ligand relative to dppz.[17] In fact, complexes of the type $[Re(CO)_3(py\text{-}R)(dppn)]^+$ (py-R = pyridine or

modified pyridine) exhibit broad, structureless steady-state emission bands with peak maxima at ca. 587-595 nm, comparable to other Re(I) polypyridine ^{3}MLCT emitters.[18,19] Experimental evidence suggests that emission from $[Re(CO)_3(py\text{-}R)(dppn)]^+$ includes both ^{3}IL(dppn) and ^{3}MLCT $d\pi(Re)\text{-}\pi^*(dppn)$ excited-state character.[17] Thus, it was proposed that $[Re(CO)_3(pyOEt)(dppn)]^+$ (Figure 7.2) might possess more distinct MLCT TRIR spectral signals compared to its dppz derivative. However, like dppz, dppn is a strong DNA intercalator; thus, $Re(CO)_3$ complexes bearing this ligand are readily capable of binding to DNA.[20,21]

7.3.2 Synthesis and Photophysical Characterization

The $[Re(CO)_3(pyOEt)(dppn)]^+$ complex is synthesized in an analogous fashion to that reported for its dppz counterpart (Scheme 7.1).[22,23] In experiments with DNA, the final product $[Re(CO)_3(pyOEt)(dppn)](PF_6)$ is converted to its Cl salt to assist in water solubility; however, $[Re(CO)_3(pyOEt)(dppn)]Cl$ still exhibits relatively poor solubility in water. The synthesis of $[Ru(tpy)(CN)(dppz)](PF_6)$ is relatively straightforward, although caution should be applied in the final reaction ($[Ru(tpy)(Cl)(dppz)]^+$ with KCN), because KCN is quite hazardous (NaOH is included in the reaction to minimize the formation of HCN vapors). This final step is based on a literature protocol for the synthesis of $[Ru(tpy)(CN)(bpy)]^+$ (Scheme 7.1).[24] Again, $[Ru(tpy)(CN)(dppz)](PF_6)$ is converted to its Cl salt for investigations with DNA, although this complex is also sparingly soluble in aqueous solution.

The absorption profile of $[Re(CO)_3(pyOEt)(dppn)]^+$ (Figure 7.3) bears very close resemblance to dppz- and dppn-containing $Re(CO)_3$ complexes.[20-23,25,26] The complex exhibits absorption maxima at ca. 400 and 420 nm and a weak tail extending in the visible to approximately 500 nm. The absorption maxima at 400 and 420 nm are tentatively assigned to π-π^* (dppn) intraligand (IL) transitions, considering the fact that free dppn absorbs at relatively low energies

(391 and 413 nm in CH_2Cl_2).[17,20,21] However, the lower-energy tail that extends into the visible region, along with the red-shift of the 400 and 420 nm bands relative to free dppn, is indicative of a dπ(Re)-π*(dppn) MLCT transition.[25,26] As anticipated for $Re(CO)_3$ complexes of dppz and dppn, the steady-state emission of $[Re(CO)_3(pyOEt)(dppn)]^+$ is quenched in aqueous solution (Figure 7.3).[20-23] Conversely, excitation of the compound in acetonitrile yields an extremely bright, broad,

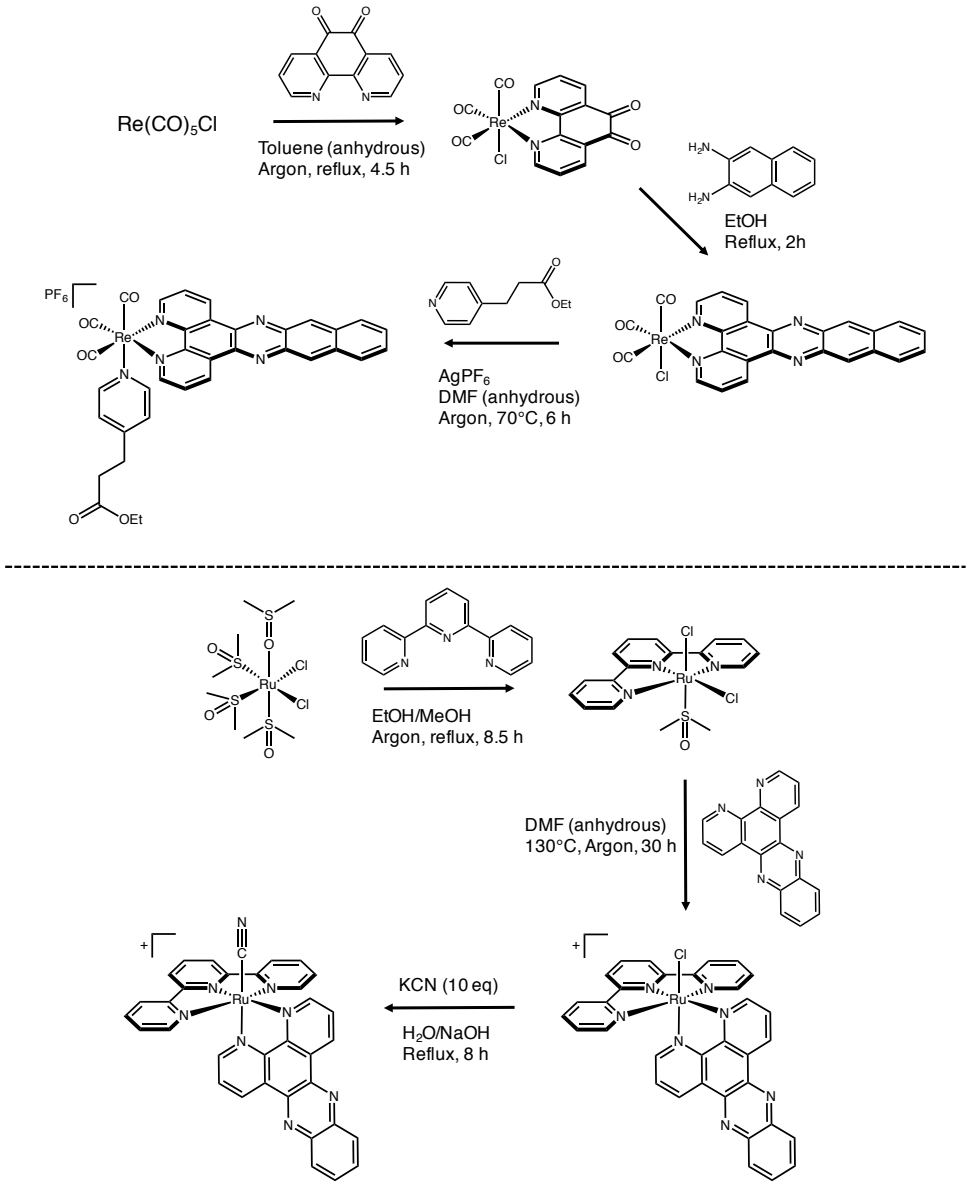

Scheme 7.1. (*Top*) Synthesis of $[Re(CO)_3(pyOEt)(dppn)]^+$. The complex is isolated as its PF_6 salt from the final reaction. (*Bottom*) Synthesis of $[Ru(tpy)(CN)(dppz)]^+$. The complex is precipitated as its PF_6 salt after the final reaction.

structureless emission band with maximum at 595 nm, in agreement with the previously reported $[Re(CO)_3(py)(dppn)]^+$ bearing an unmodified pyridine.[21]

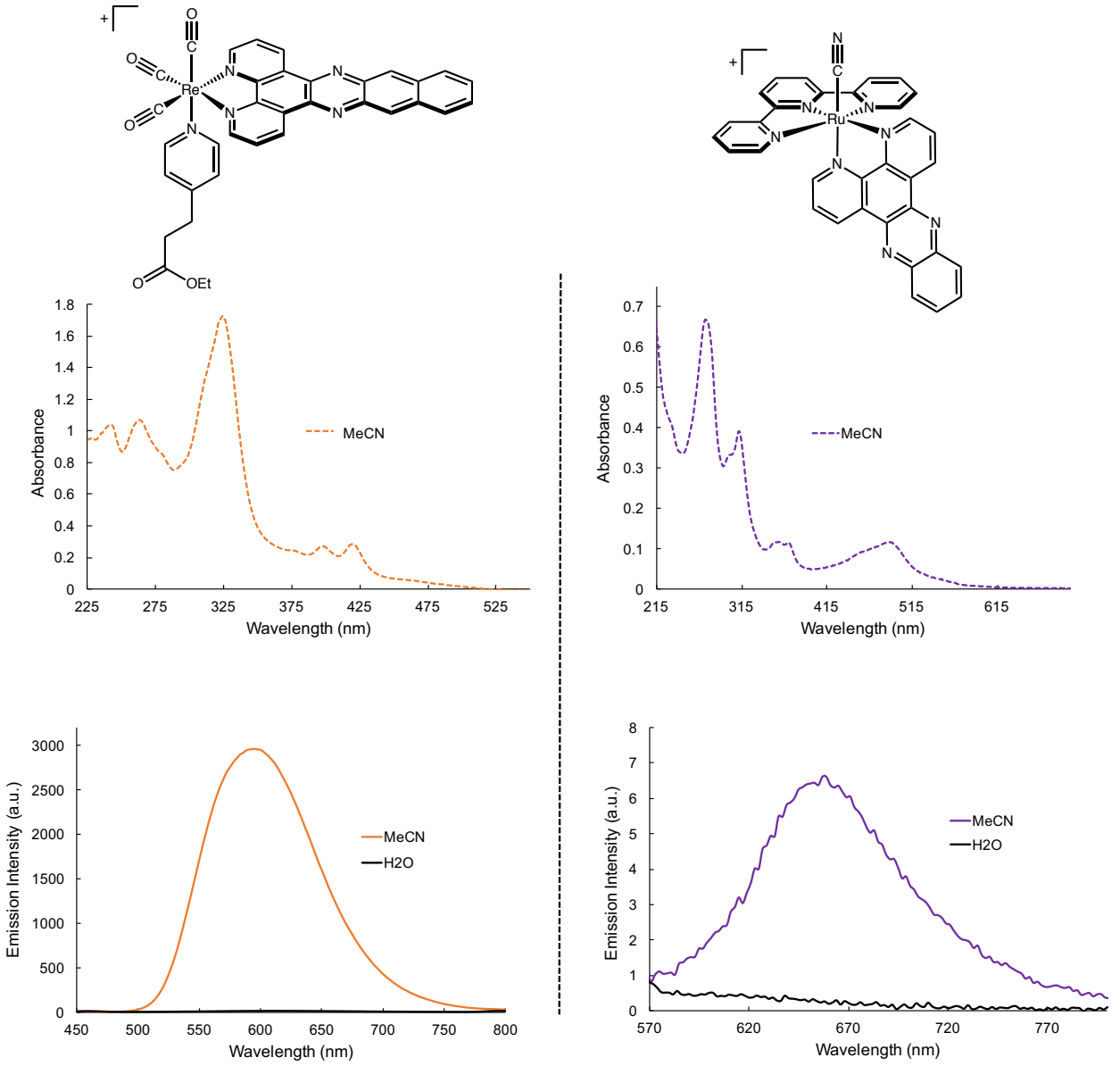

Figure 7.3. (*Top*) Chemical structures of TRIR probes investigated in this work, $[Ru(tpy)(CN)(dppz)]^+$ and $[Re(CO)_3(pyOEt)(dppn)]^+$. (*Middle-Left*) UV-Visible spectrum of $[Re(CO)_3(pyOEt)(dppn)](PF_6)$ in acetonitrile. (*Bottom-left*) Steady-state emission spectra of the Re complex in acetonitrile and water (PF_6 and Cl salts, respectively; 398 nm excitation, ~10 µM Re. (*Middle-Right*) UV-Visible spectrum of $[Ru(tpy)(CN)(dppz)](PF_6)$ in acetonitrile. (*Bottom-right*) Steady-state emission spectra of $[Ru(tpy)(CN)(dppz)]^+$ in acetonitrile (PF_6 salt) and water (Cl salt). Sample absorbances of ~0.1 at 460 nm wavelength used for excitation, or ~10 µM).

Literature precedent for compounds of the type $[Ru(tpy)(CN)(dppz)]^+$ is more limited than the $Re(CO)_3$ complexes discussed above. However, the UV-Visible spectrum of $[Ru(tpy)(CN)(dppz)]^+$ shares features of that reported for $[Ru(tpy)(CN)(bpy)]^+$, including the ligand centered π-π* transitions in the UV and an intense low-energy absorption at ca. 485 nm corresponding to an MLCT.[24] The dppz ligand π-π* also manifests at ca. 350-360 nm. Similarly to the $[Re(CO)_3(pyOEt)(dppn)]^+$ complex, the emission of $[Ru(tpy)(CN)(dppz)]^+$ is entirely quenched in water (Figure 7.3). Interestingly, the emission in acetonitrile is extremely weak; in fact, $[Ru(tpy)(CN)(bpy)]^+$ was previously reported to be a weak emitter in acetonitrile, producing an MLCT luminescence with low quantum yield[27] of 1.5 x 10^{-4} *vs*. $[Ru(bpy)_3]^{2+}$ (ϕ_{em} = 0.06)[28] and an excited state emission lifetime of ~6 ns.[24] Comparatively, the $[Re(CO)_3(pyOEt)(dppn)]^+$ complex possesses a nearly 500-fold brighter steady-state emission intensity in acetonitrile than the ruthenium complex for samples of approximately equal metal concentration (Figure 7.3).

Samples of $[Re(CO)_3(pyOEt)(dppn)]^+$ and $[Ru(tpy)(CN)(dppz)]^+$ were sent to our collaborator Tony Vlcek (Queen Mary University of London) for TRIR analysis. $[Re(CO)_3(pyOEt)(dppn)]^+$ only exhibited bands corresponding to π-π*(dppn) intraligand excited states; there was no distinct TRIR signature for an MLCT state. Thus, from a TRIR perspective, this dppn derivative is not an improvement over the previously-studied $[Re(CO)_3(pyOEt)(dppz)]^+$ complex. The excited-state TRIR spectrum of $[Ru(CN)(tpy)(dppz)]^+$ in DMF is very indistinctive, because the excited-state ν(CN) absorption is weak and strongly overlaps with the bleach. Additionally, the excited-state lifetime of the ν(CN) stretch is very sensitive to increasing water content, limiting this probe's utility in aqueous solutions with DNA. Future work will focus on methylating the CN group of $[Ru(CN)(tpy)(dppz)]^+$ to generate the isocyanide derivative $[Ru(CN\text{-}CH_3)(tpy)(dppz)]^{2+}$ with the hopes of attenuating quenching of the excited state by water.

7.3.3 Quenching of $[Re(CO)_3(pyOEt)(dppn)]^+$ Luminescence by $[Ru(CN)(tpy)(dppz)]^+$ when Bound to DNA

While $[Re(CO)_3(pyOEt)(dppn)]^+$ and $[Ru(CN)(tpy)(dppz)]^+$ will not be a useful donor-acceptor pair to monitor DNA-mediated CT by TRIR as originally designed, basic steady-state luminescence experiments can still be performed to investigate whether the Ru complex is capable

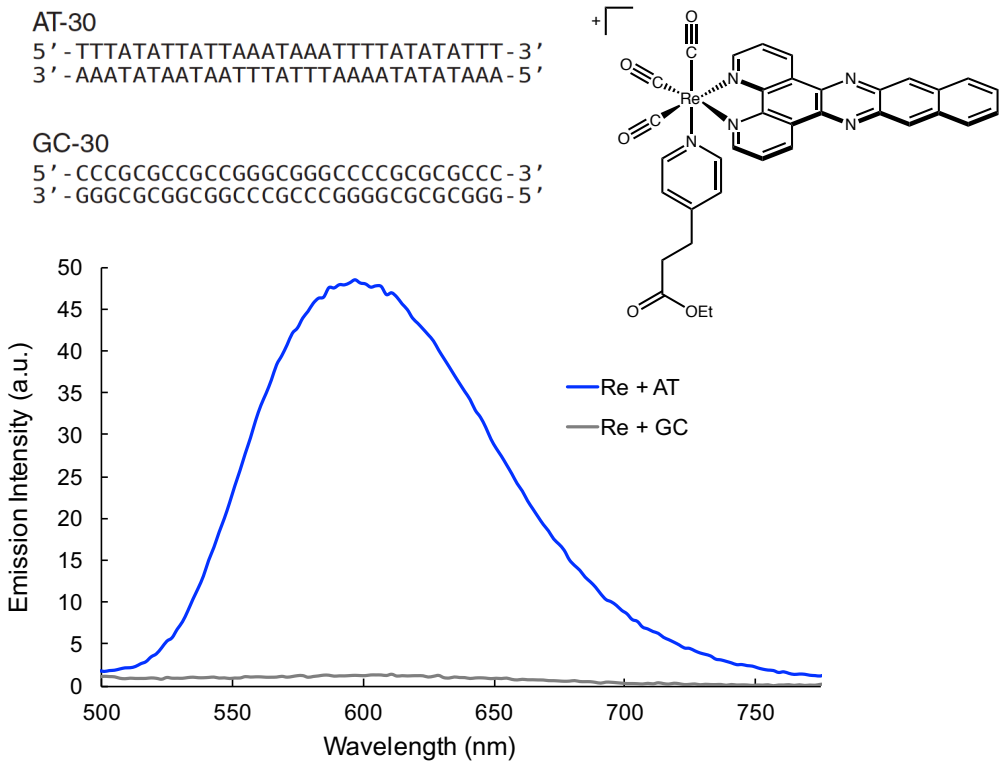

Figure 7.4. Steady-state emission spectra of $[Re(CO)_3(pyOEt)(dppn)]Cl$ (5 µM) in the presence of AT and GC 30-mer DNA duplexes (5 µM duplex or 150 µM base pair). Samples were prepared in 10 mM NaP_i, 50 mM NaCl, pH 7.0 buffer and excited at 398 nm.

of quenching the $[Re(CO)_3(pyOEt)(dppn)]^+$ emission *via* DNA-mediated electron transfer, as demonstrated previously by M. Arkin et al. for Ru(II)/Os(II) and Rh(III) noncovalent donor-acceptor pairs.[29] $Re(CO)_3$ complexes of dppn intercalate into DNA and exhibit bright emission when bound to AT-rich sequences, but are quenched in the presence of GC DNA.[20] This phenomenon is also observed for $[Re(CO)_3(pyOEt)(dppz)]^+$ and is attributed to quenching of the metal excited state by guanine.[13]

Here, two 30-mer AT and GC DNA duplexes were generated and the emission of $[Re(CO)_3(pyOEt)(dppn)]^+$ in the presence of both sequences was measured (Figure 7.4). As expected, the emission is entirely quenched when bound to the GC sequence but luminescence is observed with the AT sequence. We then investigated whether addition of the $[Ru(CN)(tpy)(dppz)]^+$ complex leads to quenching of the Re emission when bound to the AT DNA duplex. Following excitation of the Re complex, we would expect quenching of its emission when $[Ru(CN)(tpy)(dppz)]^+$ is intercalated into the same duplex as a result of electron transfer. Samples were prepared containing 5 μM Re and 250 μM base pair AT DNA (50:1 base pairs:Re) and the

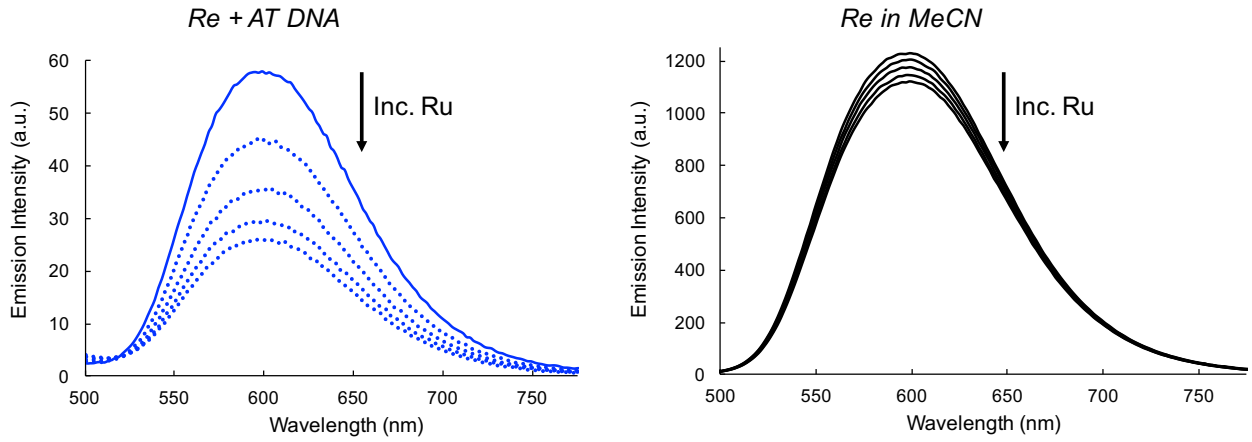

Figure 7.5. (*Left*) Steady-state luminescence quenching of $[Re(CO)_3(pyOEt)(dppn)]Cl$ (5 μM) by [Ru(CN)(tpy)(dppz)]Cl in the presence of the AT DNA sequence (250 μM base pair). Ru was titrated into the solution to 0.4, 0.8, 1.2, and 1.6 Ru:Re equivalents. Samples were prepared in 10 mM NaP_i, 50 mM NaCl, pH 7.0 buffer and excited at 398 nm. (*Right*) Ru was titrated into a 5 μM acetonitrile solution of the Re complex in the same fashion, exciting at 398 nm.

Ru complex was titrated in to 0.4, 0.8, 1.2, and 1.6 equivalents. The 50:1 base pair:Re concentration ratio was chosen such that the compounds were relatively dilute on the helix.[29] Dramatic quenching of the Re emission is observed (Figure 7.5). However, it must be noted that the two complexes under study possess absorption spectra that overlap significantly with each other - that is, there is no wavelength at which the Re complex absorbs that the Ru complex does not (refer to Figure 7.3). Such a wavelength would be ideal for the system so as to selectively

excite the Re complex. As a control, samples of the Re compound were prepared in acetonitrile and the Ru was titrated in with no DNA present (Figure 7.5). This was performed to see whether the decrease in Re emission intensity observed upon Ru addition with the AT sequence was the result of true quenching or simply a "filtering" effect resulting from the Ru compound absorbing the excitation light. We see that upon adding Ru to the Re alone, there is only a small decrease in emission intensity (Figure 7.5). As such, the quenching observed for $[Re(CO)_3(pyOEt)(dppn)]^+$ when bound to the AT sequence is likely a DNA-mediated transfer mechanism.

7.4 Conclusions

In this work, $[Re(CO)_3(pyOEt)(dppn)]^+$ and $[Ru(CN)(tpy)(dppz)]^+$, which bear IR-active CO and CN ligands, were synthesized with the intention of using them as TRIR probes to monitor the kinetics of DNA-mediated electron transfer. It was originally hypothesized that the Re complex might have an MLCT lowest excited state, which would provide a TRIR signature that is spectrally distinct from the reduced-state complex. However, TRIR analysis of $[Re(CO)_3(pyOEt)(dppn)]^+$ revealed no evidence of an MLCT; the complex, like its dppz derivative studied previously, exhibits intense bands corresponding to intraligand excited states, which makes TRIR spectral analysis of the reduced-state complex challenging. From a TRIR perspective, this dppn derivative is not an improvement over $[Re(CO)_3(pyOEt)(dppz)]^+$. Additionally, the CN stretching band of $[Ru(CN)(tpy)(dppz)]^+$ is highly solvent-sensitive, owing to hydrogen bonding with water molecules. This leads to rapid quenching of the excited state as observed by TRIR. Synthesis of a methylated $[Ru(CN\text{-}Me)(tpy)(dppz)]^{2+}$ isocyanide derivative may enhance this compound's excited state lifetime and alleviate the rapid quenching by water.

Because of the unfavorable TRIR properties exhibited by these two probes, further TRIR experiments with DNA were not conducted. However, steady-state luminescence experiments were performed to see whether electron transfer between this donor-acceptor pair was capable of quenching the $[Re(CO)_3(pyOEt)(dppn)]^+$ emission when bound to AT DNA. Upon titrating $[Ru(CN)(tpy)(dppz)]^+$ into solutions of the Re complex with AT DNA, quenching of the Re emission was observed, consistent with a DNA-mediated electron transfer mechanism.

References

1. Barton, J.K.; Olmon, E.D.; Sontz, P.A. *Coord. Chem. Rev.* **2011**, *255*, 619-634.

2. Grodick, M.A.; Muren, N.B.; Barton, J.K. *Biochemistry* **2015**, *54*, 962-973.

3. Kopelevich, Y.; Esquinazi, P. *Adv. Mat.* **2007**, *19*, 4559-4563.

4. Murphy, C.J.; Arkin, M.R.; Jenkins, Y.; Ghatlia, N.D.; Bossmann, S.H.; Turro, N.J.; Barton, J.K. *Science* **1993**, *262*, 1025-1029.

5. Holmlin, R.E.; Stemp, E.D.A.; Barton, J.K. *J. Am. Chem. Soc.* **1996**, *118*, 5236-5244.

6. Elias, B.; Shao, F.; Barton, J.K. *J. Am. Chem. Soc.* **2008**, *130*, 1152-1153.

7. Hall, D.B.; Holmlin, R.E.; Barton, J.K. *Nature* **1996**, *382*, 731-735.

8. Glyn, P.; George, M.W.; Hodges, P.M.; Turner, J.J. *J. Chem. Soc., Chem. Commun.* **1989**, 1655-1657.

9. George, M.W.; Turner, J.J. *Coord. Chem. Rev.* **1998**, *177*, 201-217.

10. Vlcek, A. *Top. Organomet. Chem.* **2010**, *29*, 73-114.

11. Adams, H. et al. *Dalton Trans.* **2006**, 39-50.

12. Encinas, S. et al. *J. Chem. Soc., Dalton Trans.* **2001**, 3312-3319.

13. Olmon, E.D. et al. *J. Am. Chem. Soc.* **2011**, *133*, 13718-13730.

14. Cao, Q. et al. *Photochem. Photobiol. Sci.* **2011**, *10*, 1355-1364.

15. Dickerson, J.E.; Summers, L.A. *Aust. J. Chem.* **1970**, *23*, 1023-1027.

16. Alston, J.R.; Kobayashi, S.; Younts, T.J.; Poler. J.C. *Polyhedron* **2010,** *29,* 2696-2702.

17. Lo, K.K.; Tsang, K.H. *Organometallics* **2004**, *23*, 3062-3070.

18. Sacksteder, L.; Lee, M.; Demas, J.N.; DeGraff, B.A. *J. Am. Chem. Soc.* **1993**, *115*, 8230-8238.

19. Lees, A.J. *Chem. Rev.* **1987**, *87*, 711-743.

20. Yam, V.; Lo, K.K.; Cheung, K.-K.; Kong, R.Y. *J. Chem. Soc., Dalton Trans.* **1997**, 2067-2072.

21. Yam, V.; Lo, K.K.; Cheung, K.-K.; Kong, R.Y. *J. Chem. Soc., Chem. Commun.* **1995**, 1191-1193.

22. Stoeffler, H.D.; Thornton, N.B.; Temkin, S.L.; Schanze, K.S. *J. Am. Chem. Soc.* **1995**, *117*, 7119-7128.

23. Olmon, E.D. *Investigating DNA-Mediated Charge Transport by Time-Resolved Spectroscopy*. Ph.D. Thesis, California Institute of Technology, Pasadena, CA, **2012**.

24. Cadranel, A.; Albores, P.; Yamazaki, S.; Kleiman, V.D.; Baraldo, L.M. *Dalton Trans.* **2012**, *41*, 5343-5350.

25. Dyer, J. et al. *Photochem. Photobiol. Sci.* **2003**, *2*, 5420-554.

26. Ruiz, G.T. et al. *Dalton Trans.* **2007**, *3*, 2020-2029.

27. Ponce, A.; Bachrach, M.; Farmer, P.J.; Winkler, J.R. *Inorg. Chim. Acta*. **1996**, *243*, 135-140.

28. Caspar, J.V.; Meyer, T.J. *J. Am. Chem. Soc.* **1983**, *105*, 5583-5590.

29. Arkin, M.R.; Stemp, E.D.A.; Holmlin, R.E.; Barton, J.K.; Hormann, A.; Olson, E.J.C.; Barbara, P.F. *Science* **1996**, *273*, 475-480.

Chapter 8

Conclusions

The work described in this thesis involves the design, synthesis, and characterization of transition metal complexes that bind to DNA through non-covalent interactions, with a focus on developing luminescent ruthenium compounds that specifically target DNA base pair mismatches. Chapter 2 presented the light switch complex $[Ru(Me_4phen)_2(dppz)]^{2+}$, which makes use of its bulky Me_4phen ligands to discriminate against intercalation at well-matched base pairs and thus favor metalloinsertion at a mismatch. The complex possesses a higher binding affinity for a DNA mismatch compared to well-matched base pairs, and exhibits a longer excited-state emission lifetime when bound to a mismatch. Furthermore, it was found that Δ-$[Ru(Me_4phen)_2(dppz)]^{2+}$ is the enantiomer which imparts all mismatch selectivity, consistent with the handedness of B-form DNA.

The work presented in Chapter 3 represents an alternate approach for achieving mismatch specificity. Instead of incorporating bulky ancillary ligands, $[Ru(bpy)_2(BNIQ)]^{2+}$ possesses a sterically expansive aromatic inserting ligand (BNIQ) that is capable of selectively undergoing metalloinsertion at a mismatch. This design strategy is more akin to the development of mismatch-targeting rhodium metalloinsertors such as $[Rh(bpy)_2(chrysi)]^{3+}$. In Chapter 4, we rationalized that perhaps incorporating extra steric bulk into the dppz ligand to generate tetramethyl-dppz (tmdppz) might also improve mismatch selectivity compared to the parent $[Ru(bpy)_2(dppz)]^{2+}$. However, we quickly learned that even the addition of simple methyl groups into dppz can lead to a loss of the light switch effect due to the close proximity of the methyl substituents to the phenazine nitrogen atoms. Through this same mechanism, we see that all luminescence discrimination for mismatched *vs*. well-matched DNA is lost.

In Chapter 5, we explored the biological activity of the mismatch-specific ruthenium complexes and used confocal microscopy to visualize $[Ru(Me_4phen)_2(dppz)]^{2+}$ in MMR-proficient

and MMR-deficient cancer cells. Visualization of $[Ru(Me_4phen)_2(dppz)]^{2+}$ in live and fixed cells revealed that the complex does localize significantly to mitochondria, and is capable of staining cytoplasmic regions of the cell. However, the compound does exhibit nuclear entry. Furthermore, much still needs to be learned regarding the mechanism of cell death induced by rhodium metalloinsertors such as $[Rh(phen)(chrysi)(PPO)]^{2+}$, specifically with respect to what proteins and pathways are activated that cause a DNA damage response. In this context, a mismatch-specific luminescent probe may have utility, and current efforts are investigating the *in cellulo* co-localization of $[Ru(Me_4phen)_2(dppz)]^{2+}$ with proteins involved in the DNA damage response.

Chapter 6 described work that was conducted to improve the efficacy of an earlier-generation rhodium metalloinsertor, $[Rh(HDPA)_2(chrysi)]^{3+}$, through amino acid conjugation. Interestingly, this resulted in a loss of cell-selective activity, possibly due to altered uptake and localization. Since these investigations, metalloinsertors that are more robust to functionalization, such as $[Rh(phen)(chrysi)(PPO)]^{2+}$, have been established, and are currently being developed as antibody drug conjugates to improve tumor specificity.

Lastly, outside the realm of mismatch-targeting – but still under the umbrella of DNA-binding transition metal complexes – a portion of work was devoted to the study of ruthenium and rhenium intercalators that were designed as TRIR probes to investigate the kinetics of DNA-mediated CT. While $[Ru(tpy)(CN)(dppz)]^{+}$ and $[Re(CO)_3(pyOEt)(dppn)]^{+}$ do not possess the spectral properties to allow for the desired analysis by TRIR, steady-state luminescence experiments do suggest that this donor-acceptor pair is capable of undergoing DNA-mediated electron transfer. However, there is still room for optimizing the structures of these complexes to improve their TRIR spectral response.

Taken together, the work described here illustrates the incredible utility of octahedral transition metal complexes for probing DNA structure. Importantly, we have learned that through the logical design of new ligands and the modification of existing ligand scaffolds, we can achieve recognition of specific biomarkers such as DNA mismatches. Mismatch-targeting rhodium and ruthenium complexes represent a new strategy for therapeutic and diagnostic design, and we hope that the work presented here will fuel future research endeavors aimed at developing therapeutic and diagnostic small molecule agents directed towards MMR-deficient cancers.

In a broader sense, this work speaks to the incredible value of conducting scientific research in an interdisciplinary setting. The opportunity to 1) rationally design and synthesize novel small molecules, 2) explore their spectroscopic properties, and 3) investigate their biological activity in clinically relevant cancer cells has truly been a rewarding experience. There is a definite satisfaction that comes with synthesizing a compound at the benchtop and then directly studying its potential therapeutic or diagnostic utility. The interdisciplinary nature of our research has forced me to acquire a diverse scientific skill set, which has been extremely gratifying. Furthermore, through collaborations with other research groups, we have been able to answer key questions that otherwise would have been difficult to approach in our lab alone, allowing us to push the boundaries of scientific discovery at a rapid, exciting pace.

Appendix

A.1 $[Ru(Me_4phen)_2(dppz)]^{2+}$ DNA Titrations

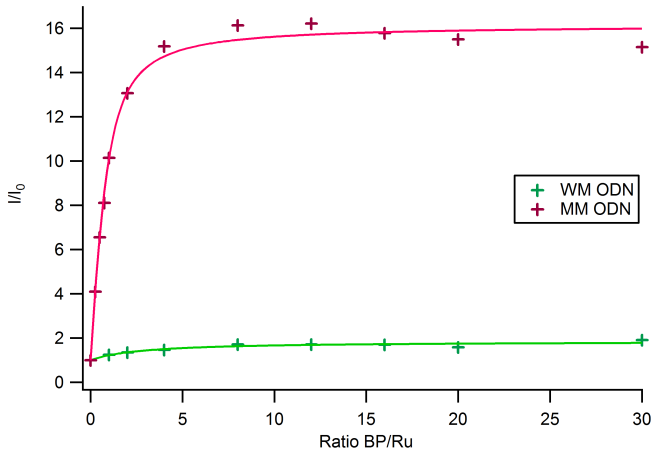

Figure A1: Steady-state luminescence titrations of *rac*-$[Ru(Me_4phen)_2(dppz)]^{2+}$ with well-matched (green) and mismatched (red) 27-mer DNA duplexes (ODN). Samples were run in 5 mM tris, 200 mM NaCl, pH 7.5. [Ru] = 2 μM, λ_{ex} = 440 nm. Emission spectra were integrated from 564-820 nm.

The luminescence intensity of the complex upon addition of DNA (well-matched or mismatched duplexes) was used to determine the binding affinity of *rac*-$[Ru(Me_4phen)_2(dppz)]^{2+}$ towards well-matched and mismatched DNA base pair sites. For the titration with well-matched DNA, the binding affinity was evaluated using the McGhee-Von Hippel method,[1] and a value of $6.8 \times 10^4\ M^{-1}$ per well-matched base pair was obtained with an occupational factor, *p*, of 2.3 (also known as the size-covering parameter; that is, the consecutive base pair residues covered or occupied by a single bound complex. A value of $p = 2$ corresponds to nearest-neighbor exclusion).[2]

In order to evaluate the binding affinity of the complex for the mismatched site, we must consider two competing equilibria (expressed below) for the intercalation at well-matched sites and insertion at the CC mismatch.

$$C + BP \rightleftharpoons [C\_BP] \qquad K_{ass} = \frac{[C\_BP]}{[C]\,[BP]}$$

$$C + MM \rightleftharpoons [C\_MM] \quad K_{MM} = \frac{[C\_MM]}{[C]\,[MM]}$$

K_{ass} describes the binding equilibrium between the complex, *C*, and well-matched base pair sites, *BP*, in the DNA. K_{MM} describes the binding equilibrium between the complex and the mismatched site, *MM*.

Next, we will express the total concentration of complex as C_c; this is kept constant throughout the titration. We can then define the various molar fractions for the complex as follows:

$f = \frac{[C]}{C_C}$, the molar fraction of free complex.

$b = \frac{[C\_BP]}{C_C}$, the molar fraction of complex bound to WM base pairs.

$m = \frac{[C\_MM]}{C_C}$, the molar fraction of complex bound to MM sites.

Additionally, we express the total concentration of duplex as C_{ODN}; this value increased throughout the titration. The variable *R* is introduced as being equal to the ratio C_{ODN}/C_C, and in our titration the luminescence of the complex is measured as the value of *R* is increased. The luminescence intensity, I/I_0, can be expressed as a function of *R* as follows:

$$I/I_0 = f + \alpha\, b + \beta\, m$$

where α and β are equal to the relative emissivity of complex when bound to *BP* and *MM*, respectively.

We must define a few more final parameters: *x* is the ratio of mismatched sites to total base pairs in the duplex (so 1/27, or 0.037); *p*, as mentioned above, is the occupational factor which takes into account the possible inhibition of binding by two complexes in close vicinity; and *n* is the total number of base pairs in the duplex (27). We can now express the equilibrium

concentrations of free *BP* and *MM* sites as follows:

$$[BP] = n\,(1-x)\,C_{ODN} - p\,[C\_BP] = n\,(1-x)\,C_{ODN} - p\,b\,C_C$$

$$[MM] = n\,x\,C_{ODN} - [C\_MM] = n\,x\,C_{ODN} - m\,C_C$$

Thus,

$\frac{[BP]}{C_C} = n\,(1-x)\,R - p\,b$ and $\frac{[MM]}{C_C} = n\,x\,R - m$

The binding equilibrium equations are thus rewritten as:

$K_{ass} = \frac{b}{f\,C_C(n\,(1-x)\,R - p\,b)}$ and $K_{MM} = \frac{m}{f\,C_C(n\,x\,R - m)}$

The expression of b and m as functions of f can thus be obtained:

$$K_{ass}\,f\,C_C(n\,(1-x)\,R - p\,b) - b = 0$$

$$b = \frac{K_{ass}\,C_C\,n\,(1-x)\,R\,f}{1 + K_{ass}\,C_C\,p\,f}$$

$$K_{MM}\,f\,C_C(n\,x\,R - m) - m = 0$$

$$m = \frac{K_{MM}\,C_C\,n\,x\,R\,f}{1 + K_{ass}\,C_C\,f}$$

With

$$1 = f + b + m$$

$$0 = f - 1 + \frac{K_{ass}\,C_C\,n\,(1-x)\,R\,f}{1 + K_{ass}\,C_C\,p\,f} + \frac{K_{MM}\,C_C\,n\,x\,R\,f}{1 + K_{ass}\,C_C\,f}$$

$$0 = (f-1)(1 + K_{ass}\,C_C\,p\,f)(1 + K_{ass}\,C_C\,f) + K_{ass}\,C_C\,n\,(1-x)\,R\,f\,(1 + K_{ass}\,C_C\,f)$$
$$+ K_{MM}\,C_C\,n\,x\,R\,f(1 + K_{ass}\,C_C\,p\,f) \qquad \textbf{(eq. 1)}$$

The expression of the intensity of luminescence, I/I_0 can be written as follows:

$$I/I_0 = f + \alpha\,\frac{K_{ass}\,f\,C_C\,n\,(1-x)\,R}{1 + p\,K_{ass}\,f\,C_C} + \beta\,\frac{K_{MM}\,f\,C_C\,n\,x\,R}{1 + K_{MM}\,f\,C_C} \qquad \textbf{(eq. 2)}$$

The fitting process using equation **2** is realized by an iterative solving to the expression of *f* using equation **1**. Moreover, a global fitting approach is used to fit the data on both the CC mismatch sequence and the well-matched sequence. The binding affinity K_{ass} and the factors p and α are linked for the global fit. In the case of the well-matched sequence (x=0), the parameters K_{MM} and β are kept constant at 1 and 0, respectively.

A global fitting on the data obtained from the well-matched and mismatched titrations is performed and yield the values of $K_{ass} = 6.8\ 10^4\ M^{-1}$ per well-matched base pair and $K_{MM} = 1.8\ 10^6\ M^{-1}$ per mismatched site. The errors are evaluated to be equal to 10%.

A.2 $[Ru(bpy)_2(BNIQ)]^{2+}$ DNA Titrations

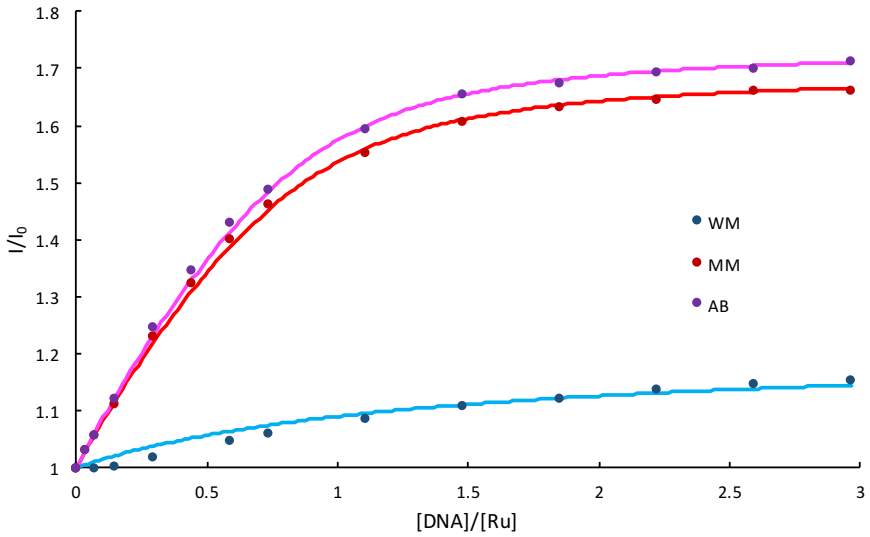

Figure A2: Steady-state luminescence titrations of *rac*-$[Ru(bpy)_2(BNIQ)]^{2+}$ (4 µM) with well-matched (blue), mismatched (red), and abasic (pink) DNA. Samples were prepared in 5 mM Tris, 200 mM NaCl, pH 7.5. [Ru] = 4 µM, λ_{ex} = 440 nm. [DNA] reflects the concentration of full sequence. Emission spectra were integrated from 590-850 nm.

The global fitting on the three data sets is performed (occupational factor set to 2) and yields the values of $K_a = 7.3\ 10^3\ M^{-1}$ per well-matched base pair, $K_a = 3.5\ 10^6\ M^{-1}$ per CC mismatch, and $K_a = 3.8\ 10^6\ M^{-1}$ per abasic site. The emissivities for the complex associated with these sites,

relative to the luminescence of the free complex, are estimated to be 1.36, 1.42 and 1.46 for well-matched, mismatched, and abasic sites, respectively. The errors are evaluated to be equal to 10%.

References

1. McGhee, J.D.; von Hippel, P.H. *J. Mol. Biol.* **1974**, *86*, 469-489.

2. Hiort, C.; Lincoln, P.; Norden, B. *J. Am. Chem. Soc.* **1993**, *115*, 3448-3454.